공학박사 학위논문

NEW INNOVATIVE IMPLANTABLE DEVICES FOR CONTROLLED DRUG DELIVERY

약물 조절전달을 위한 혁신적 이식형 약물주입장치

2017 년 7 월

서울대학교 대학원

협동과정 바이오엔지니어링 전공

이 승 호

Ph. D. Dissertation

NEW INNOVATIVE IMPLANTABLE DEVICES FOR CONTROLLED DRUG DELIVERY

BY

SEUNG HO LEE

JULY 2017

INTERDISCIPLINARY PROGRAM IN BIOENGINEERING

THE GRADUATE SCHOOL

SEOUL NATIONAL UNIVERSITY

Abstract

NEW INNOVATIVE IMPLANTABLE DEVICES FOR CONTROLLED DRUG DELIVERY

By

Seung Ho Lee

Interdisciplinary Program in Bioengineering

The Graduate School

Seoul National University

This dissertation focuses on the design, development and evaluation of implantable drug delivery devices that can replace frequent injections and oral administrations with single implantation and maximize the therapeutic effect of chronic diseases. Currently, implantable drug delivery devices have been widely developed and used in clinical practice, but there are still a number of limitations. Therefore, I propose new innovative implantable drug delivery devices based on a new operating principle.

First, I developed a microchannel-based implantable microchip that

can be pre-programmed prior to implantation and released in a self-controlled manner after implantation. The key of this study is that the device can control the desired amount of drug release by adjusting channel dimensions (i.e., cross-sectional area (A) and length (L)) based on the Diffusion flux and Fick's first law of diffusion equation. The microchip was made of poly(methyl methacrylate), where a pair of micro-channels and micro-wells was embedded to serve as a drug diffusion barrier and a reservoir, respectively. Micro-channel can be precisely fabricated by controlling the CO_2 laser output, processing speed, and irradiation height. To achieve both almost immediate onset and continuous release of DS, a single microchip equipped with the micro-channels with A/Ls of 0.0280 mm, 0.0217 mm and 0.0108 mm was prepared and exhibited continuous drug release for 70 days (almost zero-order pattern for 31 days, $R^2 > 0.996$). When the resulting microchip was implanted in living rats, the drug concentration in the blood could be maintained at 148 ng/ml-225 ng/ml for the first 30 days while showing good biocompatibility. In addition, I also designed an implantable battery-less device enabled with patient-driven, on-demand insulin release to be actuated by an externally applied magnetic field. The key of this study is that the device can be operated without battery. So just apply a magnetic field on the skin instead of an injection needle, the exact amount of drug can be delivered. Unlike other active implantable drug delivery devices where an internal battery is required, MDP does not require a battery. Therefore, it is small in size and does not require

re-surgery, so it can be used semi-permanently. To demonstrate *in vivo* feasibility, it was proved that the insulin concentration and decreased glucose level in the STZ-induced diabetes rat model were maintained at 741.8 ± 4.13 μUml^{-1} and 300.3 ± 10.8 mg dl^{-1}, respectively in the MDP group similar to the values of 683.3±16.9 μUml^{-1} and 251.1 ± 6.41mg dl^{-1} in the S.C injection group for 60 days.

Through these studies, I envision that microchannel-based implantable microchip and implantable battery-less device can offer a patient-oriented new concept biomedical technology.

Keywords : Implantable drug delivery device, Microchannel, Magnetically driven, Battery-less, Controlled drug release, Continuous drug release, Pulsatile drug release

Student Number : 2011-21126

Contents

List of Tables

List of Figures

Chapter 1

Introduction

1.1 Chronic Diseases and its Current Therapy

Chronic diseases are one lasting 3 months or more and generally cannot be prevented and nor do they just appear(1). The most common way to treat them is drug therapy such as, injection and oral administration. However, since long-term continuous and / or pulsatile drug release profiles are required depending on the disease, frequent injection and oral administration are inevitable (Figure 1.1). Thus, it causes a lot of suffering and economic burden to patients.

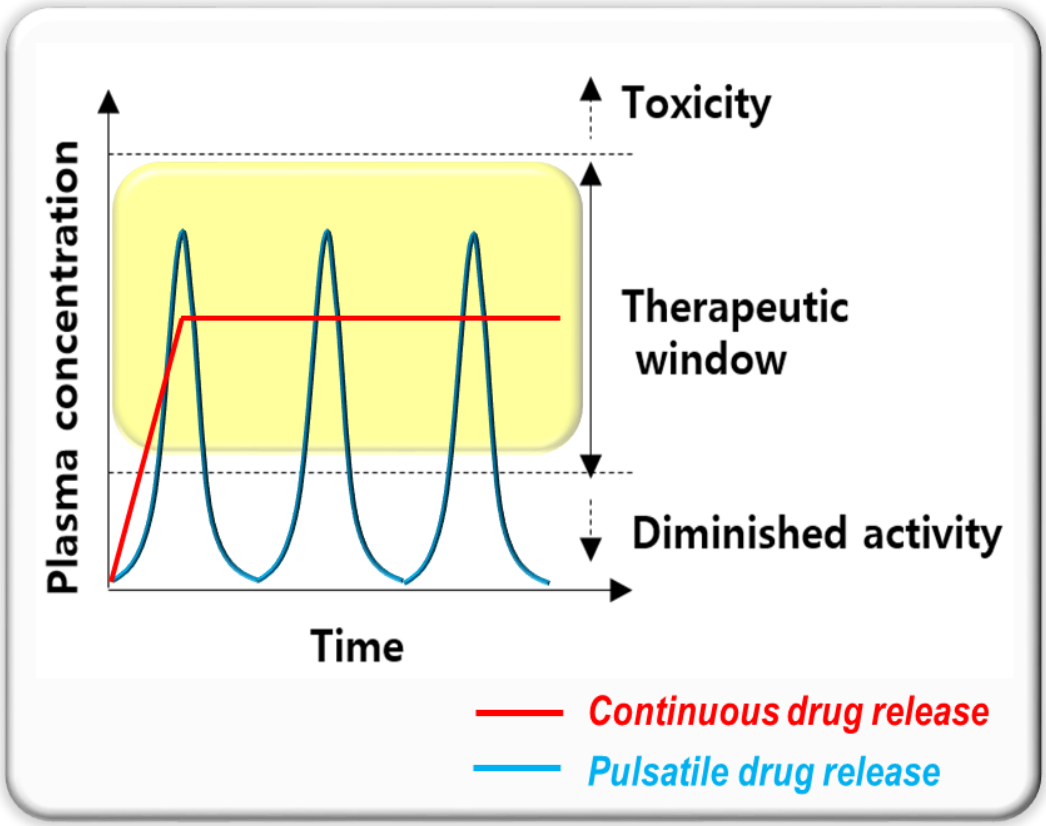

Figure 1.1 Drug efficacy and drug release profiles

1.2 Implantable Drug Delivery Device

Therefore, my solution to solve this is an implantable drug delivery device that can replace frequent injections and oral administrations with a single implantation, and can deliver the desired amounts of drugs at desired time points and periods.

In general, the implantable drug delivery device enabled with controlled drug delivery can be divided into 1) passive drug delivery device and 2) active drug delivery device.

In addition, marketability of implantable drug delivery device has been increasing as one of the next-generation promising fields. It accounts for 12% of the total drug delivery market in 2012 and is expected to reach $ 21.1 billion in 2018, with a CAGR of 8.8% (Fig. 1.2).

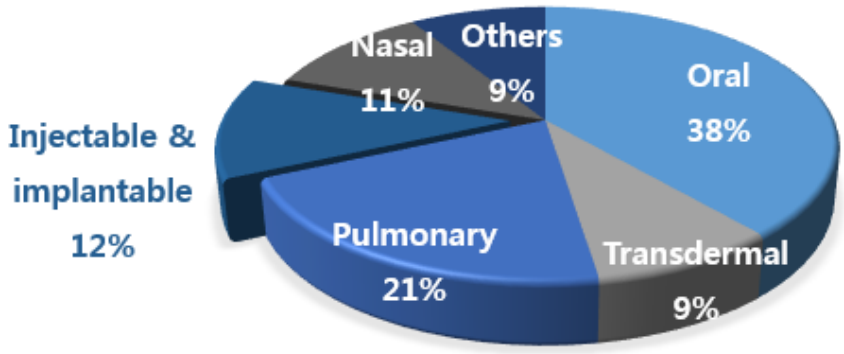

	2006	2010	2011	2018	CAGR (%)[a]
Market sales (unit : USD billion)	7.3	9	11.6	21.1	8.8

[a] Compound Annual Growth Rate

Figure 1.2 Drug delivery market (2)

1.3 Passive Drug Delivery Device

A passive drug delivery device can preprogram drug release rate and release the drug in a self-controlled manner after implantation. Most of them exhibit continuous drug release based on diffusion. Particularly, since there is no need for a battery and driving parts inside the device, the device can be miniaturized and is easy to implant. In general, it is classified matrix controlled system (3, 4), microscale constrained system (5, 6), nanoscale constrained system (7), and osmotic based system (8, 9).

1.3.1. Matrix Controlled System

The matrix controlled system is a system that regulates drug release rate by controlling the properties of the polymer matrix, such as composition, molecular weight and thickness.

The most representative device is the Gliadel wafer, which is currently being used as a brain tumor treatment in clinical practice. It consists of a blend of biodegradable polifeprosan 20 (i.e, poly [bix (p-carboxyphenoxy) propane and sebacic acid] in 20:80 molar ratio) and tumor treatment carmustine(BCNU). The actual size is 14.5 mm in diameter and 1 mm thick, and usually implies six implants in the surgical cavity after tumor is removed(4).

1.3.2 Microscale Constrained System

Microscale constrained system is a system that uses micro-conduit (i.e., 1 mm, less hydraulic diameter of one side of each side), as diffusion barrier. The most representative device is an Implanon, which is currently being used for birth control in clinical practice. Rod shaped device has a diameter of 2 mm and a length of 40 mm. The device consists of an ethylene vinyl acetate (EVA) membrane, which can control the drug release rate, and etonogestrel. The drug release rate was 60-67 μg day^{-1} in week 5-6, 35-45 μg day^{-1} at the end of the first year, 30-40 μg day^{-1} at the end of the second year and 25-30 μg day^{-1} at the end of the third year. In particular, implantation can be easily accomplished in minutes, with no local anesthesia on the forearm (6).

1.3.3 Nanoscale Constrained System

Nanoscale constrained system is a system that can exhibit continuous drug release by adjusting the dimensions of the nanochannel to match the hydrodynamic diameter of drug.

Nanoprecison medical's Nanoplatform is available for long-term continuous release of GLP-1 for Type 2 diabetes treatment. It consists of a tube-shaped titanium outer case to serve as a drug reservoir and a rate controlling membrane where multi-

nanochannels are formed by titania etching (7).

1.3.4 Osmotic Based System

Osmotic based system is a system that releases the drug by using expansion of osmotic agent as a driving force. Typically, the device consists of a drug reservoir, a semipermeable membrane, a piston, and an osmotic agent. The principle of drug release is as follows; the water enters the semipermeable membrane due to the osmotic gradient between the moisture in the surrounding interstitial fluid and the osmotic agent, and the drug is released by pushing the drug in the drug reservoir to the piston due to the volume expansion of the osmotic agent.

First, the osmotic implant developed by Duros is 45 mm in length and 4 mm in diameter, and is filled with GnRH analogue leuprolide for the treatment of prostate cancer(8).

In addition, Intarcia has been developing a matchstick-sized osmotic device, ITCA 650, with a diameter of 44 mm and a diameter of 4 mm for Type 2 diabetes, obesity and HIV treatment (9).

1.4 Active Drug Delivery Device

On the other hand, the active drug delivery device can adjust the drug release rate after the device implantation.

In particular, it is suitable for diseases requiring precise and complex

drug regimens, as the drug release can be adjusted on-demand to the situation.

In general, it is classified to peristaltic actuated system (10, 11), electrochemical dissolution system (12), electrothermal ablation system (13, 14), piezoelectric actuated system (15), electrolysis based system (16, 17).

1.4.1 Peristaltic Actuated System

Peristaltic actuated system is a system uses positive displacement which is inspired by the intestinal motility of animals. Thus, the drug is released when the roller pump runs and squeezes the tube filled with the drug.

First, Medtronics's synchromed Ⅱ for intrathecal drug delivery in clinical practice is a prime example. It consists of a drug reservoir, a peristaltic roller, a propellant, a refill septum and an outer case of titanium. The device has a diameter of 87.5 mm, a thickness of 19.5 mm and a maximum flow rate of 24 ml day^{-1}. In addition, the volume of the drug reservoir is 20 ml, and the refill septum is composed, and the drug can be recharged(11).

The Iprecio pump, which is specially designed for preclinical studies, also consists of a rotary finger pump (peristaltic), a drug reservoir and a refill septum. The device has a length of 24.8 mm, a width of 15 mm, and a height of 7.2 mm and the drug release rate can be adjusted to 0-10 μl h^{-1} infusion flow rate. In addition, the volume of

the drug reservoir composed of Medical grade SEBS (Styrene-Ethylene-Butylene-Styrene) is 900 μl, and the refill septum is constituted thus, drug recharge is possible (10).

1.4.2 Electrochemical Dissolution System

Electrochemical dissolution system is a system that uses electric potential to make membrane soluble, and then body fluids dissolve the membrane and drug.

The most representative device is the electrochemical dissolution microchip introduced by MIT Robert Langer group in 1999 Nature.

The device is sealed with a gold cap in a multi-drug reservoir enclosed with the drug. And this gold cap is connected with electric circuit, respectively. Applying electric potential will change the gold cap to soluble gold salt. Then, soluble gold cap and drug are dissolved from the body fluids. After that, it is released in pulsatile manner that most devices cannot implement (18).

1.4.3 Electrothermal Actuation System

Electrothermal ablation system utilizes electric potential to rupture the membrane that is sealing the drug within the microsecond and deliver the drug at the desired time. This study was jointly developed by MIT and Microchip Inc. and firstly introduced in Nature

biotechnology in 2006. After that the miniaturized device was introduced to science translational medicine in 2012 by demonstrating its efficacy in osteoporosis patients. Unlike previous electrochemical dissolution devices, the gold cap can be ablated and ruptured within microseconds to deliver the drug faster. The device size is 54 mm in length, 31 mm in width, 11 mm in height and has a total of 200 individually addressable reservoirs(13, 14).

1.4.4 Piezoelectric Actuated System

Piezoelectric actuated system is a system that uses the driving force which is increased or shrunk when a voltage is applied to a crystal where atoms are regularly arranged like ceramics to control the drug release rate. A typical device is a piezo-actuated MIP pump from Debiotech. The device consists of a pair of check valves and a reciprocating pumping membrane having a piezoelectric ceramic disk and titanium fluid connectors that allow the liquid drug to flow properly from the drug reservoir to the target location, and the drug release rate is typically 1 ml min^{-1}(15).

1.4.5 Electrolysis based System

Electrolysis based system is a system that adjusts the drug release rate by using the expansion force of gas generated by water electrolysis. Representative device is electrochemical pumping

device, which was introduced at IEEE from Kim et al., in 1999. In addition, another electrolysis based device was introduced at Biomedical Microdevice from Ellis Meng Group in 2012. It consists of a reservoir, which acts as an external case drug reservoir, a Nafion coated PT electrode, and a parylene bellow with an electrolysis reaction. First, when an electric current is applied to the electrode, oxygen and hydrogen gas are generated by the electrolysis of the electrolyte inside the parylene bellow, thereby expanding the bellow. Thereafter, the drug in the drug reservoir is released by the expanded volume (16, 17).

1.5 Current Drawback & Research Aims

Implantable drug delivery device capable of controlled drug release has been extensively studied and developed in clinical and preclinical applications. However, conventional devices still have many drawbacks.

First, the passive drug delivery devices introduced in section 1.3 have advantages that can be pre-programmed prior to implantation and then released in a self-controlled fashion.

However, in the case of matrix-controlled systems, there is an issue with initial burst effect in which the drug release rapidly occurs in the early stage, thereby causing uncontrolled and unpredictable release profile. Thus, systems such as micro/nano scale constrained system and osmotic based system capable of controlled drug release

without an initial burst effect have been recently developed. However, they still have some limitations. For example, nanoscale constrained system and osmotic based system also require complex fabrication procedures when fabricating nanochannel-based membrane and constructing osmotic-based materials. To overcome these limitations, I developed a microchannel-based implantable microchip capable of long-term controlled drug release without initial burst effect. This work will be presented in chapter 2.

In addition, the active drug delivery devices introduced in section 1.4 have advantages that can control the drug release rate after implantation from outside the body. However, since most of them require a battery inside the device, the total volume of the device becomes larger and the re-surgery is inevitable when the battery life is over.

To resolve this, therefore, I also designed an implantable battery-less device enabled with patient-driven, on-demand insulin release to be actuated by an externally applied magnetic field. This work will be presented in Chapter 3.

Chapter 2

Multi-channel Based Implantable Micro-chip for Controlled Drug Delivery

2.1 Introduction

Diclofenac sodium (DS), a non-steroidal anti-inflammatory drug (NSAID), is widely used for the long-term treatment of inflammatory disorders, especially musculoskeletal diseases such as rheumatoid arthritis, osteoarthritis, and ankylosing spondylitis (19). However, due to its short biological half-life, long-term continuous infusion or multiple dosing schedules are often required (20). Therefore, a device enabled for continuous drug release is considered

advantageous for DS delivery; a therapeutic drug concentration can be maintained in the blood stream for a long period of time with less frequent administrations. Many systems have been suggested for this purpose (21-24). Those conventional systems, primarily employing biocompatible polymers as encapsulants, could release drug by diffusion or polymer degradation. However, a high initial burst of drug release remains a challenge (25), creating difficulty in precisely controlled drug release. This could be problematic to achieving the realization of zero-order release of DS, which is considered an ideal regimen for most NSAIDs (26).

To overcome these limitations and precisely control drug delivery, microfabricated devices have been introduced (27, 28). Aided by microfabrication technology, a precisely controlled geometry can be made for accurately tailored drug release. Despite those advantages, the devices often required multiple complex fabrication procedures, such as photolithography, deposition, and etching (29). In addition, to actively deliver the drug, the devices often need an additional unit, such as an electric power supply, which inevitably makes the device large, and possibly not advantageous for implantation. However, these complex procedures may not be needed to achieve a desirable regimen for DS, i.e., zero-order drug delivery.

In this work, I suggest a drug-delivery micro-chip (DMC) with a simple structure for controlled delivery of DS. The DMC described herein was made on a poly (methylmethacrylate) (PMMA) plate, where the only two compartments, a micro-channel and a micro-well,

were prepared by etching with a CO_2 laser. The micro-well was located inside a DMC and filled with a fine powder of DS, which served as the drug depot. One end of the micro-channel was located inside the MC and connected to a micro-well, and the other end was open to the outer boundary of the MC, serving as diffusion barrier. The channel was filled with a water-soluble, biocompatible polymer, polyethylene glycol (PEG). Thus, the water could first infiltrate via the channel to reach a micro-well containing the drug, and then, the solubilized drug in the well could diffuse out via the same channel. In this way, DS could be released in a sustained manner with a minimized initial burst. Moreover, the release pattern could be precisely modulated by the dimensions of the microfabricated channels (30): the drug release rate could be determined by the cross-sectional area to length ratio of the channel (i.e., A/L, where A and L are the cross-sectional area and length, respectively). Therefore, for a long-term, continuous drug release, one may need a channel with a small A/L. However, with only this one type of channel, the onset of drug release would also be delayed due to hindered water infiltration via the channel towards the well.

To achieve both almost immediate onset and prolonged drug release, I propose a more integrated design of the DMC equipped with multiple types of micro-channels. For example, a channel with a large A/L starts drug release almost immediately, but the period of drug release is not long. When the drug release is about to be completed from this channel, the channel with a smaller A/L can initiate drug release, and

the release can be more sustained. This process can be continued with a channel with a next smaller A/L. In this sense, with a proper combination of these different channels, I also attempted to realize zero-order release of DS.

For this, I first evaluated eight different types of micro-channels: their cross-sectional areas and lengths were varied from 0.021 mm^2 to 0.087 mm^2 and from 2 mm to 8 mm, respectively. Thus, eight different types of MCs were prepared in this work, each embedded with a single pair of a micro-well and a specific type of micro-channel. Based on their *in vitro* drug release profiles, I then predicted the drug release from various combinations of the micro-channels, among which the combination showing the best fit for zero-order release for the most prolonged period was found. An integrated DMC (I_DMC) was prepared with the resulting combination, and its predicted release profile was confirmed in an *in vitro* drug release test environment for 70 days. The I_DMC was also implanted subcutaneously in Sprague-Dawley (SD) rats to perform an in vivo pharmacokinetic test for 30 days. To examine the biocompatibility, the tissue around the implanted I_DMC was biopsied 30 days after implantation and analyzed histologically.

2.2 Materials and Methods

2.2.1 Materials

Polyethylene glycol (PEG; average MW = 6 kDa) and PMMA plates (thickness = 1.8 mm) were purchased from Acros Organics (Geel, Belgium) and EunSung Polytechnology (Seoul, Korea), respectively. Ideal 9144 Masking Tape was obtained from American Biltrite (Lowell, Massachusetts, USA). Diclofenac sodium (DS; 99.0% purity), naproxen sodium, acetonitrile, phosphoric acid, and triethylamine (HPLC grade) were purchased from Sigma (St. Louis, MO, USA). Phosphate-buffered saline (PBS; pH 7.4), ethylendiaminetetraacetic acid (EDTA) tubes, and i.v. catheters were obtained from the Seoul National University Hospital Biomedical Research Institute. Zoletil® 50 and Rompun® were obtained from Bayer (Seoul, Korea). Betadine and paraformaldehyde (4%) were purchased from Hyundai Pharm (Seoul, Korea) and Dreamcell (Seoul, Korea), respectively. For hematoxylin and eosin staining (H&E), xylene, ethanol and hydrochloric acid (35%-37%) were purchased from Duksan Pure Chemicals (Ansan, Korea).

2.2.2 Fabrication of DMCs

A DMC, containing a single pair of micro-channels and micro-wells, was prepared on a PMMA plate of 1.8 mm in thickness to examine the drug-release property of each of the micro-channels (Fig. 2.1). In this work, both cross-sectional area and length of the micro-channels were varied to give eight different types of DMCs: the cross-sectional areas and lengths of the channel were varied to

0.021 mm^2 and 2 mm (i.e., DMC of channel type S2 (DMC_S2)), 0.021 mm^2 and 4 mm (i.e., DMC of channel type S4 (DMC_S4)), 0.021 mm^2 and 8 mm (i.e., DMC of channel type S8 (DMC_S8)), 0.056 mm^2 and 2 mm (i.e., DMC of channel type M2 (DMC_M2)), 0.056 mm^2 and 4 mm (i.e., DMC of channel type M4 (DMC_M4)), 0.056 mm^2 and 8 mm (i.e., DMC of channel type M8 (DMC_M8)), 0.087 mm^2 and 4 mm (i.e., DMC of channel type L4 (DMC_L4)), and 0.087 mm^2 and 8 mm (i.e., DMC of channel type L8 (DMC_L8)). To prepare a DMC, the PMMA plate was first cut into a circular shape, 15 mm in diameter, and the micro-channel and micro-well were prepared using a CO_2 laser (FC-200RA LASER Machinery, Bucheon, South Korea) (Fig. 2.1(a)). The channel was etched within the thickness of the plate, while a through-and-through hole was made for the micro-well. The resulting circular plate was then thoroughly cleaned with a 10% ethanol solution. To serve as a conduit for water infiltration, the channel was densely filled with a water-soluble polymer, PEG, in a molten form at 80℃, which was then solidified at room temperature for 5 h (Fig. 2.1(b)). After that, the top side of the DMC, where the channel was formed, was sealed with biocompatible Ideal 9144 silicone tape (Fig. 2.1(c))(3, 31). Through the bottom side of the DMC, the micro-well was then densely filled with a fine DS powder using the doctor blade method (Fig. 2.1(d)) and was sealed with the same Ideal 9144 silicone tape (Fig. 2.1(e)). To fabricate DMCs enabled for zero-order release, the same procedure as described above was employed, and the selected combination of

multiple pairs of micro-channels and micro-wells was created in a single circular plate of 13 mm in diameter.

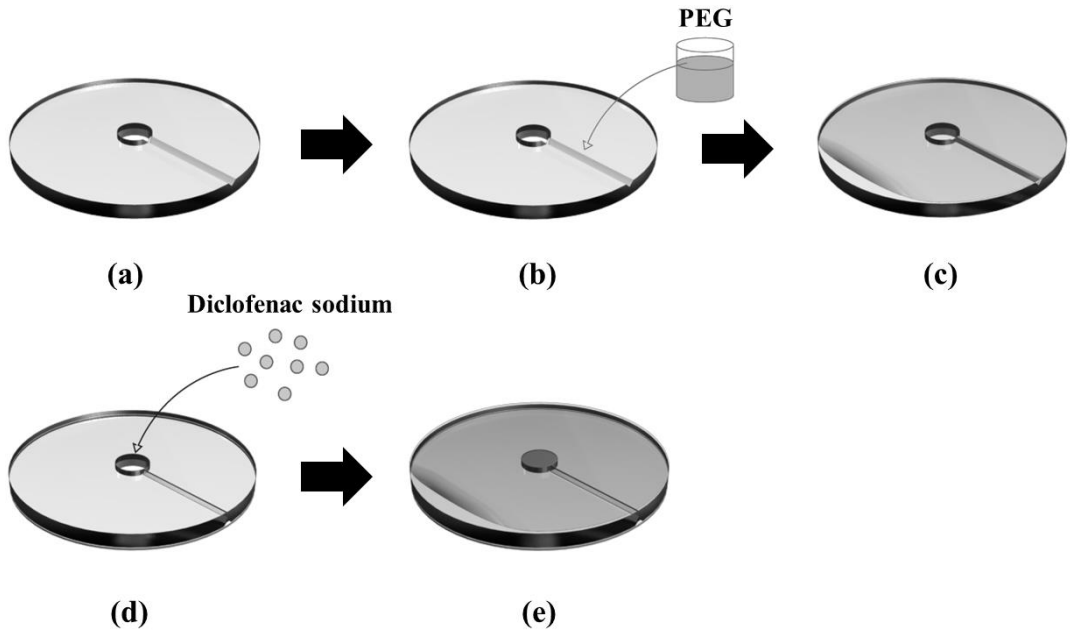

Fig. 2.1 Schematic procedure of DMC fabrication

Through the top side of a circular PMMA plate, (a) a micro-channel was etched within the thickness of the plate and a through-and-through hole was made for a micro-well (drug reservoir). (b) The micro-channel was filled with PEG. (c) The top side of the DMC was sealed with a biocompatible tape. Through the bottom side of the plate, (d) the micro-well was densely filled with a fine powder of DS with the doctor blade method. (e) The bottom side of the DMC was sealed with a biocompatible tape.

2.2.3 Characterization of Micro-channels and Micro-wells

The morphology of the micro-channels was examined by scanning electron microscopy (SEM; 7501F, Jeol, Japan). For this, the micro-channels, either empty or filled with PEG from the DMC_S8, DMC_M8 and DMC_L8 were each placed on a sample mount and sputter-coated with platinum for 10 min (208HR, Cressington Scientific, UK) before imaging. To assess the reproducibility of drug loading, a DMC in which a micro-well was filled with DS powder but not yet sealed was immersed in 100 ml of PBS to fully dissolve the drug. The aliquot was then measured spectrophotometrically at 275 nm using a UV-Vis spectrophotometer (UV-1800, SHIMADZU, Japan). The experiments were performed with at least three distinct DMCs.

2.2.4 *In Vitro* Drug Release Study

The *in vitro* drug release experiment was performed in pH 7.4 PBS at 37° C with continuous stirring at 125 rpm in a shaking incubator (SI-600R, Jeio Tech, Korea). The DMCs of different types were each immersed in the release media, and aliquots were collected at scheduled intervals for 54 days. Then, the collected samples were measured spectrophotometrically at 275 nm (UV-1800, SHIMADZU, Japan) to determine the amount of drug that was released. All experiments were performed in triplicate for each type of DMC.

2.2.5 Selection of Micro-channel Combination for Zero-order Release

I sought to find the best combination of multiple micro-channels for integrated design of a DMC enabled with zero-order release for a prolonged period of time, as well as an almost immediate onset of drug release. For this, I first generated all possible combinations of two or three different micro-channels, giving a total of 84 combinations (Table 2.1), where their drug release profiles were predicted mathematically by summing the experimental data obtained from the eight different individual DMCs prepared in this work. I then selected the combinations with an almost immediate onset of drug release (i.e., onset on day 0.5), giving a total of 28 different combinations (Table 2.2). From each of the selected combinations, I assessed the longest possible period of zero-order drug release, satisfying $R^2 > 0.993$. From those, I finally chose the combination that showed the best fit for zero-order release (i.e., R^2 closest to 1) for the most prolonged period of time, which was employed to prepare the I_DMC used in this work.

Table 2.1. Onset times of drug release from all possible combinations of the two or three different micro-channels prepared in this work. The combinations, showing the drug release onset on day 0.5, were first selected for further consideration.

	Micro-channel combination	Drug release onset time (day)	Selection mark
1	S2, S4	2	
2	S2, S8	2	
3	**S2, M2**	**0.5**	**V**
4	S2, M4	1	
5	S2, M8	2	
6	S2, L4	1	
7	S2, L8	2	
8	S4, S8	5	
9	**S4, M2**	**0.5**	**V**
10	S4, M4	1	
11	S4, M8	4	
12	S4, L4	1	
13	S4, L8	2	
14	**S8, M2**	**0.5**	**V**
15	S8, M4	1	
16	S8, M8	4	
17	S8, L4	1	
18	S8, L8	2	
19	**M2, M4**	**0.5**	**V**
20	**M2, M8**	**0.5**	**V**
21	**M2, L4**	**0.5**	**V**
22	**M2, L8**	**0.5**	**V**

(Continued)

	Micro-channel combination	Drug release onset time (day)	Selection mark
23	M4, M8	1	
24	M4, L4	1	
25	M4, L8	1	
26	M8, L4	1	
27	M8, L8	2	
28	L4, L8	1	
29	S2, S4, S8	2	
30	**S2, S4, M2**	**0.5**	**V**
31	S2, S4, M4	1	
32	S2, S4, S8	2	
33	S2, S4, L4	1	
34	S2, S4, L8	2	
35	**S2, S8, M2**	**0.5**	**V**
36	S2, S8, M4	1	
37	S2, S8, M8	2	
38	S2, S8, L4	1	
39	S2, S8, L8	2	
40	**S2, M2, M4**	**0.5**	**V**
41	**S2, M2, M8**	**0.5**	**V**
42	**S2, M2, L4**	**0.5**	**V**
43	**S2, M2, L8**	**0.5**	**V**
44	S2, M4, M8	1	
45	S2, M4, L4	1	
46	S2, M4, L8	1	
47	S2, M8, L4	1	
48	S2, M8, L8	2	
49	S2, L4, L8	1	
50	**S4, S8, M2**	**0.5**	**V**
51	S4, S8, M4	1	
52	S4, S8, M8	4	
53	S4, S8, L4	1	
54	S4, S8, L8	2	
55	**S4, M2, M4**	**0.5**	**V**
56	**S4, M2, M8**	**0.5**	**V**
57	**S4, M2, L4**	**0.5**	**V**
58	**S4, M2**	**0.5**	**V**

	Micro-channel combination	Drug release onset time (day)	Selection mark
59	S4, M4, M8	1	
60	S4, M4, L4	1	
61	S4, M4, L8	1	
62	S4, M8, L4	1	
63	S4, M8, L8	2	
64	S4, L4, L8	1	
65	**S8, M2, M4**	**0.5**	**V**
66	**S8, M2, M8**	**0.5**	**V**
67	**S8, M2, L4**	**0.5**	**V**
68	**S8, M2, L8**	**0.5**	**V**
69	S8, M4, M8	1	
70	S8, M4, L4	1	
71	S8, M4, L8	1	
72	S8, M8, L4	1	
73	S8, M8, L8	2	
74	S8, L4, L8	1	
75	**M2, M4, M8**	**0.5**	**V**
76	**M2, M4, L4**	**0.5**	**V**
77	**M2, M4, L8**	**0.5**	**V**
78	**M2, M8, L4**	**0.5**	**V**
79	**M2, M8, L8**	**0.5**	**V**
80	**M2, L4, L8**	**0.5**	**V**
81	M4, M8, L4	1	
82	M4, M8, L8	1	
83	M4, L4, L8	1	
84	M8, L4, L8	1	

Table 2.2. Micro-channel combinations enabled with almost immediate drug release. For each of the combinations, the longest possible period of zero-order drug release, satisfying $R^2 > 0.993$, was found and their actual values of R^2 were listed.

Micro-channel combinations	R^2	Longest possible period of zero-order release (days)
S2, M2	0.9952	23
S4, M2	0.9931	16
S8, M2	0.9943	16
M2, M4	0.9935	23
M2, M8	0.9931	16
M2, L4	0.9942	23
M2, L8	0.9948	23
S2, S4, M2	0.9947	23
S2, S8, M2	0.9953	23
S2, M2, M4	0.9945	23
S2, M2, M8	0.9945	23
S2, M2, L4	0.9955	23
S2, M2, L8	0.9943	23
S4, S8, M2	0.9936	23
S4, M2, M4	0.9947	23
S4, M2, M8	0.9934	23
S4, M2, L4	0.9947	23
S4, M2, L8	0.9950	23
S8, M2, M4	0.9947	23
S8, M2, M8	0.9931	16
S8, M2, L4	0.9946	23
S8, M2, L8	0.9951	23
M2, M4, M8	0.9937	31
M2, M4, L4	0.9948	23
M2, M4, L8	0.9956	31
M2, M8, L4	0.9941	23
M2, M8, L8	0.9954	31
M2, L4, L8	**0.9960**	**31[a]**

[a] The combination, M2, L4 and L8, showed the best fit for zero-order release (i.e., R^2 closest to 1) for the most prolonged period of time and thus, was chosen to design the I_DMC

2.2.6 Implantation of I_DMC

To examine the in vivo drug-release property, the I_DMC was implanted in animals, and a pharmacokinetic study was performed for 30 days. For this *in vivo* evaluation, male Sprague-Dawley rats, aged 7 weeks and weighing 190-230 g, were used. All in vivo studies were approved by the Institutional Animal Care and Use Committee (IACUC No. 12-0039) at Seoul National University Hospital Biomedical Research Institute. The animals were housed under a 12/12 h light/dark cycle and were provided with food and water ad libitum.

For implantation, the animals were anesthetized using an intraperitoneal injection of a mixture (1 ml/kg) of Zoletil® 50 and Rompun® (1:1 v/v; Fig. 2.2(a)). Then, the hair on the dorsal area of each rat was shaved and disinfected with betadine. After that, a pocket was formed via the subpanniculus plane, followed by a 2-cm incision on the skin along the vertebra (Fig. 2.2(b)). Then, the I_DMC was inserted in the pocket (Fig. 2.2(c)), which was closed with a nylon 3-0 thread (Ethicon, USA), and the surgical site was disinfected again with betadine (Fig. 2.2(d)). For the control group, animals were also implanted with an I_DMC without DS loading.

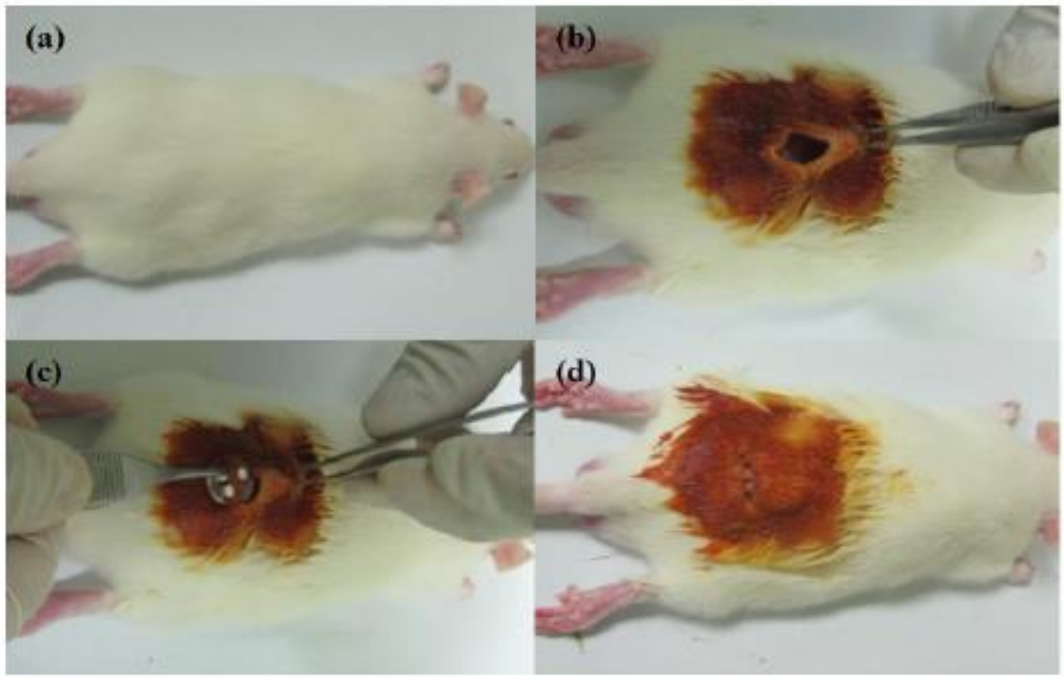

Figure 2.2 Surgical procedure for I_DMC implantation

2.2.7 *In Vivo* Pharmacokinetic Study

At scheduled time points after implantation of the I_DMC, a 0.5 ml blood sample was collected in an EDTA tube from the lateral tail vein. The collected sample was immediately centrifuged at 3000 x g for 15 min at 4 ° C to separate the plasma, which was then stored at −20 ° C. For measurement, 600 μl methanol and 200 μl of an internal standard (50 μg/ml naproxen sodium) were added to 200 μl of thawed plasma. The mixture was vortexed and centrifuged at 3000 x g for 15 min. Next, 900 μl of the mixture was evaporated using a Concentrator plus (Eppendorf, Hamburg, Germany) for 4 h at 30 ° C. The residue was mixed with 100 μl of a mobile phase, which consisted of a mixture of acetonitrile and 0.2
% triethylamine (TEA; 60:40, v/v) at pH 2.75 adjusted with 85% phosphoric acid. The resulting solution (50 μl) was loaded on an HPLC system consisting of an Agilent 1260 series HPLC pump, autosamplers, and a UV multi−wavelength detector (MWD; Agilent Technologies, CA, USA). In this work, the HPLC analysis was performed in isocratic mode on a reverse phase Hypersil BDS C_{18} column (5 μm, 250 mm x 4.6 mm i.d., Thermo Scientific, IL, USA). The flow rate and column temperature were set at 0.8 ml/min and 20℃, respectively, and the peaks were detected at a wavelength of 275 nm (32).

2.2.8 Histopathologic Evaluation

For histopathologic evaluation, the rats were sacrificed by CO_2 asphyxiation 30 days after implantation, and dorsal region tissues around the I_DMC were harvested. The resulting tissue sample was then fixed in 4% paraformaldehyde in a conical tube for 24 h and embedded with paraffin wax. The paraffinized samples were cut into 4−μm−thick slices, which were mounted on glass slides. The slides were then deparaffinized with xylene, rehydrated with ethanol, and washed in distilled water. Next, the slides were processed with hematoxylin solution for 10 min and rinsed with distilled water for 5 min. Then, the slides were treated with acid alcohol (0.3 % (v/v) hydrochloric acid in 70% (v/v) ethanol) and 0.1% (v/v) ammonium hydroxide three consecutive times, respectively. Afterwards, the slides were treated with eosin Y solution for 1 min and rinsed with distilled water. Lastly, the slides underwent a dehydration process, which consisted of sequential treatment with xylene for 20 min and ethanol (i.e., 50 %, 70 %, 80 %, 90 %, 95 % and 100 % ethyl alcohol) for 5 min. The samples were examined by a professional pathologist using a light microscope (X4, Carl Zeiss, Germany). I also assessed the fibrotic capsule formed around the I_DMC. In this work, the capsule was defined as possessing three distinct layers, i.e., an internal layer of synovial−like metaplasia, an intermediate layer of conjunctive tissue and an external layer of collagen formed on the surface of the I_DMC, where the thinnest region from each of the

sample images was chosen to measure the capsule thickness (33).

2.3 Results

2.3.1 Characterization of DMC

To allow controlled delivery of DS, I first prepared a DMC on which a single pair of a specific micro-channel and micro-well was embedded in a micro-chip of PMMA, as shown in Fig. 2.1. In this work, I varied the dimensions of the micro-channels, i.e., the cross-sectional areas and lengths of the micro-channels, to give eight different DMCs, as listed in Table 2.3 (i.e., DMC_S2, DMC_S4, DMC_S8, DMC_M2, DMC_M4 DMC_M8, DMC_L4 and DMC_L8). In this way, I attempted to evaluate the drug release property of each of the micro-channels according to its cross-sectional area to length ratio (i.e., A/L). The DMCs were 15 mm in diameter and 1.85 mm in thickness, giving a total volume of approximately 326 μl.

To fabricate a micro-channel, I etched the PMMA plate with a CO_2 laser (FC-200RA LASER Machinery, Korea). In this process, I varied the channel lengths from 2 mm to 4 mm to 8 mm by scanning the laser for the different lengths on the PMMA plate. To vary the cross-sectional area from 0.021 mm^2 to 0.056 mm^2 to 0.087 mm^2, I varied the applied laser energy, employing different laser scanning speeds of 15 mm/s, 10 mm/s, and 5 mm/s with equal laser power of 6 W, respectively.

Fig. 2.3 (A) shows the micro-channels of three different cross-

sectional areas before being filled with PEG. The width of the micro-channels did not change appreciably, possibly due to the pre-set size of the laser spot. However, the depth of the micro-channels increased as the laser scanning energy increased (i.e., as the laser scanning speed decreased). To serve as water-infiltration conduits towards the micro-well of the drug reservoir, the micro-channels were filled with a water-soluble polymer, PEG. As shown in Fig. 2.3(B), regardless of the dimensions, the micro-channels were seamlessly filled with PEG with the method employed in this work. The micro-well was also fabricated with a CO_2 laser, where a through-and-through hole, 3 mm in diameter, was made on a PMMA plate. The micro-well was densely filled with a fine powder of the drug, DS, in a reproducible manner, giving a loading amount of 8.32 $\pm$ 0.21 mg DS per well.

Table 2.3 Properties of the micro-channels.

Type of DMC	A/L (mm)	Drug release onset time (day)	Average release rate (%/day) [a]
DMC_S2	0.0105	3	1.43
DMC_S4	0.0052	5	0.73
DMC_S8	0.0026	8	0.32
DMC_M2	0.0280	0.5	3.68
DMC_M4	0.0140	2	2.06
DMC_M8	0.0070	4	0.80
DMC_L4	0.0217	1	2.71
DMC_L8	0.0108	3	1.44

[a] The average release rate of DS was obtained for the first 23 days after the drug release onset.

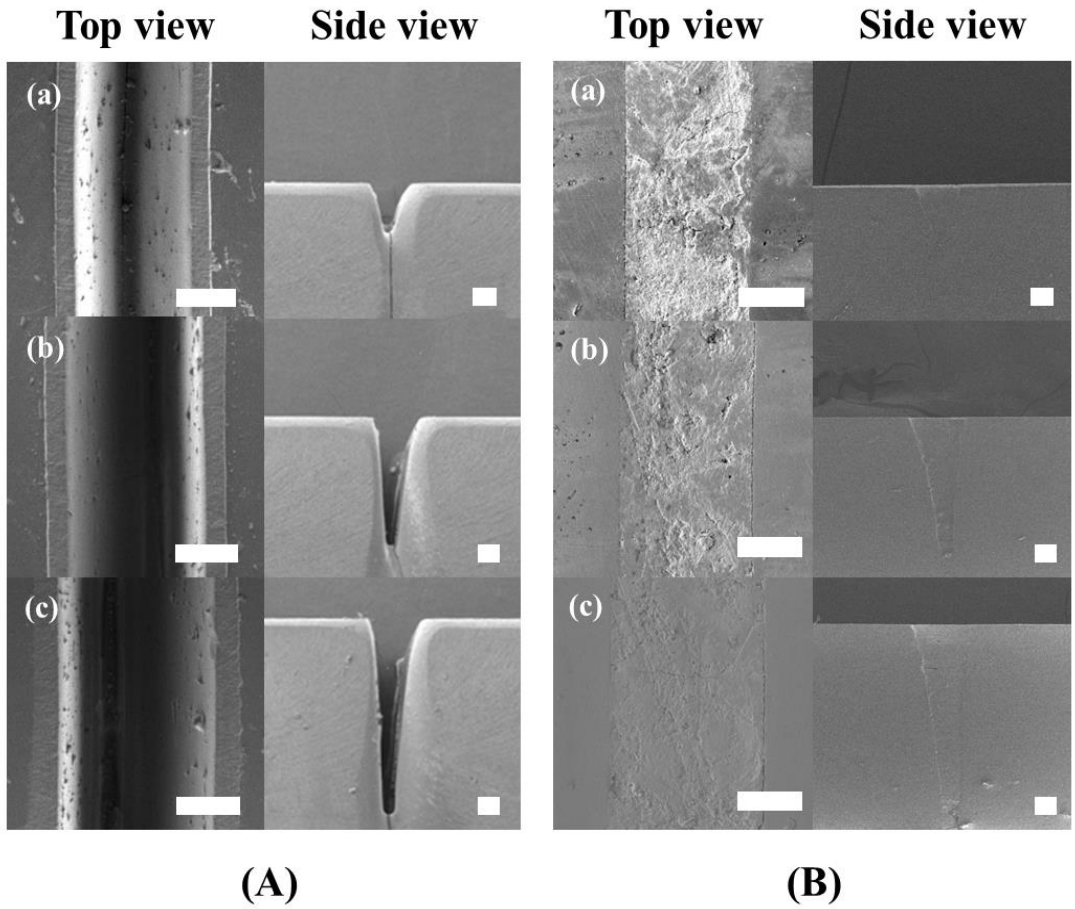

Figure 2.3 SEM micrographs of the micro-channels (A) before and (B) after filling with PEG. The cross-sectional areas of the micro-channels were (a) 0.021 mm^2, (b) 0.056 mm^2 and (c) 0.087 mm^2. The scale bars = 100 μm

2.3.2 *In Vitro* Drug Release Profiles of DMC

The *in vitro* drug release test was performed with the DMCs to first evaluate the drug release from each specific type of micro-channel prepared in this work. I attempted to control drug release by modulating the dimensions of the micro-channel, i.e., the A/L, according to the Fick's first law of diffusion and diffusion flux eqn. (Table 2.4) (30): drug release is slower and more sustained as the A/L becomes smaller. Here, I have listed the DMCs in the order of the A/L value: DMC_M2 > DMC_L4 > DMC_M4 > DMC_L8 ≈ DMC_S2 > DMC_M8 > DMC_S4 > DMC_S8. DMC_S2 and DMC_L8 possessed similar A/L values, which were 0.0105 mm and 0.0108 mm, respectively (Table 2.3). To initiate drug release from the DMC, the water first infiltrated via the PEG-filled micro-channel to reach the micro-well with the drug; then, the solubilized drug molecules diffused out via the same micro-channel. For this reason, the onset time of drug release was delayed as the A/L decreased, as shown in Table 2.3. Thus, DMC_S8, with the smallest A/L (0.0026 mm), showed the latest onset of drug release, on day 8; the earliest onset was observed on day 0.5 with DMC_M2, which had the largest A/L (0.0280 mm). Even when the respective cross-sectional areas and lengths of the micro-channels were different, the DMCs with a similar A/Ls showed similar onset times for drug release: both DMC_L8 and DMC_S2 exhibited the onset of drug release on day 3 due to their similar A/Ls of 0.0108 mm and 0.0105 mm, respectively.

Fig. 2.4 shows the drug release profiles of the eight different DMCs evaluated in this work. For all DMCs, drug was released in an almost zero-order pattern for the first 23 days (i.e., until the time at which less than 70% cumulative release was reached) after the release onset ($R^2 > 0.993$) (30). Depending on the dimensions of the micro-channels, the release rates could be modulated from 0.32 %/day to 3.68 %/day. Notably, for the first 23 days after the release onset, the drug release rate decreased proportionally to the decrease in A/L. For both DMC_S2 and DMC_L8, which possessed similar A/L values, the release rates were also similar: 1.43 %/day and 1.44 %/day, respectively (Table 2.3 and Fig. 2.5).

Table 2.4 Fick' s first law of diffusion and diffusion flux equation

Diffusion flux

$$J = \frac{dM}{dt * A}$$

J : mass flux (mol $m^{-2}s^{-1}$)

M : the mass (or number of atoms) (mol)

A : the unit cross-sectional are (m^2)

t : the observation time for the diffusion (s)

Fick's 1st law of diffusion

$$J = -D * \frac{dC}{dx}$$

J : mass flux (mol $m^{-2}s^{-1}$)

D : diffusion coefficient (m^2s^{-1})

C : concentration (mol m^{-3})

x : position (m)

$$\frac{dM}{dt * A} = -D * \frac{dC}{dx}$$

$$\frac{dM}{dt} = -D * A * \frac{dC}{dx}$$

$$\frac{dM}{dt} = -D * A * \frac{S}{L}$$

** dC = S (Solubility of the drug – concentration of the drug in dissolution medium)*

** dx = L (length of channel)*

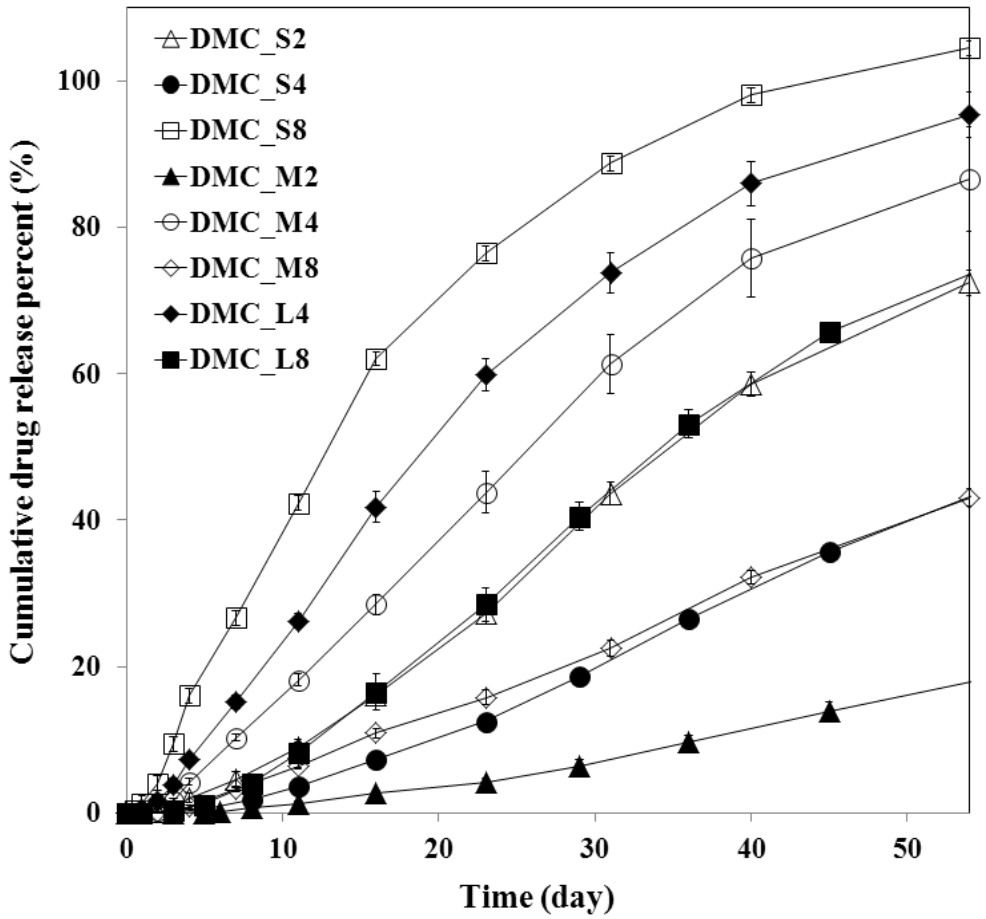

Figure 2.4 *In vitro* drug release profiles of the DMCs. The experiments were performed in pH 7.4 PBS at 37℃.

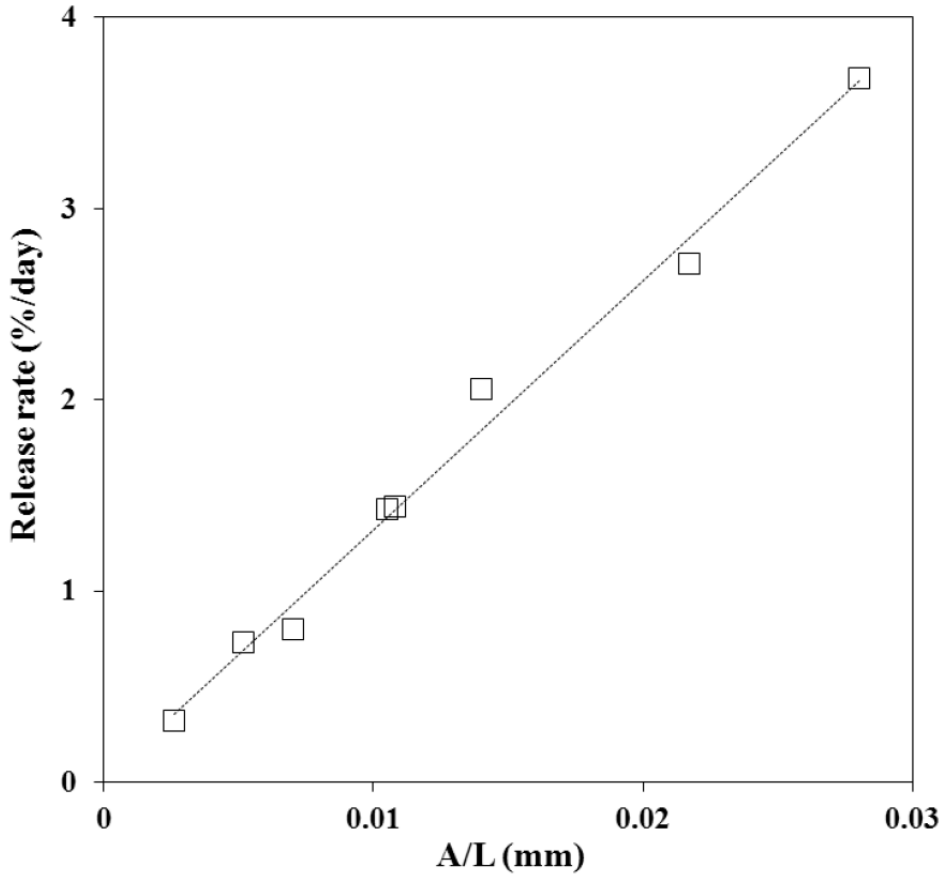

Figure 2.5 Release rates of the DMCs, depending on the cross-sectional area to length ratio (A/L) of the micro-channels.

2.3.3 I_DMC for Zero-order Drug Release

I proposed an integrated design for the DMC (i.e., the I_DMC), where micro-channels of various A/Ls were embedded to realize both immediate onset and prolonged drug release. Moreover, in this work, I sought to find a combination that showed zero-order release, which could be considered an advantageous regimen of DS (26). For this, I first generated all possible combinations of two or three of the individual micro-channels proposed herein (Table 2.1) and mathematically predicted their drug release profile based on the data shown in Fig. 2.4.

Table 2.2 shows the combinations selected by the criteria described in "Selection of Micro-channel Combination for Zero-order Release". Among them, the combination of the M2, L4 and L8 micro-channels showed the best fit for zero-order release (i.e., the R^2 value closest to 1) for the most prolonged period of time (31 days). Therefore, I used this combination to prepare the I_DMC in this work. Fig. 2.6 shows an optical image of the I_DMC used herein, where the three different types of micro-channels selected were each paired with three respective micro-wells. I prepared the micro-wells with the same size used in the DMC of a single type of micro-channel; hence, each contained approximately 8.3 mg DS per well and thus a total load of 24.9 mg drug in the three micro-wells of a single I_DMC. The dimensions of the I_DMC were 13 mm in diameter and 1.85 mm in thickness, giving a volume of 245 μl. As I performed the *in vitro*

drug release test, the I_DMC exhibited almost immediate drug release on day 0.5, which could be ascribed to the micro-channel with the largest A/L, M2. The drug release was sustained for more than 70 days with the other two micro-channels of smaller A/Ls. Notably, drug release for the first 31 days after onset showed an excellent fit for zero-order release kinetics ($R^2 > 0.998$), with a release rate of 563.2 μg/day (2.29 %/day), which was in good agreement with the predicted drug release profile (Figs 2.7 and 2.8).

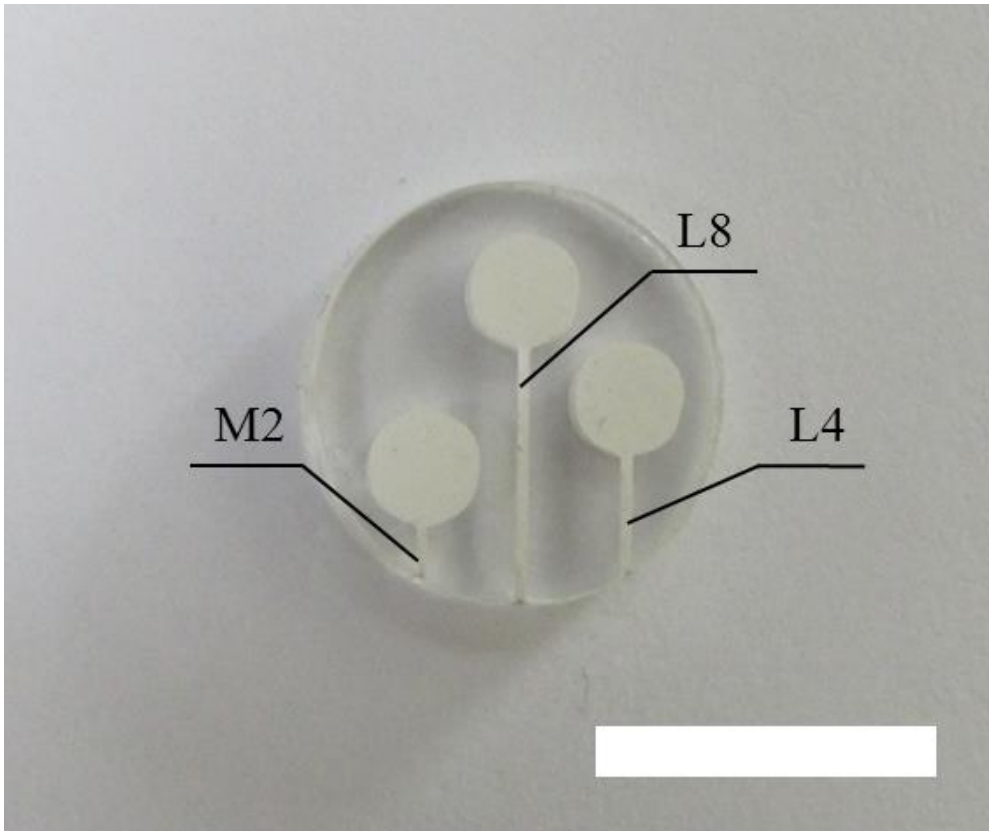

Figure 2.6 Optical images of the I_DMC. The scale bar = 10 mm.

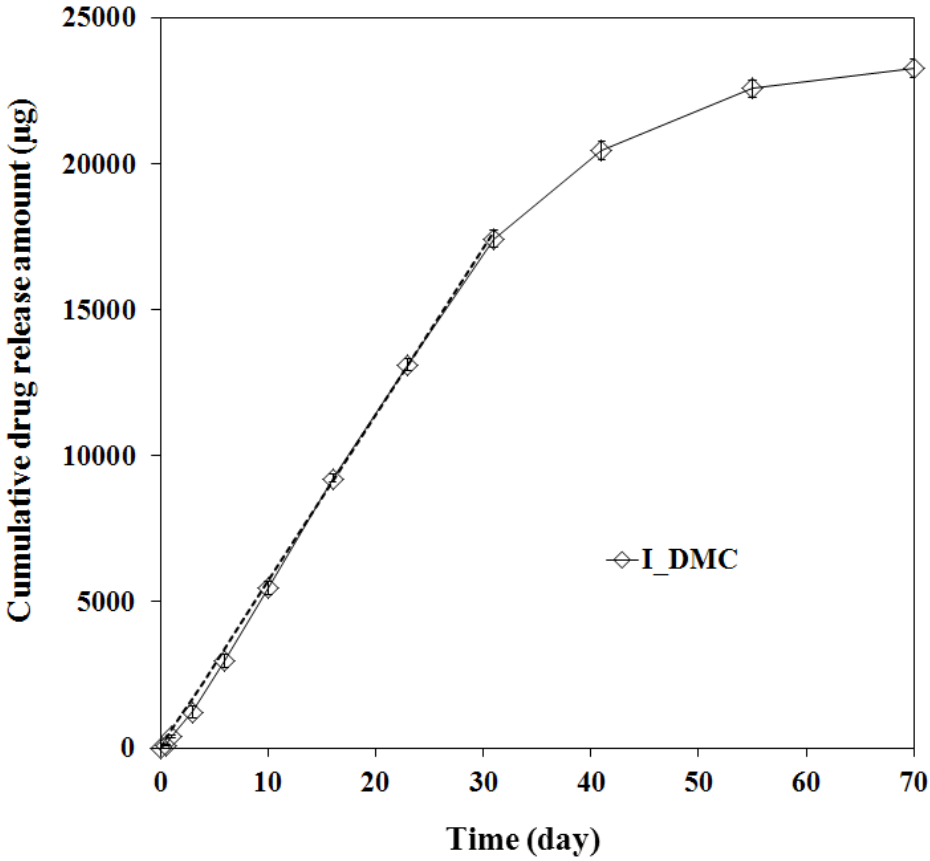

Figure 2.7 *In vitro* drug release profiles of the I_DMC. The experiments were performed in pH 7.4 PBS at 37℃. The dashed line shows a linear trend line fit to the release profile of the I_DMC for the first 31 days.

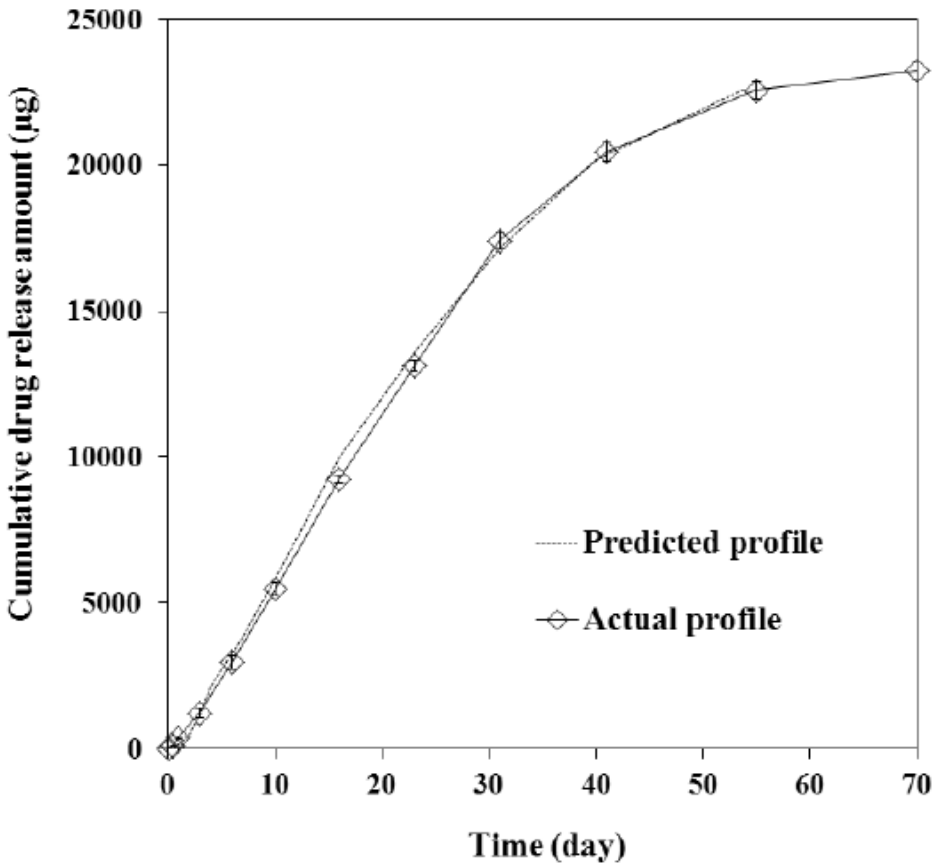

Figure 2.8 *In vitro* drug release profiles of I_DMC. The *in vitro* drug release experiment was performed with the I_DMC immersed in pH 7.4 PBS at 37° C to obtain the actual release profile (solid line), which was in good agreement with the predicted one (dashed line) obtained with the experimental data from the individual DMCs (i.e., DMC_M2, DMC_L4 and DMC_L8) in Fig. 2.4.

2.3.4 *In Vivo* Pharmacokinetics Study from the I_DMC

To assess the in vivo performance, I implanted the I_DMCs in living rats and carried out a pharmacokinetics study for 30 days. As shown in Fig. 2.9, the DS appeared to be continuously released and thus, systemically detected during the whole test period. The average drug concentrations in the blood serum were observed to be maintained within a relatively narrow range of 148 ng/ml – 225 ng/ml during the first 23 days after implantation, possibly due to the almost zero-order release from the I_DMC without an initial burst release. The decrease in drug concentration after 23 days could be due to the formation of a fibrous capsule around the I_DMC, hindering drug diffusion from the subcutaneous space into the bloodstream (34). For the control groups, which were implanted with the I_DMC without DS, no drug was detected during the whole test period of 30 days.

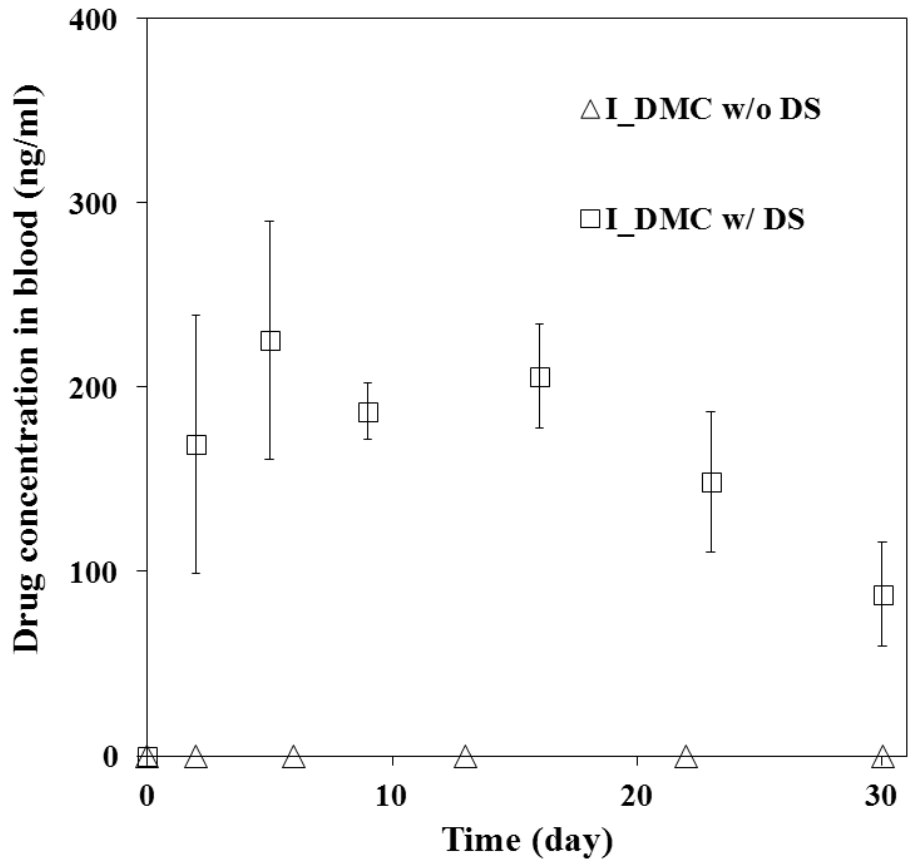

Figure 2.9 *In vivo* pharmacokinetics of the I_DMC loaded with DS (□). The I_DMC without DS was also implanted to give the control group (△).

2.3.5 Histopathology

At 30 days after implantation, which was the end point of the in vivo pharmacokinetics study, the tissues around the implanted I_DMCs, with and without DS, were harvested for histological evaluation. Regardless of the presence of DS, the overall inflammatory and foreign body reactions were minimal on H&E staining (Fig. 2.10) and were not significantly different between the different groups. The tissue surrounding the I_DMC showed the formation of a fibrous capsule composed of fibroblasts, collagen and capillaries, which had been observed in previous reports of various implanted devices (35). The thickness of the fibrous capsule was 903.9 ± 48.91 μm, which was similar to that of the controls (909.0 ± 48.27 μm).

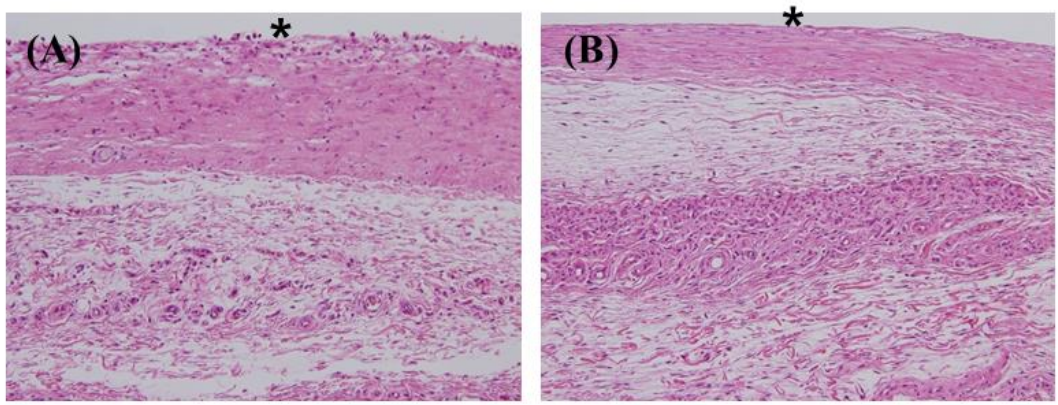

Figure 2.10 Histological images of the tissues around the implanted I_DMC. The tissue samples around the I_DMC (A) without DS and (B) with DS were stained on H&E. The mark indicates the location of the I_DMC and tissue interface.

2.4 Discussion

Long-term, zero-order delivery of DS is considered an ideal regimen for the treatment of chronic inflammatory disorders (36). In this sense, microfabricated devices have attracted interest in the field of zero-order drug delivery: the geometry of the drug diffusion barrier and reservoir can be precisely tailored; thus, highly controlled drug delivery would be possible. Many conventional polymeric devices could deliver DS in a sustained manner; however, a large initial burst of drug release was often problematic, especially with hydrophilic drugs, such as DS (37).

Previously, a micro-chip embedded with micro-channels was reported to realize almost zero-order release for several days (38). Many channels of the same dimensions were connected in parallel to a single drug reservoir, where, therefore, the drug release rate could be modulated by varying the number of those channels. However, due to the hydrophobic material of which they were composed (poly(lactic-co-glycolic acid)), the channels were difficult to wet, causing some of the channels to be frequently occluded in an irregular manner and leading to a high chance of drug release inaccuracy. Nano-scaled channels were also employed as diffusion barriers to achieve zero-order drug release (39, 40). The drug release was modulated depending on the hydrodynamic diameter of the drug molecules; however, this approach could only be used for macromolecular drugs and is therefore not suitable for small-

molecule drugs, such as DS. A tubular device was also prepared with a perforated micro-hole as a drug diffusion barrier for zero-order release (41). This device could accurately modulate drug release by controlling the hole size (i.e., the exposed hole area). With a thin tube wall, water could rapidly infiltrate via the hole into the tube filled with the drug, thereby initiating the almost immediate onset of drug release. On the other hand, the area of the hole is the only parameter for controlling the drug release, thus potentially allowing less variation of the drug release rate.

The micro-chip proposed in this work also possessed micro-channels as a diffusion barrier. Therefore, the drug release from each channel showed a zero-order release pattern, as in the previous works mentioned above (38, 41). On the other hand, the micro-chip described herein was designed to modulate drug release by varying two distinct parameters of the micro-channel dimensions, i.e., the cross-sectional area and the length of the micro-channels, thereby permitting more controllability of the drug release (Fig. 2.4). For long-term release, I used channels with a small A/L, which delayed the onset of drug release; however, this could be resolved by integrating a variety of sizes of micro-channels into a single micro-chip (i.e., the I_DMC), including one enabled for rapid drug onset. From a theoretical perspective, therefore, I could envision more prolonged zero-order release by adding and integrating more micro-channels with smaller A/Ls into a single micro-chip. The micro-channels herein were filled with a hydrophilic polymer, PEG, leading

to expedited wetting of the channels, thus providing a reproducible drug release profile.

The *in vitro* drug release study revealed that the I_DMC in this work could release drug in a zero-order pattern for up to 31 days (Fig. 2.7). Accordingly, therefore, the drug concentration in the blood was maintained within a relatively narrow range for the first 23 days after in vivo implantation of the I_DMC. Notably, the drug concentration in the blood was not very high early after implantation (day 2), which could be ascribed to the absence of initial burst release from the I_DMC. The decrease in drug concentration after day 23 could be due to the formation of a fibrous capsule around the implanted I_DMC (Fig. 2.8). One of the possible scenarios for reproducible systemic drug exposure, therefore, would be to delay the onset of drug release until complete formation of the fibrous capsule, as previously suggested (14): reproducible drug diffusion via the completed capsule into the bloodstream. This is expected to be achievable with the strategy proposed in this work: one can easily modulate the geometry and combination of the micro-channels to achieve the required delay of drug release onset.

Although suggested as a proof-of-principle device, the micro-chips in this work were fabricated with biocompatible materials, considering their implantation. The body of the micro-chip was made of PMMA, which is a material that has already been approved for clinical use; e.g., it is a component of bone cement (42, 43). PEG, which was used to fill the micro-channels, is also known to be highly

biocompatible (44). The top and bottom sides of the micro-chip were sealed with Ideal 9144 silicone tape, which has already been proven safe for clinical use (31). For those reasons, the micro-chips described herein exhibited no significantly adverse tissue reactions after implantation (Fig. 2.10).

2.5 Conclusion

For controlled delivery of DS, I propose an implantable micro-chip equipped with pairs of micro-channels and micro-wells. The micro-channels are filled with a water-soluble polymer, PEG, and can work as a drug diffusion barrier where the release rate can be tailored according to the channel dimensions, i.e., cross-sectional area and length. In this work, as I increased the cross-sectional area-to-length ratio (A/L) from 0.0026 mm to 0.0280 mm, the average drug release rate decreased proportionally from 3.68%/day to 0.32%/day. Additionally, with the increase in A/L, the onset time of drug release was delayed to day 8. Therefore, for the almost immediate onset and continuous release of DS, I suggest an integrated design for the micro-chip, i.e., a single micro-chip embedded with multiple pairs of micro-channels and micro-wells. Moreover, when properly selected, a combination of micro-channels of different dimensions can achieve zero-order release. In this work, a micro-chip with micro-channels of three distinct A/Ls (0.0280 mm, 0.0217 mm and 0.0108 mm) exhibited almost zero-order drug release *in vitro* for 31 days (R^2 >

0.996). Due to the micro-channel with a large A/L, 0.028 mm, the release onset was almost immediate on day 0.5. For this reason, the *in vivo* pharmacokinetics study revealed that the drug concentration in the blood could be maintained between 148 ng/ml and 225 ng/ml for the first 23 days after micro-chip implantation. Therefore, I conclude that a micro-chip employing multiple pairs of micro-wells and micro-channels of different dimensions as drug reservoirs and diffusion barriers, respectively, can be a novel implantable system for zero-order drug delivery.

Chapter 3

Implantable Battery-less Device for On-demand, Controlled Delivery of Insulin

3.1 Introduction

All types of diabetes mellitus are characterized by insufficient insulin secretion(45). Type 1 diabetes is characterized by absolute insulin deficiency and thus requires insulin injections covering both basal and prandial requirements(45). Type 2 diabetes is a consequence of both insulin resistance and insulin deficiency(45). However, insulin therapy is necessary for people with type 2 diabetes who have

severe hyperglycemia or hyperglycemia that is inadequately controlled by oral agents(46). Multiple daily injections (MDIs) and continuous subcutaneous insulin infusion (CSII) can provide plasma insulin profiles similar to normal physiology(47). However, MDIs are often painful and erroneous, and CSII requires a bulky, external device(48).

Therefore, a more patient-friendly system with controlled delivery of insulin has been actively sought. After one-time implantation (or injection), such a system must permit pulsatile insulin release to mimic physiological secretion following food intake(49). More importantly, this release pattern must be controlled in a patient-driven, on-demand manner from outside the body without invasive multiple skin punctures. Stimulus-responsive biomaterials previously used to deliver insulin(50-52) are subject to ruptures, leaks or deformations that lead to a lack of reproducibility over multiple release cycles. More sophisticated, implantable microdevices operated by the principles of peristaltic actuation(53, 54) electrochemical dissolution(12, 55), electrothermal ablation(13, 14), electrolysis(16, 17) or piezoelectric actuation(56) often require electrical power supplies (e.g., batteries) and electronic circuit components and are thus too large for implantation. Moreover, when the battery expires, device explantation is inevitable and requires additional major surgery, making this method unsuitable for long-time insulin delivery.

Therefore, in this work, I developed an implantable pump enabled

with patient-driven, on-demand insulin release and, most importantly, without electric power sources, thus allowing semi-permanent use after implantation. I designed the pump to be actuated by an externally applied magnetic field (i.e., a magnetically driven pump (MDP)). I prepared the pump by simple assembly of magnets and constituent units. The pump comprises a drug reservoir and an actuator to store and infuse insulin, respectively. The actuator is equipped with a plunger and barrel, each possessing a magnet. The plunger in the actuator moves to release an accurate amount of insulin stored in the reservoir only when a magnetic field is applied outside the body. To our knowledge, this study is the first to describe a simple-assembly, fully-implantable pump for batteryless, on-demand insulin infusion via a magnetic field. I assessed the *in vivo* performance of the MDP in diabetic rats by comparing the profiles of plasma insulin concentration and blood glucose levels with those treated with conventional subcutaneous insulin injection.

3.2 Materials and Methods

3.2.1 MDP Fabrication

The three-dimensional structure of the MDP was drawn using 3D modeling software (SolidWorks 2014, USA, Seoul National University Academic License). The composing units and their subunits were separately fabricated from polyurethane copolymer (Fullcure® 720 photopolymer) using a rapid prototyping PolyJet

technique on a 3D printer (Eden 350V, Objet Geometries, Israel). The resulting units and subunits were then assembled with the magnets (~ 0.1 T) and seamlessly attached with medical epoxy (Epo-Tek 301, Epoxy Technology, USA). A more detailed description of the MDP fabrication procedure is provided in Fig. 3.1.

3.2.2 Measurement of Insulin Concentration

The insulin concentration was measured using an Agilent 1260 series HPLC system (USA) equipped with a UV detector set at 210 nm and a reversed-phase poroshell 300SB-C18 column (5 μm, 75 mm × 2.1 mm i.d., Thermo Scientific, USA). The mobile phase was a mixture of acetonitrile with 0.08 % trifluoroacetic acid (ACN/TFA) and 0.1 % trifluoroacetic acid aqueous solution (TFA). The mobile phase was fed at a flow rate of 0.8 ml min^{-1} in gradient mode, in which the volume ratio of ACN/TFA:TFA was 25:75 for the first 1.5 min and 40:60 for the remaining 5 min.

3.2.3 *In Vivo* Experiments

The protocol for *in vivo* experiments was approved by the Institutional Animal Care and Use Committee (IACUC No. 14-0165) at Seoul National University Hospital Biomedical Research Institute. To induce a diabetic animal model, male Sprague-Dawley (SD) rats weighing 350-400 g were fasted for 8 h with free access to water

and then intraperitoneally injected with 60 mg kg^{-1} streptozotocin (STZ; Sigma-Aldrich) dissolved in 0.09 M citrate buffer solution (pH 4.0) to destroy the insulin-producing beta cells of the pancreas(57). Five days after STZ treatment, the rats were fasted for 8 h, and then approximately 5 μl of blood was sampled from the tail vein and analyzed with a glucose meter (Accu-Chek® Performa, Roche Diagnostics, Germany). Only rats with blood glucose levels greater than 300 mg dl^{-1} were employed as diabetic rats. The STZ-induced diabetic rats were divided into four groups: i) control group, ii) S.C. injection group, iii) MDP_1A group and iv) MDP_1A/2A group. No randomization was used. Details on the surgical procedure for MDP implantation are described in Fig. 3.2.

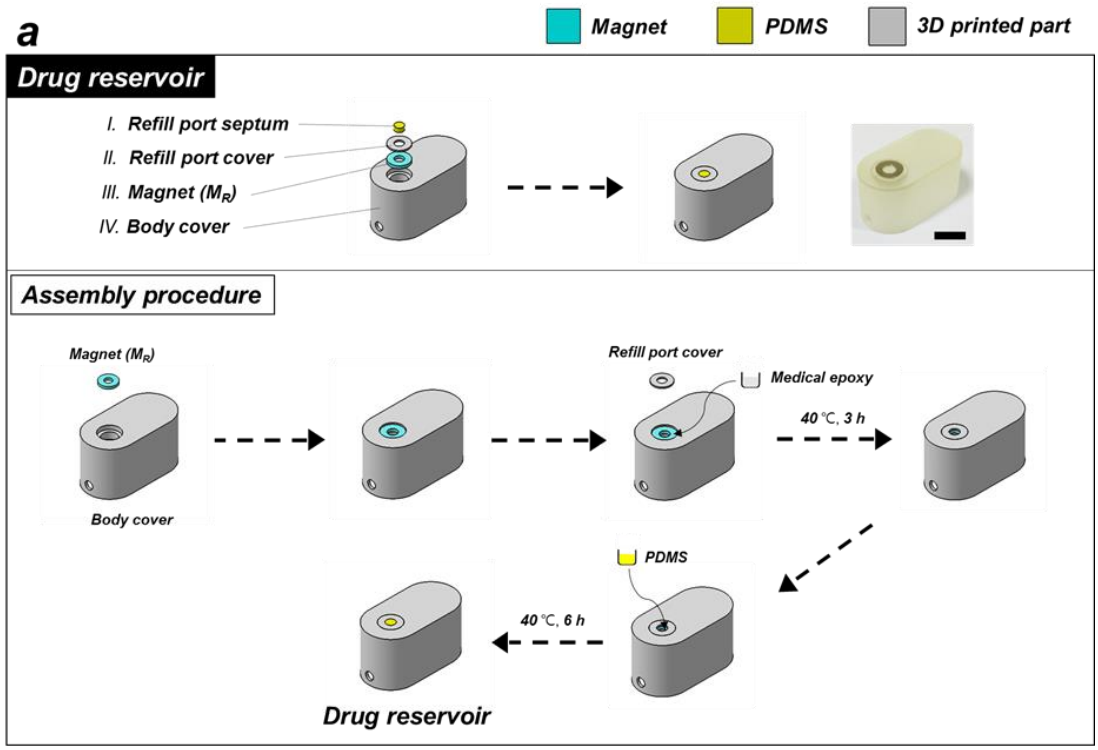
a
Magnet
PDMS
3D printed part
Drug reservoir
I. Refill port septum
II. Refill port cover
III. Magnet (M_R)
IV. Body cover
Assembly procedure
Magnet (M_R)
Body cover
Refill port cover
Medical epoxy
40 ℃, 3 h
PDMS
40 ℃, 6 h
Drug reservoir

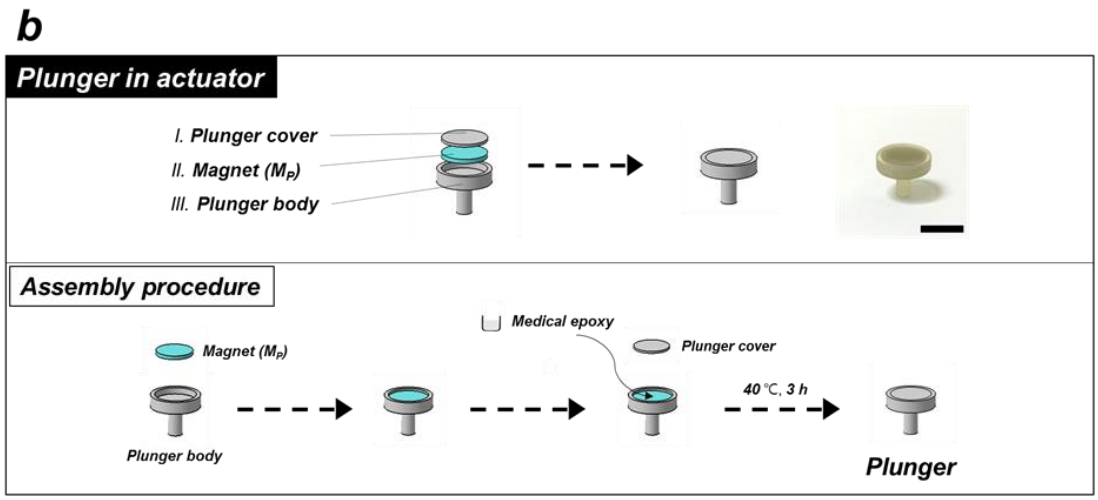
b
Plunger in actuator
I. Plunger cover
II. Magnet (M_P)
III. Plunger body
Assembly procedure
Magnet (M_P)
Plunger body
Medical epoxy
Plunger cover
40 ℃, 3 h
Plunger

(Continued)

c

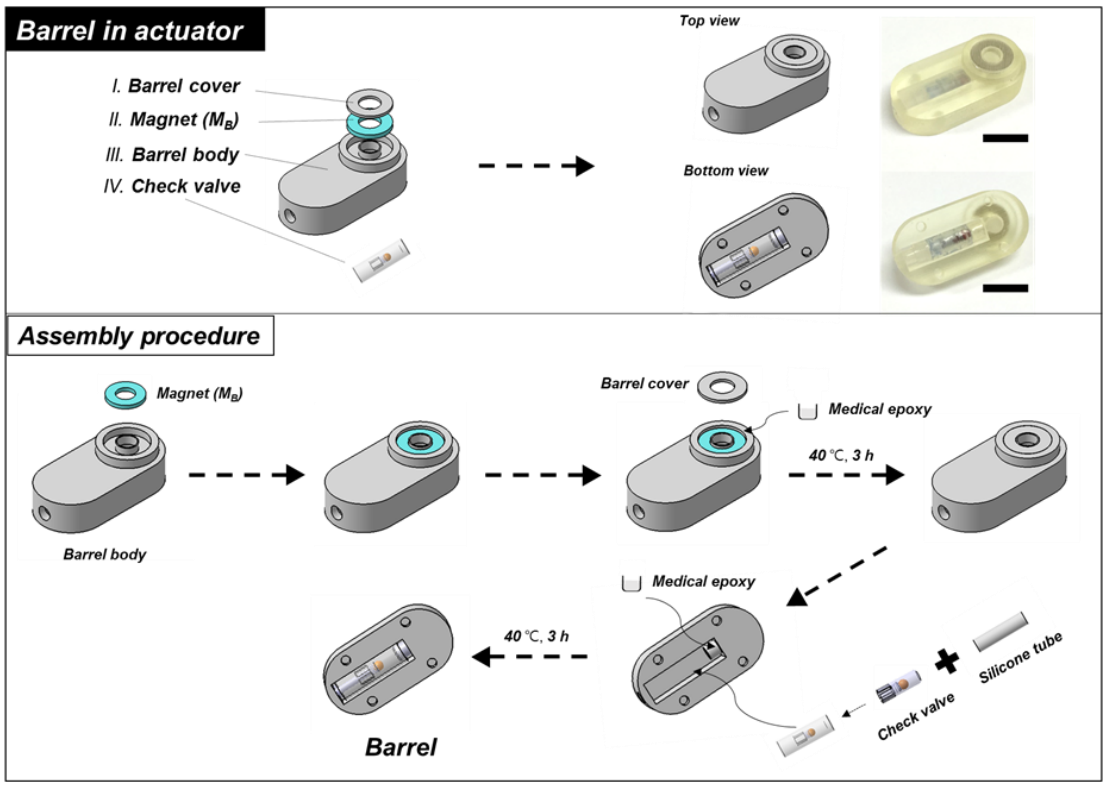

d

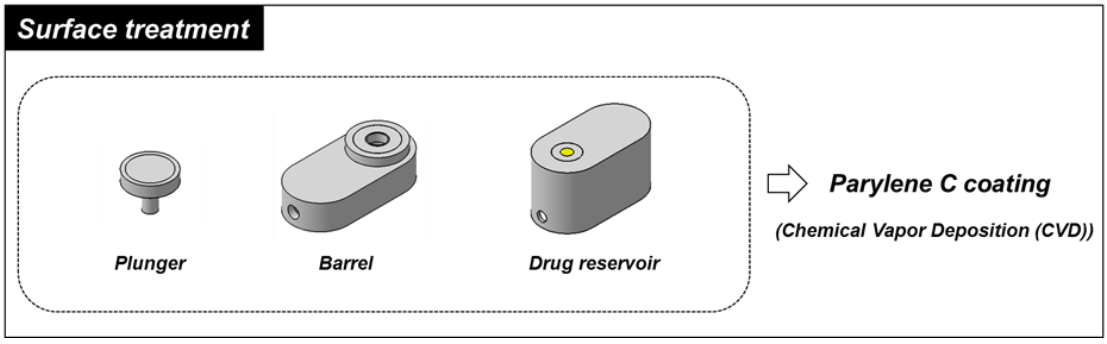

(Continued)

e

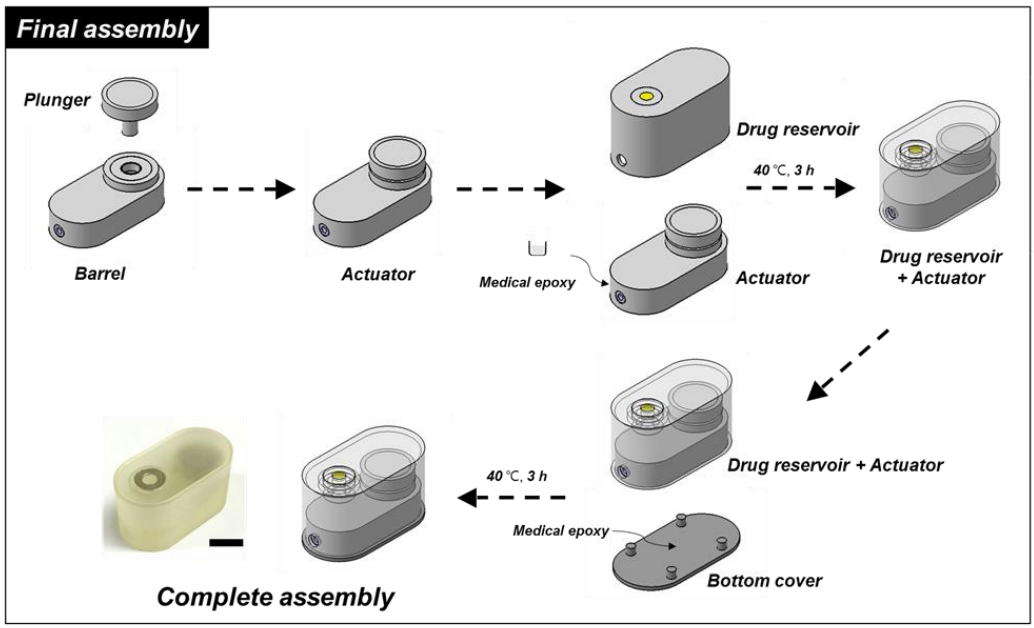
Final assembly
Plunger
Barrel
Actuator
Medical epoxy
Drug reservoir
Actuator
40 ℃, 3 h
Drug reservoir
+ Actuator
Drug reservoir + Actuator
Medical epoxy
Bottom cover
40 ℃, 3 h
Complete assembly

f

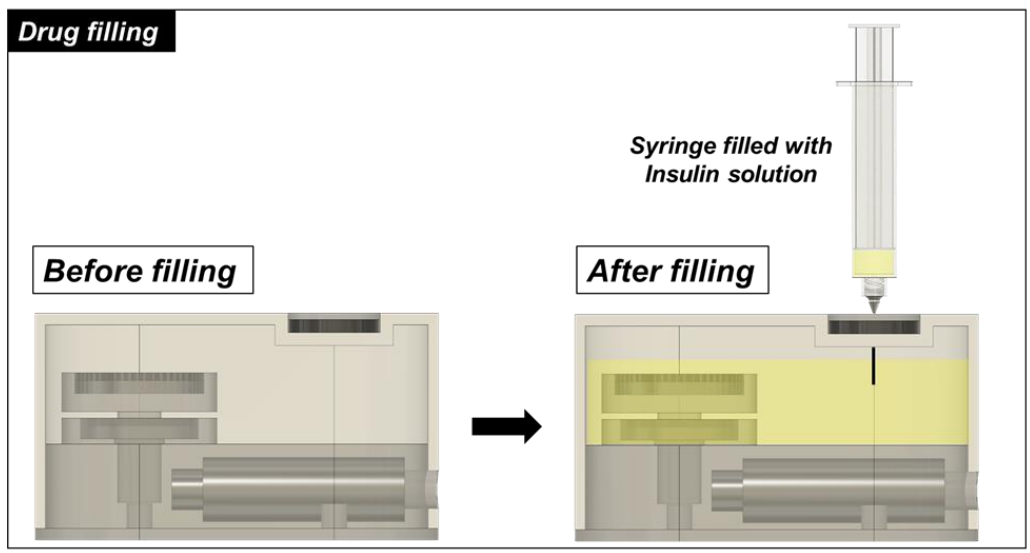
Drug filling
Syringe filled with
Insulin solution
Before filling
After filling

Figure 3.1 Detailed description of the MDP fabrication procedures. The MDP consists of two distinct units: a drug reservoir and an actuator. **(a)** To prepare the drug reservoir, a body cover was assembled with a donut-shaped magnet (M_R), which was then assembled and bonded with a refill port cover. The hole formed in the refill port was then filled with PDMS to prepare a septum. **(b)** To prepare the plunger in the actuator, a plunger body was assembled with a coin-shaped magnet (M_P), which was then assembled and bonded with the plunger cover. **(c)** To prepare the barrel in the actuator, a barrel body was assembled with a donut-shaped magnet (M_B), which was then assembled and bonded with a barrel cover. The resulting product was then assembled and bonded with a check valve inserted into a silicone tube. **(d)** The plunger, barrel and drug reservoir were coated with Parylene C by chemical vapor deposition. **(e)** The plunger was assembled with the barrel to form the actuator unit. Then, the actuator was assembled and bonded with the drug reservoir, which was then bonded with a bottom cover to complete the assembly. **(f)** The MDP was filled with 1.2 ml of an aqueous solution of insulin with a 30G syringe needle through the septum port into the drug reservoir.

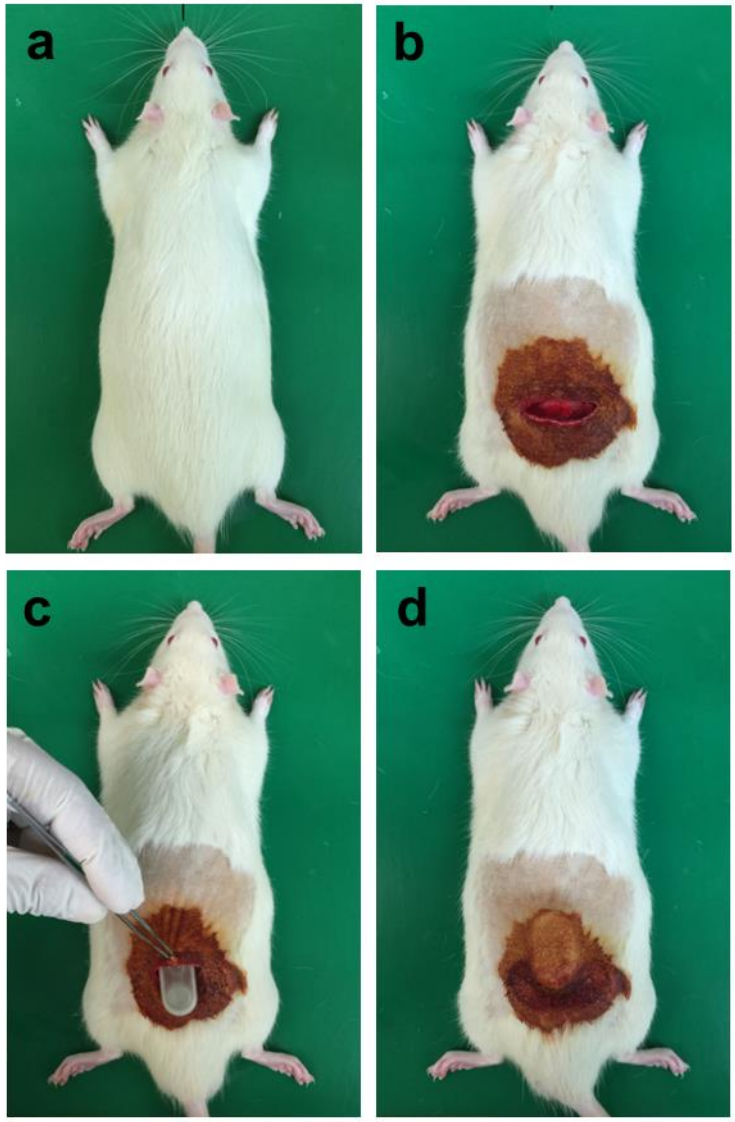

Figure 3.2 Surgical procedure for MDP implantation. (a) A diabetic rat was anesthetized via intraperitoneal injection of a mixture (1 ml/kg) of Zoletil® 50 and Rompun® (1:1 v/v). (b) The dorsal area was shaved and sterilized with betadine. (c) A 4–5 cm skin incision was made, and the MDP was implanted into the dorsal subcutaneous pocket. (d) The wound was closed with a surgical suture and disinfected with betadine.

During the experiments, the animals were freely accessible to food and water. To measure the plasma insulin concentration at each scheduled time, 0.5 ml of blood was withdrawn from the tail vein 60 min after insulin administration while the animal was sedated by inhalation of isoflurane. For the MDP_1A and MDP_1A/2A groups, blood was also withdrawn at −1 min (i.e., at 1 min before MDP actuation), and the insulin concentration was measured to monitor any possible leak of insulin from the MDP (Fig. 3.3).

At 1, 16 and 30 days, blood was also withdrawn at shorter time scales at −1, 30, 60, 120, 240, 360 and 720 min after insulin administration (Fig. 3.4a). The blood plasma was separated by centrifugation and stored in the freezer at −20° C before analysis. The insulin concentration in plasma was measured using an Insulin ELISA kit (Mercodia Insulin ELISA, Mercodia AB, Sweden). To measure the blood glucose levels at each scheduled time, approximately 5 μl of blood was sampled at 120 min after insulin administration and analyzed using a glucose meter. The decreased glucose level was calculated by subtracting the glucose level at 120 min from that measured at − 1 min (i.e., at 1 min prior to insulin administration). At 1, 16 and 30 days, the blood glucose level was also obtained at shorter time scales at −1, 30, 60, 120, 240, 360 and 720 min after insulin administration (Fig. 3.4b).

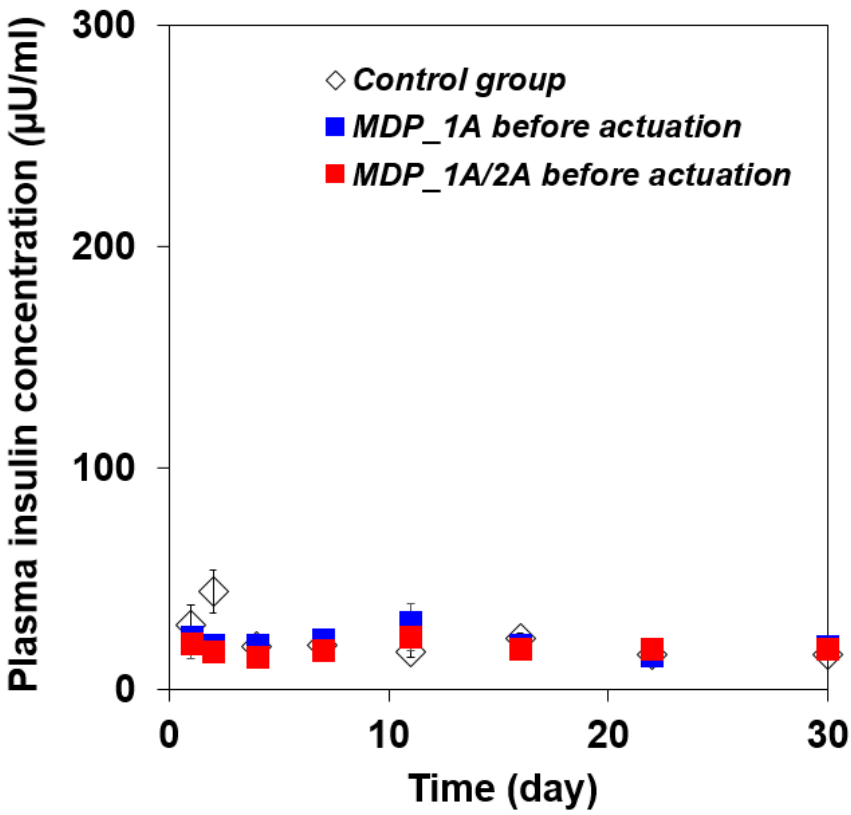

Figure 3.3 Leak test results of the MDP. The plasma insulin concentration was measured immediately before actuation and compared to that of the control group (i.e., diabetic rats without treatment) (n = 4 ; control, n = 4 ; MDP_1A, n = 4 ; MDP_1A/2A).

a

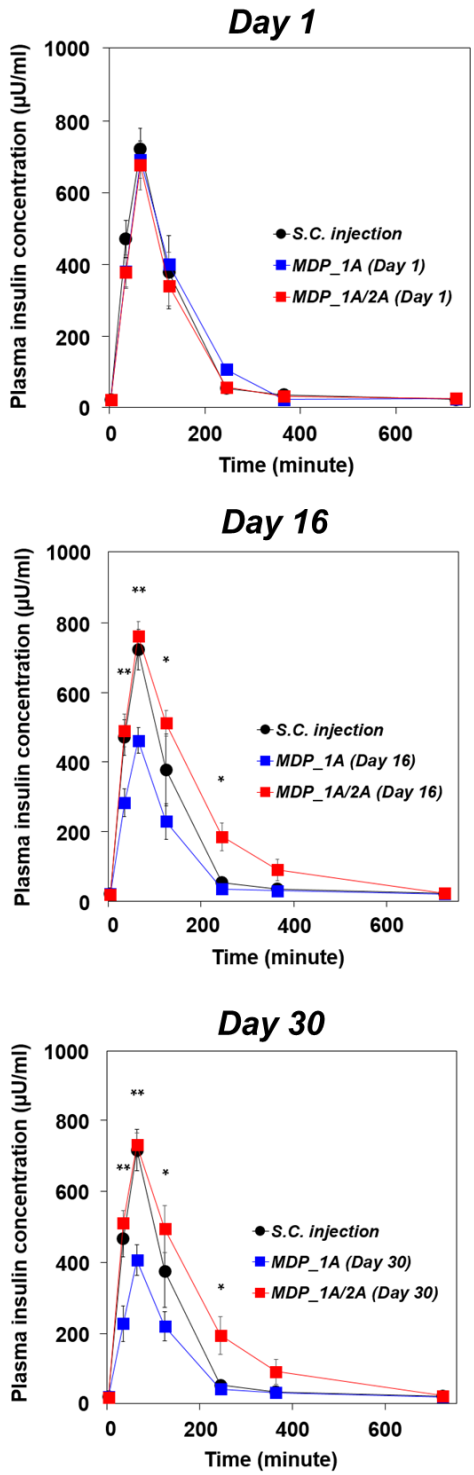
Day 1
Plasma insulin concentration (μU/ml)
1000
800
600
400
200
0
0
200
400
600
Time (minute)
S.C. injection
MDP_1A (Day 1)
MDP_1A/2A (Day 1)
Day 16
Plasma insulin concentration (μU/ml)
Time (minute)
S.C. injection
MDP_1A (Day 16)
MDP_1A/2A (Day 16)
**
**
*
*
Day 30
Plasma insulin concentration (μU/ml)
Time (minute)
S.C. injection
MDP_1A (Day 30)
MDP_1A/2A (Day 30)
**
**
*
*

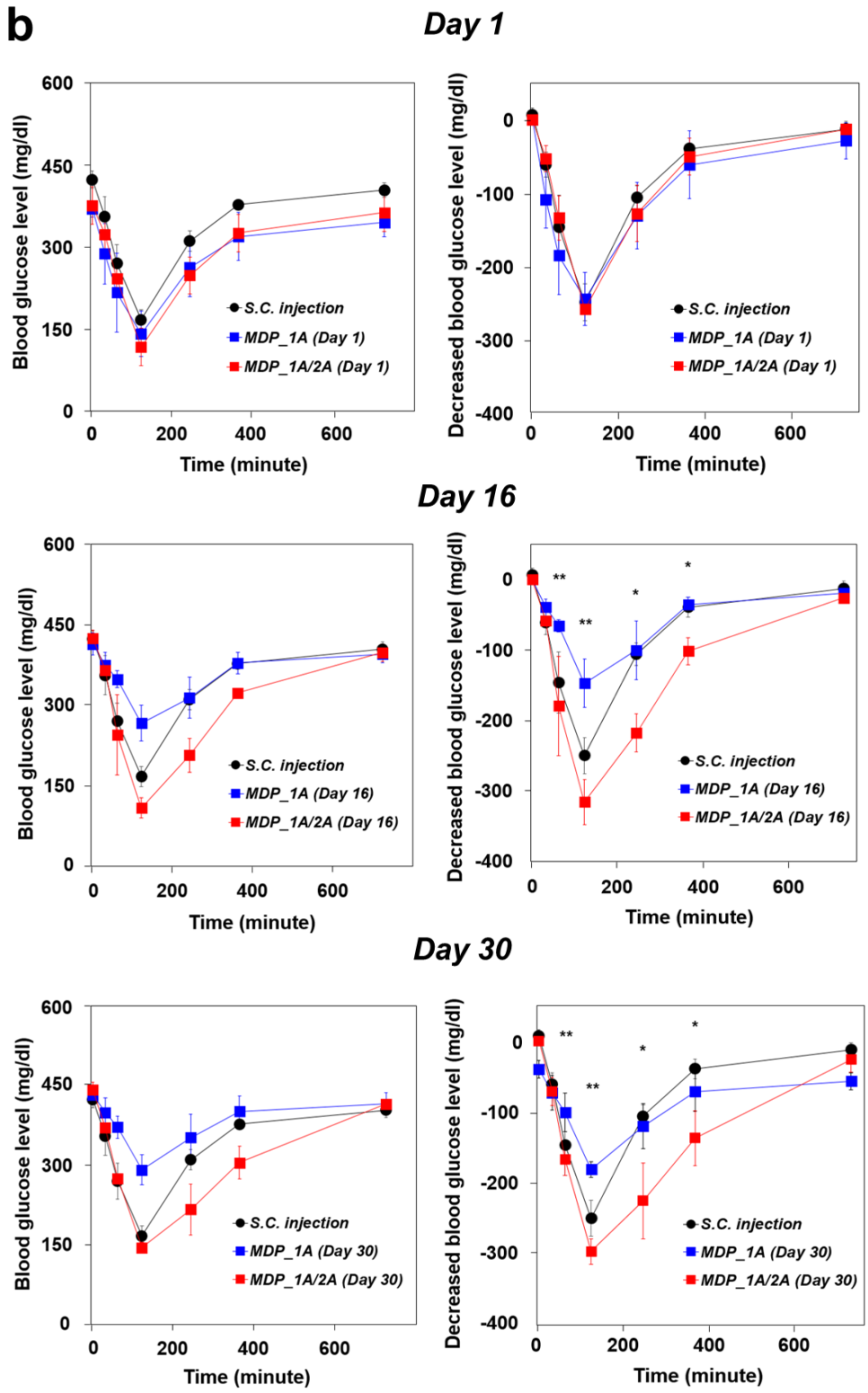
b
Day 1
Blood glucose level (mg/dl)
Time (minute)
S.C. injection
MDP_1A (Day 1)
MDP_1A/2A (Day 1)
Decreased blood glucose level (mg/dl)
Day 16
MDP_1A (Day 16)
MDP_1A/2A (Day 16)
Day 30
MDP_1A (Day 30)
MDP_1A/2A (Day 30)

Figure 3.4 Profiles of (a) plasma insulin concentration and (b) blood glucose level at shorter time scales at −1 to 720 min on days 0, 16 and 30, obtained from the four different animal groups: i) control group (n = 4), ii) S.C. injection group (n = 4), iii) MDP_1A group (n = 4) and iv) MDP_1A/2A group (n = 4). Error bars are s.d. ** The MDP_1A group was significantly different from both the S.C. injection and MDP_1A/2A groups ($P < 0.05$). * The MDP_1A group was statistically significantly different from the MDP_1A/2A group ($P < 0.05$).

3.2.4 Histopathology

The rats in the MDP_1A/2A group were sacrificed by carbon dioxide inhalation at 16 and 30 days after implantation, and the dorsal region tissues around the implanted MDP were harvested for histopathological analysis. The tissues were fixed in 10 % buffered formalin in a conical tube and embedded in paraffin wax for sectioning and staining. The paraffin blocks were then cut into 4-μm-thick slices and prepared on glass slides. The slides were then stained with hematoxylin and eosin (H&E), CD68 and Masson's trichrome (MT). Finally, the stained slides were assessed by a board-certified professional pathologist using an optical microscope (BX53, Olympus, Japan). No blinding was done. In this work, I observed tissue near the reservoir body surface and tissue near the outlet of the MDP. At each biopsy time and for each tissue location, at least three images were obtained from each of the four rats; a total of at least 12 images were analyzed.

3.2.5 Statistical Analysis

All data for plasma insulin concentration and decreased glucose level in blood at each scheduled time were compared among the S.C. injection, MDP_1A and MDP_1A/2A groups for statistical significance via non-parametric methods (Kruskal-Wallis ANOVA). $P < 0.05$ was considered statistically significant. The statistical software

application used was SPSS (SPSS version 22, IBM, USA).

3.3 Results

3.3.1 MDP Design and Working Principles

I prepared the MDP by assembling the two distinct drug reservoir and actuator units, as shown in Fig. 3.5a. The drug reservoir unit formed the exterior of the MDP. In the reservoir body cover, a refill port was formed with a septum, cover and donut-shaped magnet (M_R). Inside the drug reservoir, I prepared the actuator unit, which, like a typical syringe, was composed of two subunits, the plunger and barrel. The plunger subunit was composed of a plunger cover, coin-shaped magnet (M_P) and plunger body. The barrel subunit was composed of a barrel cover, donut-shaped magnet (M_B), barrel body and check valve. The refill port septum was composed of polydimethylsiloxane (PDMS) elastomer. All magnets and the check valve were used as obtained from commercial sources. All other units were fabricated from polyurethane copolymer using a PolyJet 3D printer to ensure high reproducibility of their precise dimensions. The units were then assembled and seamlessly attached with medical epoxy to produce the MDP. Detailed assembly procedures are provided in the Methods and Fig. 3.1.

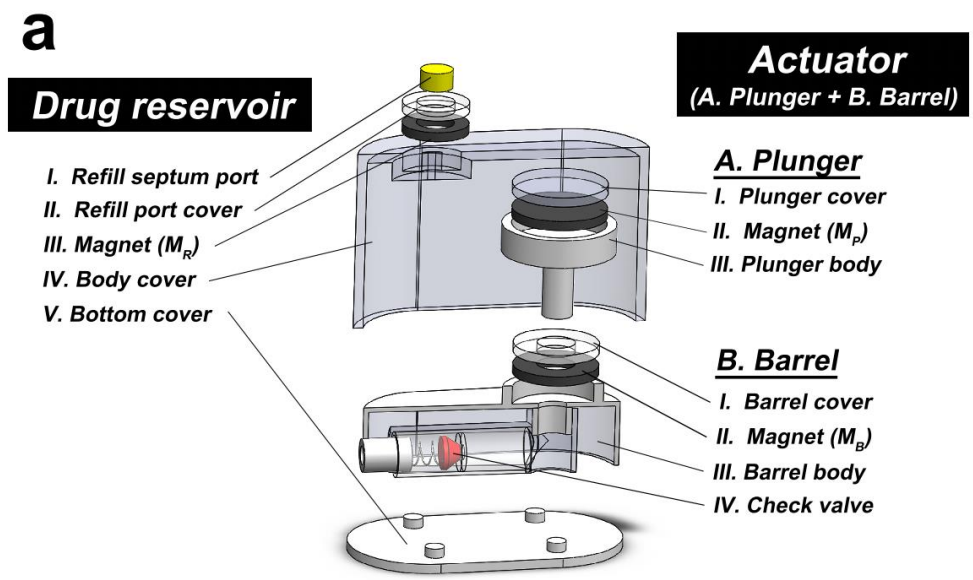
a
Drug reservoir
I. Refill septum port
II. Refill port cover
III. Magnet (M_R)
IV. Body cover
V. Bottom cover
Actuator
(A. Plunger + B. Barrel)
A. Plunger
I. Plunger cover
II. Magnet (M_P)
III. Plunger body
B. Barrel
I. Barrel cover
II. Magnet (M_B)
III. Barrel body
IV. Check valve

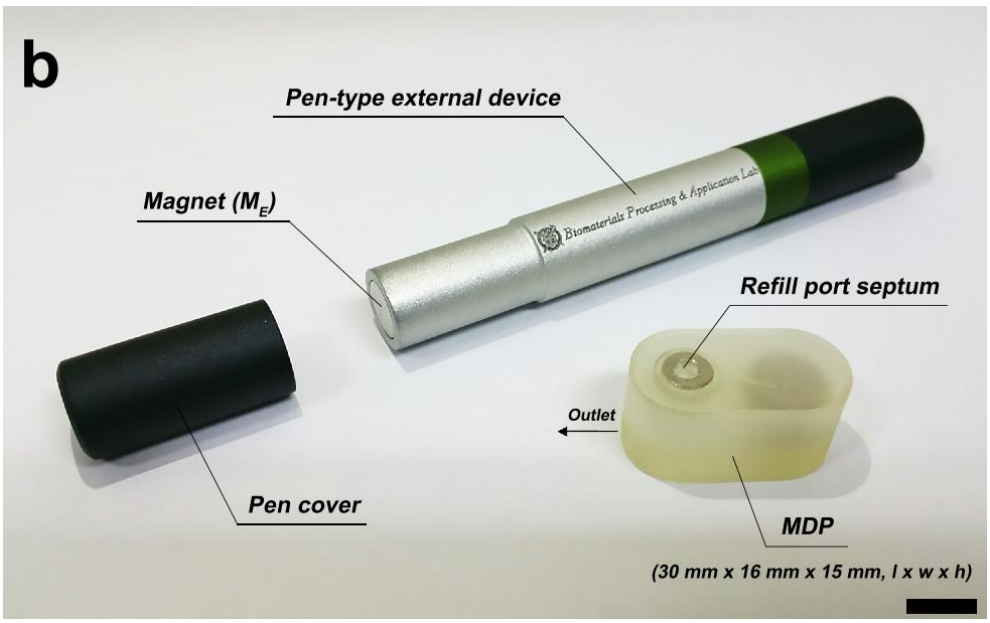
b
Pen-type external device
Magnet (M_E)
Biomaterials Processing & Application Lab
Refill port septum
Outlet
Pen cover
MDP
(30 mm x 16 mm x 15 mm, l x w x h)

(Continued)

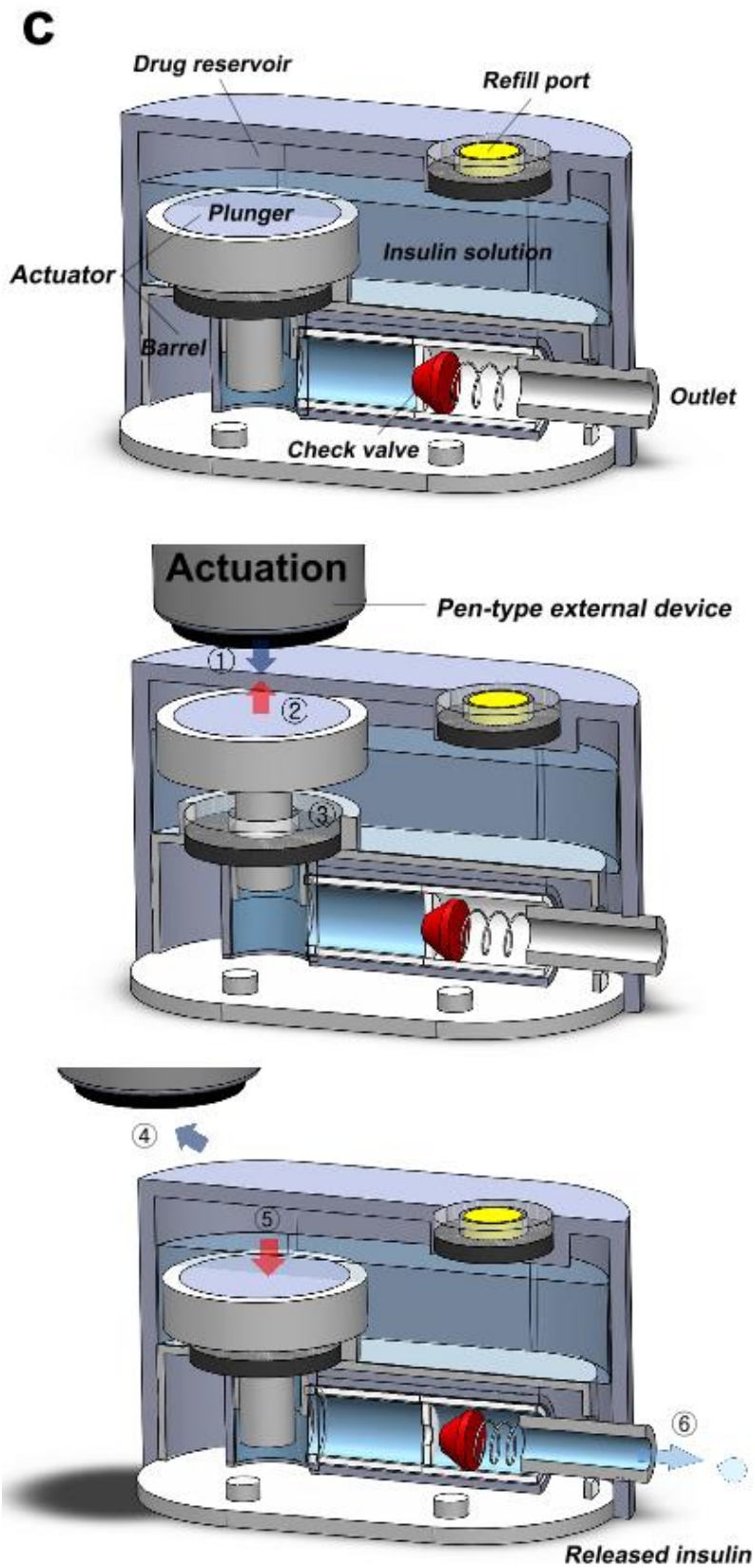
C
Drug reservoir
Refill port
Plunger
Insulin solution
Actuator
Barrel
Outlet
Check valve
Actuation
Pen-type external device
①
②
③
④
⑤
⑥
Released insulin

Figure 3.5 Descriptive images of the MDP. (a) 3D schematic of the MDP. The MDP is composed of two distinct units: a drug reservoir and an actuator. The actuator is composed of a plunger and barrel. The drug reservoir is filled with insulin solution (109 U ml^{-1}) after assembly. To prepare the insulin solution, insulin in powder form (short acting; Sigma-Aldrich, MO, USA) was dissolved in sterile PBS at pH 7.4. **(b)** Optical image of the MDP and pen-type external device. The scale bar is 1 cm. **(c)** The actuation principle of the MDP is as follows: ① the external magnet is applied; ② the plunger moves upward; ③ the drug solution in the reservoir is aspirated into the barrel; ④ the external magnet is removed; ⑤ the plunger moves downward; and ⑥ the insulin is released through the one-way check valve.

Fig. 3.5b presents an optical image of the MDP and the external device prepared in this work. The total volume of the MDP was approximately 7.2 ml (30 mm x 16 mm x 15 mm, *l* x *w* x *h*), in which a 3-ml volume was used as the drug reservoir. I filled the MDP with 1.2 ml of an aqueous solution of insulin, which was injected through the septum port into the drug reservoir. The whole surface of the MDP was coated with Parylene C due to the biocompatibility of Parylene C after implantation (58). A one-way check valve was installed in series with the outlet to prevent unwanted leakage of insulin and inflow of bodily fluid. A pen-type external device was prepared following the basic design and dimensions of a commercially available insulin pen(59). A magnet (M_E) was installed at the tip of the pen, and a cover was installed on the tip when not in use (Fig. 3.6).

Figure 3.6 Image of a commercial insulin pen and the external device prepared in this work. I designed an external device closely following the size and shape of an insulin pen approved for clinical use (KwikPen®, Eli Lilly, USA). The scale bar is 5 cm.

Fig. 3.5c shows the actuation principle of the MDP in this work. Magnets were placed in the heads of the barrel and plunger (i.e., M_B and M_P, respectively) to face each other with opposite polarities and therefore attach to each other strongly enough to prevent accidental movement of the plunger. Under this non-actuation condition, pressure does not develop in the barrel, and the check valve remains closed, preventing any leakage of the insulin solution. A magnet (M_E) was installed in the external device facing the plunger magnet (M_P) with opposite polarity. The magnetic field between M_E and M_P is stronger than the one between the magnets in the barrel and plunger (i.e., M_B and M_P, respectively). Thus, when the external magnet device is applied above the MDP (Fig. 3.5c (①)), the plunger detaches from the barrel and moves upward (Fig. 3.5c (②)) to aspirate drug solution into the barrel (Fig. 3.5c (③)). Then, when the external magnet device is removed (Fig. 3.5c (④)), the plunger moves downward due to attraction from the magnet in the barrel, increasing the pressure in the barrel (Fig. 3.5c (⑤)) to open the check valve and release the insulin solution from the MDP (Fig. 3.5c (⑥)). The plunger was not tightly inserted in the barrel but with a gap of 150 μm to allow for smooth and reproducible actuations. The magnet in the drug reservoir (M_R) is for localization of the refill port, similar to medical devices such as tissue expanders(60). Although not visible after implantation, therefore, the exact location of the refill port can be determined using a magnet of opposite polarity outside the body. The refill port allows refill injection using a hypodermic

needle without damaging the body of the MDP. The M_E faces the M_R with the same polarity and is therefore repelled, preventing potential mislocation of the M_E on the refill port.

3.3.2 *In Vitro* Performance Test

To investigate the performance of the MDP, an *in vitro* drug release test was performed, where a gap of 1 mm was prepared between the external device and MDP to simulate the presence of the skin after implantation(61, 62). In this work, the MDP could be actuated with gaps of up to 3 mm with the external magnet (M_E) of 3000 G (Table 3.1). As shown in Figs 3.7a and 3.8a, the release amount per actuation, 0.81 ± 0.04 U per actuation, was highly reproducible even with repeating actuations. This result implies that the MDP infuses 7.4 μl of liquid per actuation. Therefore, because the drug reservoir contains 1.2 ml of insulin solution, the MDP allows at least 160 deliveries of insulin after implantation. With this high reproducibility, the dose amount can be varied by simply varying the number of actuations. To simulate conditions of long-term implantation, the MDP was fully submerged in release media for 28 days.

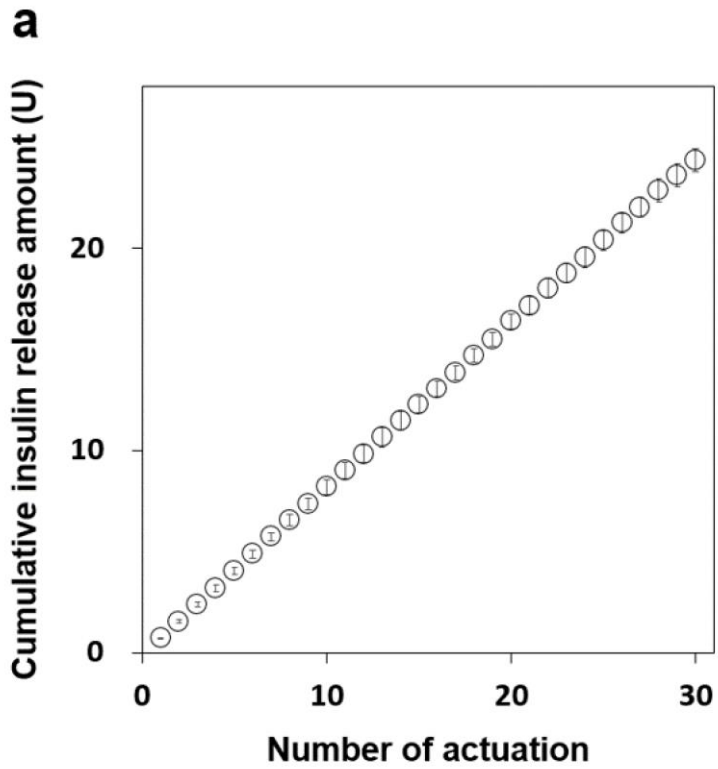
a
Cumulative insulin release amount (U)
0
10
20
0
10
20
30
Number of actuation

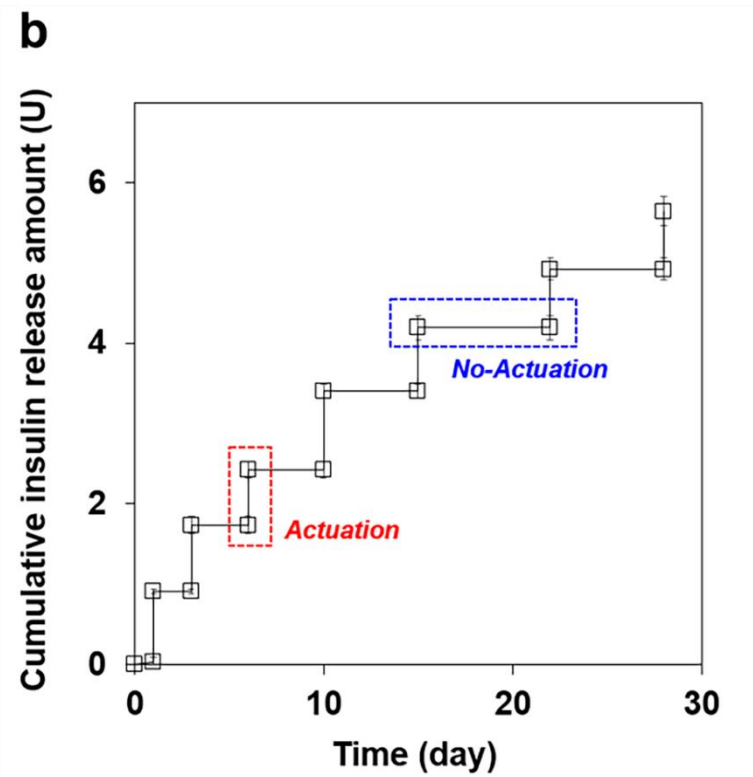
b
Cumulative insulin release amount (U)
0
2
4
6
0
10
20
30
Time (day)
No-Actuation
Actuation

Figure 3.7 *In vitro* insulin release profiles of the MDP

The MDP was fully immersed in pH 7.4 phophate buffered saline (PBS) and incubated in an incubator at 37° C while being continuously shaken at 50 rpm. At each actuation, the external magnet device was applied at a constant distance from the top of the MDP by placing a 1 mm-thick glass slide between the external magnet device and MDP to simulate the presence of tissue after implantation, and removed almost instantaneously (< 1 s) while the MDP was fully submerged in the release medium. An aliquot of the release medium was sampled at scheduled times and analyzed by high-performance liquid chromatography. Details on this procedure are described in the Methods section. **(a)** Thirty consecutive actuations were applied at intervals of 10 min, and an aliquot was sampled after each of the actuations. With five distinct MDPs tested herein, the released amount of insulin was highly reproducible and was 0.81 ± 0.04 U per actuation. Error bars are s.d. **(b)** The MDP was actuated at predetermined times of 1, 3, 6, 10, 15, 22 and 28 days while fully immersed in PBS for 28 days. Aliquots were sampled immediately before and after each of the actuations. With four distinct MDPs tested herein, there was almost no release of insulin during the period of no actuation. The released amount of insulin was also highly reproducible and was 0.80 ± 0.09 U per actuation. Error bars are s.d.

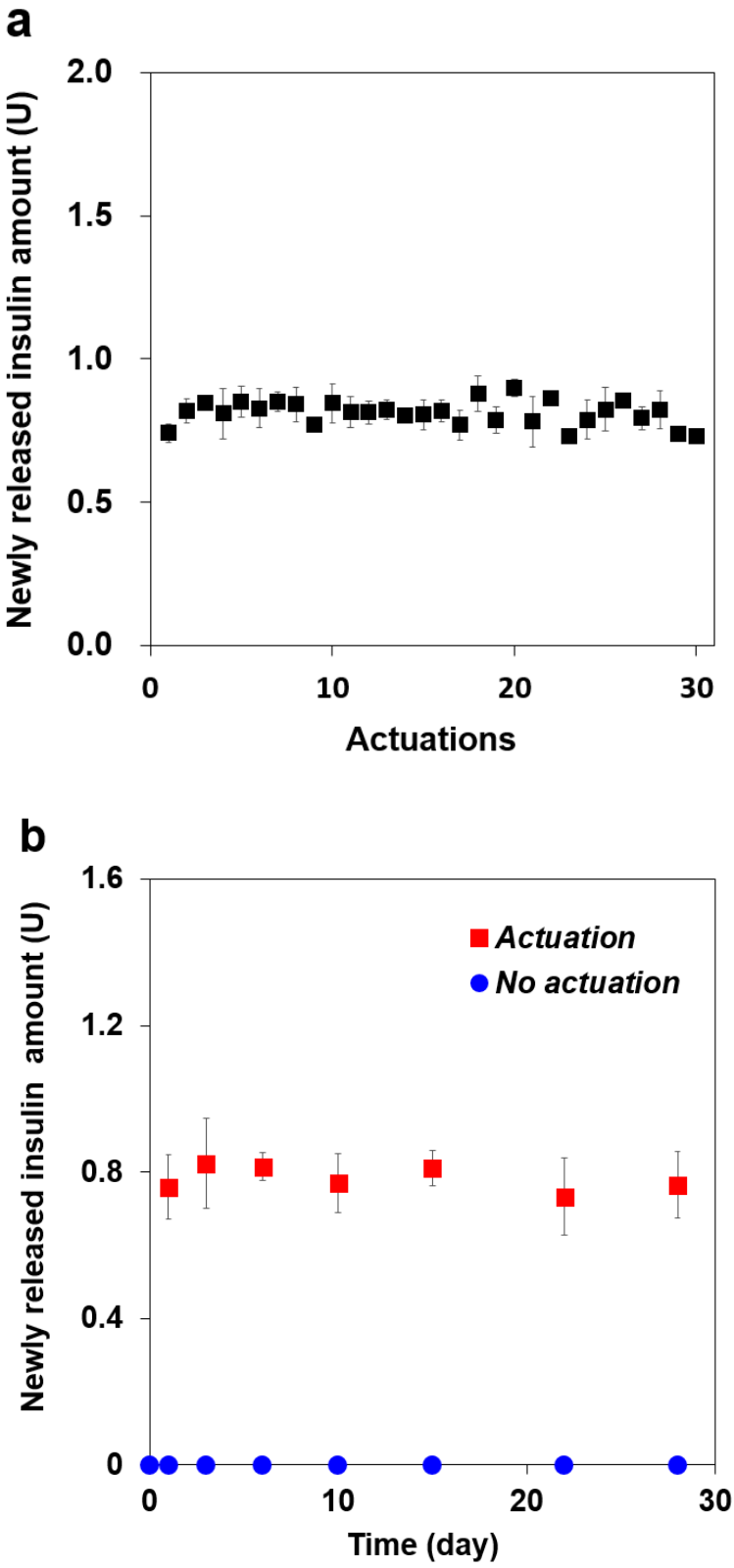
a
Newly released insulin amount (U)
2.0
1.5
1.0
0.5
0.0
0
10
20
30
Actuations
b
Newly released insulin amount (U)
1.6
1.2
0.8
0.4
0
Actuation
No actuation
0
10
20
30
Time (day)

Figure 3.8 Insulin release profiles of the MDP. Figs 3.7(a) and (b) were replotted to show the amount of newly released insulin per actuation. The released amounts of insulin were highly reproducible and were **(a)** 0.81 ± 0.04 U and **(b)** 0.80 ± 0.09 U per actuation. When there was no actuation, insulin was not detected with the measurement method employed in this work.

Table 3.1 Actuation ability of the MDP according to the gap between the external device and MDP. The MDP could be actuated at gaps of up to 3 mm and in this range, the MDP could infuse the same amount of insulin, as observed in our *in vitro* performance test. To be actuated with the skin gap of 1 mm, the MDP herein needs an external magnet with 3000 G. Therefore, considering the range of a magnetic field available in a regular life style (< 2 G), a chance for an accidental activation of the MDP is expected to be not high.

Gap between the external device and MDP (mm)	Actuation ability*
0	Y
1	Y
1.5	Y
2	Y
2.5	Y
3	Y
3.5	N

* Y : actuated; N : not actuated

As shown in Figs 3.7b, insulin was released only at the times of actuation, and no insulin was detected during the periods of non-actuation. Considering the LOQ (limit of quantification: 0.002 U ml^{-1}) with the measurement in this work, this result implied that even though there was a leak, it should be less than 0.02 U insulin during the longest non-actuation periods of 7 days (< 3 x 10^{-3} U per day). The average amount of released insulin per actuation was similar to that described above, again indicating high reproducibility. Using the aqueous solution prepared in this work, the stability and biological activity of insulin appeared to be maintained for up to 30 days under simulated biological conditions (Fig. 3.9).

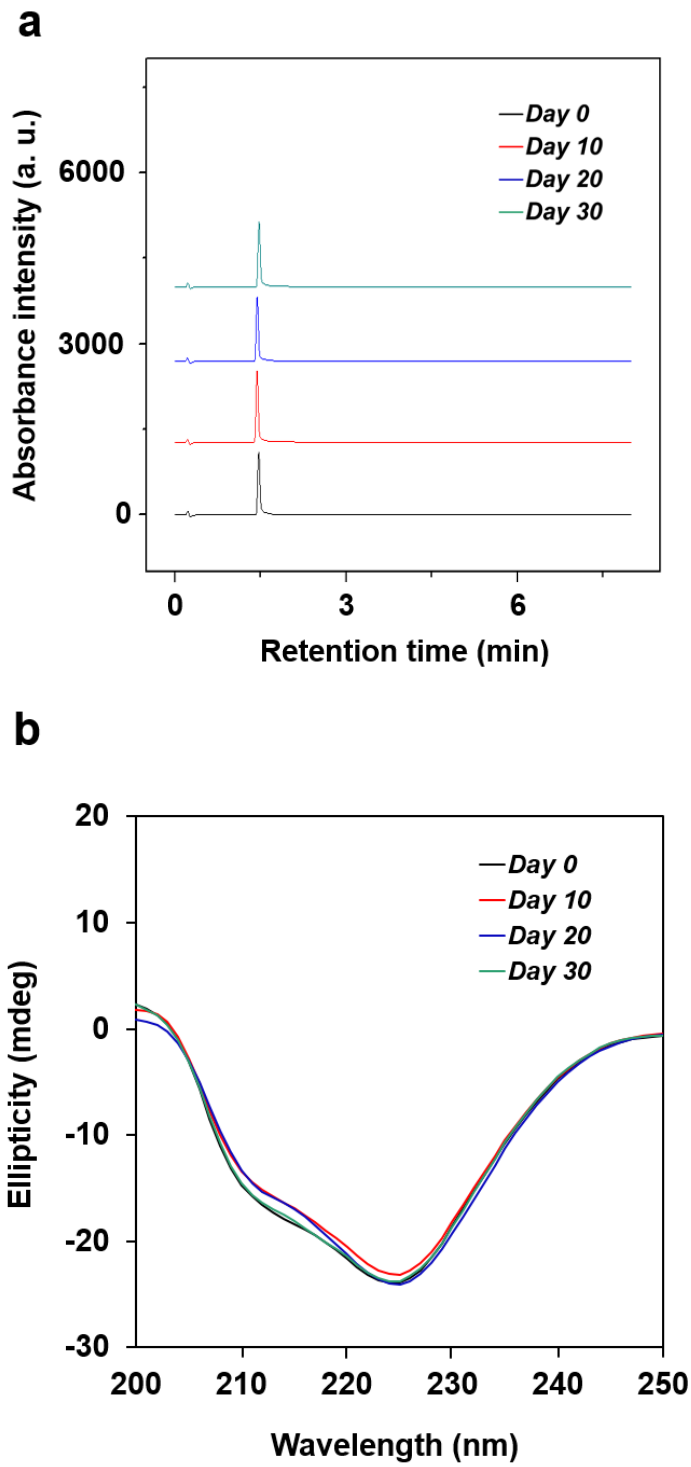
a
Absorbance intensity (a. u.)
6000
3000
0
0
3
6
Retention time (min)
Day 0
Day 10
Day 20
Day 30
b
Ellipticity (mdeg)
20
10
0
-10
-20
-30
200
210
220
230
240
250
Wavelength (nm)
Day 0
Day 10
Day 20
Day 30

(Continued)

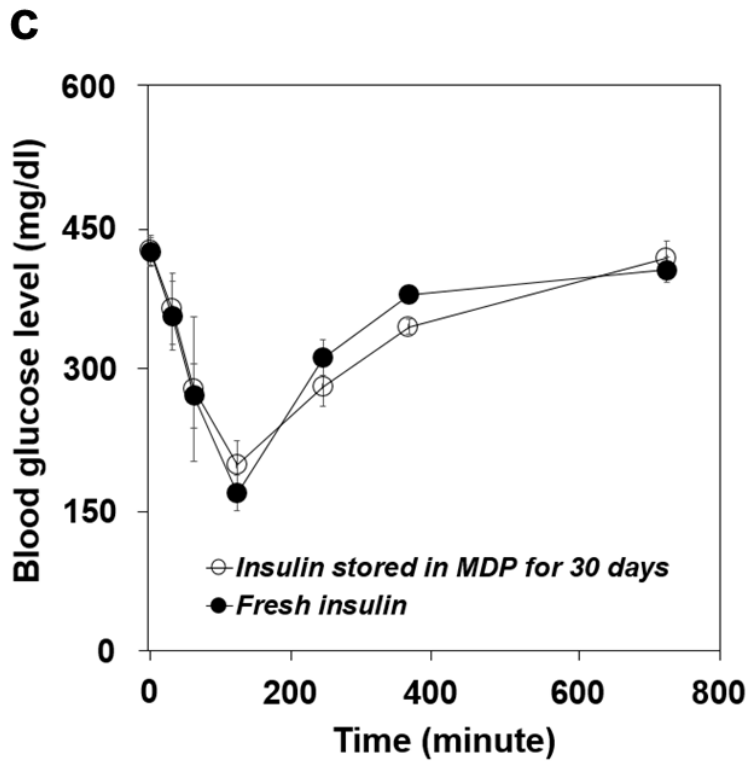
C
600
450
300
150
0
Blood glucose level (mg/dl)
0
200
400
600
800
Time (minute)
Insulin stored in MDP for 30 days
Fresh insulin

Figure 3.9 Stability evaluation of insulin. An insulin solution (109 U/ml) in PBS (pH 7.4) was stored in the MDP at 37 ° C for periods of 0, 10, 20 and 30 days and analyzed by RP-HPLC and circular dichroism (CD) spectroscopy. **(a)** The RP-HPLC analysis was performed following the same procedure described in the main text. The uniform intensity and constant retention time of insulin among the tested incubation periods indicate that the insulin stored in the MDP was retained without aggregation or degradation until day 30 of incubation at body temperature. **(b)** CD spectra were obtained using a CD spectrometer (J-810, Jasco, Japan). A quartz cuvette with a 1-mm path length was used, and spectra were scanned at 200–250 nm. The CD spectra were seen to be similar among the tested incubation periods to a large extent, implying that for most of insulin in the MDP, the secondary structure remained unchanged after 30 days of incubation at body temperature. **(c)** A fresh insulin solution and a solution extracted from the MDP after incubation for 30 days were subcutaneously injected to diabetic rats, respectively (n = 4; fresh insulin, n = 4; insulin stored in the MDP for 30 days). A fresh insulin solution was prepared at the same concentration (109 U/ml) as the one initially used for stability test with the MDP and the same volume (7.4 μl) of each of the solutions was injected. Between two groups, the profiles of blood glucose level were similar, implying that most of insulin stored in the MDP for 30 days could still effectively lower the blood glucose level.

3.3.3 In Vivo Evaluation

To assess *in vivo* performance, the MDP was subcutaneously implanted in streptozotocin (STZ)-induced diabetic rats, and pharmacokinetics and pharmacodynamics studies were performed over a 30-day period. As shown in Fig. 3.10a, the insulin concentrations between the MDP_1A and S.C. (i.e., subcutaneous injection) groups were similar until day 11. The differences in concentration among the scheduled times were not significant for each of the animal groups. During this period, the insulin concentrations were 629.4 ± 12.3 μU ml^{-1} and 683.3 ± 16.9 μU ml^{-1} in the MDP_1A and S.C. injection groups, respectively, with a fairly narrow distribution of concentration values in both groups. The blood glucose levels and their decreases between the MDP_1A and S.C. injection groups were also similar until day 11 (Fig. 3.10b), with values of 238.1 ± 7.38 mg dl^{-1} and −251.1 ± 6.41 mg dl^{-1}, respectively. This result indicates that noninvasive actuation with a magnetic field from the outside skin allowed the implanted MDP to deliver insulin as effectively and reproducibly as the conventional subcutaneous injection. In the control group, both the insulin concentrations and decrements of blood glucose levels were very low (23.08 ± 9.08 μU ml^{-1} and −19.3 ± 7.57 mg dl^{-1}, respectively) during the testing period, as expected for STZ-induced diabetic rats(63). After 11 days, the plasma insulin concentrations of the MDP_1A group decreased to as low as 430.9 ± 22.8 μU ml^{-1} (Fig.

3.10a), which was associated with an attenuated blood glucose lowering effect (Fig. 3.10b). This decrease may be due to the formation of a fibrous capsule around the MDP after long-term implantation(64), which appeared to hamper the diffusion of insulin from the subcutaneous space into the blood stream.

To compensate for this reduction and attain therapeutic levels similar to the S.C. injection group, I proposed to deliver more insulin with the MDP after 11 days. Another animal group, MDP_1A/2A, was prepared to test this method. In this group, the MDP was actuated once until day 11; the insulin concentration and decreased glucose levels (636.5 ± 29.2 μU ml^{-1} and -240.7 ± 26.4 mg dl^{-1}, respectively) were not very different from the MDP_ 1A and S.C. injection groups (Fig. 3.10).

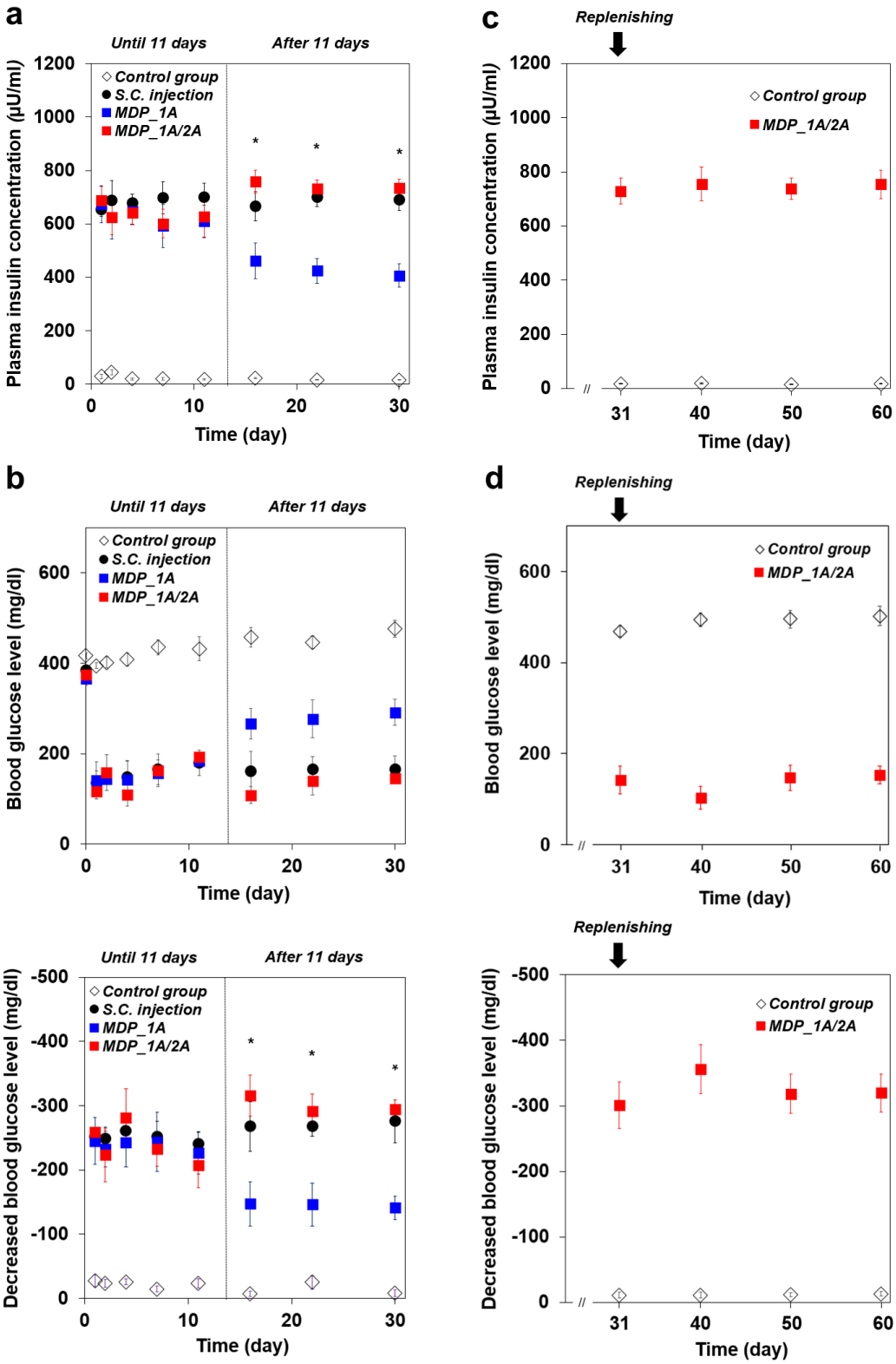
a
Until 11 days
After 11 days
Control group
S.C. injection
MDP_1A
MDP_1A/2A
Plasma insulin concentration (μU/ml)
Time (day)
b
Blood glucose level (mg/dl)
Decreased blood glucose level (mg/dl)
c
Replenishing
d

Figure 3.10 Profiles of (a,c) plasma insulin concentration and (b,d) blood glucose level with the four different animal groups: i) control group–diabetic rats with no treatment (n = 4), ii) S.C. injection group–diabetic rats subcutaneously injected with an insulin solution with a Hamilton microliter syringe at each of the scheduled times (n = 4), iii) MDP_1A group–diabetic rats implanted with the MDP in the subcutaneous space and treated with a single actuation at each of the scheduled times (n = 4); and iv) MDP_1A/2A group–diabetic rats implanted with the MDP and treated with a single actuation (0.8 U insulin) at each of the scheduled times until 11 days and two consecutive actuations (1.6 U insulin) at each of the scheduled times after 11 days (n = 4). For each actuation, the external device with M_E was applied and removed to the skin immediately above the implanted MDP. After insulin was delivered via actuation or injection, blood was withdrawn at $T_{max,\ insulin}$=60 min to measure the maximum insulin concentration and also at $T_{max,\ glucose}$=120 min to measure the minimum glucose level and its maximum decrease (Fig. 3.11). Error bars are s.d. **(a,b)** The plasma was sampled at scheduled times of 1, 2, 4, 7, 11, 16, 22 and 30 days with the four different animal groups. **(c,d)** After 30 days, I continued the experiment with the two different animals groups: i) control and iv) MDP_1A/2A groups. At 31 days, for the MDP_1A/2A group, I fully withdrew the insulin solution in the drug reservoir and refilled it with 1.2 ml of a fresh one while the MDP was still implanted (Fig. 3.12). The plasma was sampled at scheduled times of 31, 40, 50 and 60 days.

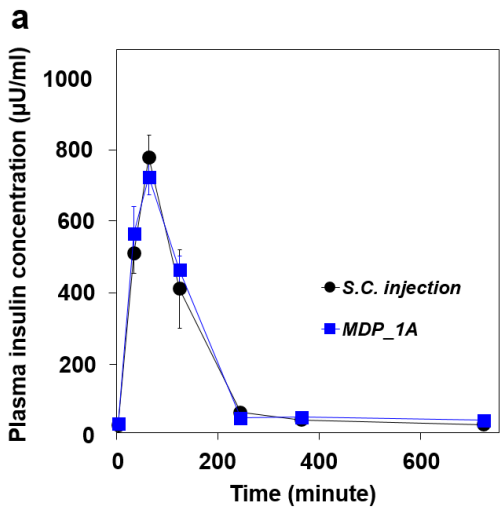
a
Plasma insulin concentration (μU/ml)
1000
800
600
400
200
0
0
200
400
600
Time (minute)
S.C. injection
MDP_1A

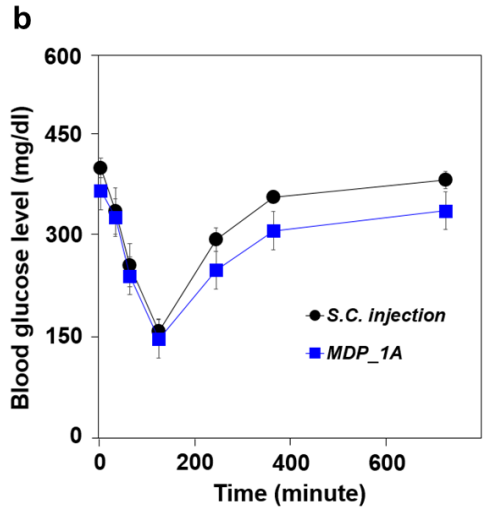
b
Blood glucose level (mg/dl)
600
450
300
150
0
0
200
400
600
Time (minute)
S.C. injection
MDP_1A

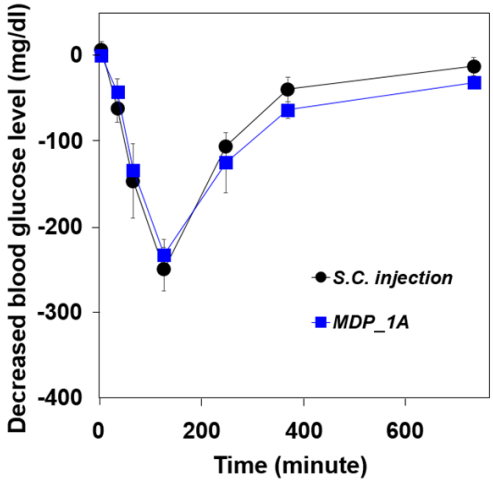
Decreased blood glucose level (mg/dl)
0
-100
-200
-300
-400
0
200
400
600
Time (minute)
S.C. injection
MDP_1A

Figure 3.11 Profiles of plasma insulin concentration and blood glucose level at shorter time scales after insulin administration in diabetic rats. (a) Blood was sampled at −1, 30, 60, 120, 240, 360 and 720 min after insulin administration. The maximum insulin concentration occurred at 60 min in both the S.C. injection and MDP groups. (b) The blood glucose level was measured at −1, 30, 60, 120, 240, 360 and 720 min after insulin administration. The maximum decrease in glucose level occurred at 120 min in both the S.C. injection and MDP groups (n = 4 ; S.C. injection, n = 4 ; MDP_1A).

a

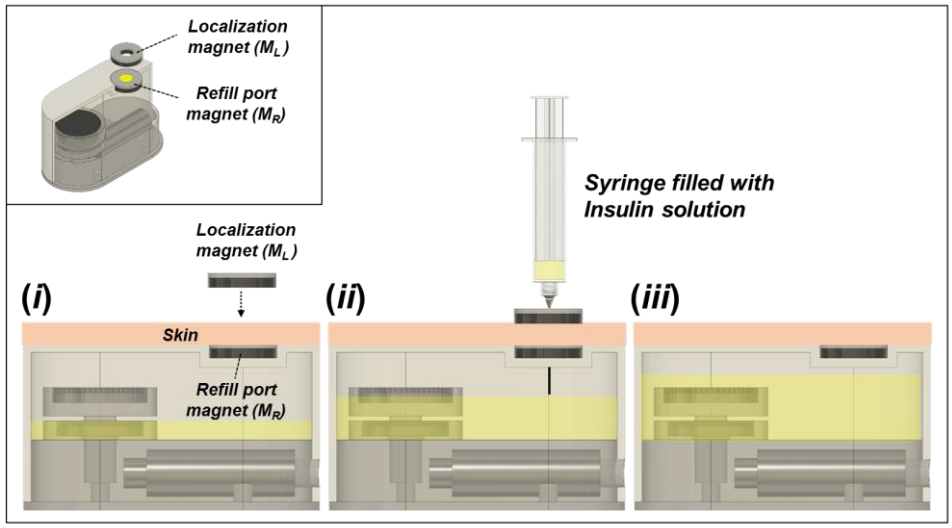
Localization magnet (M_L)
Refill port magnet (M_R)
Syringe filled with Insulin solution
Localization magnet (M_L)
(i)
(ii)
(iii)
Skin
Refill port magnet (M_R)

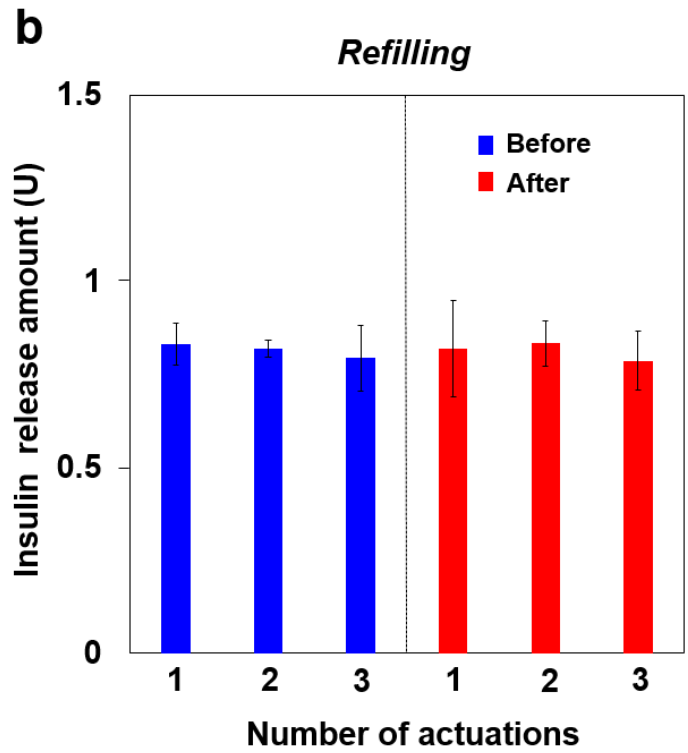
b
Refilling
1.5
1
0.5
0
Insulin release amount (U)
Before
After
1
2
3
1
2
3
Number of actuations

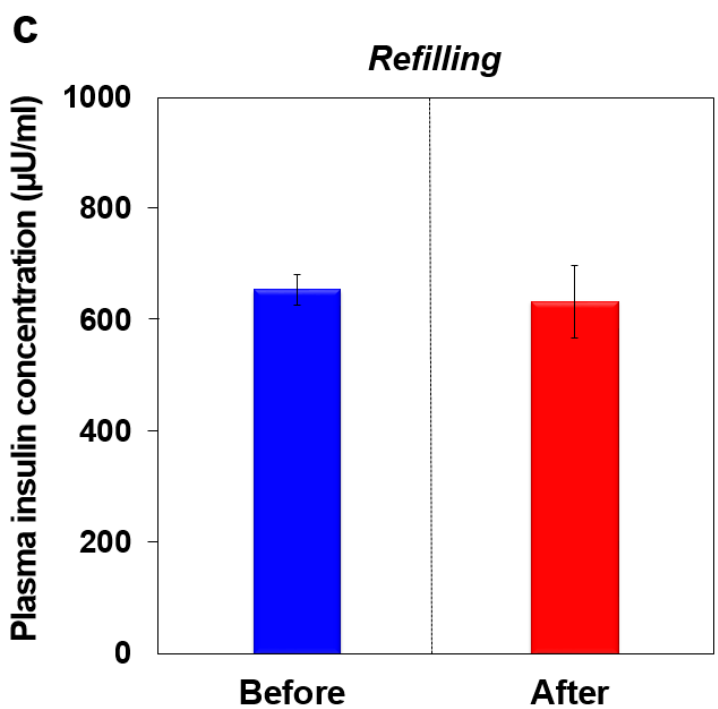
c
Refilling
1000
800
600
400
200
0
Plasma insulin concentration (μU/ml)
Before
After

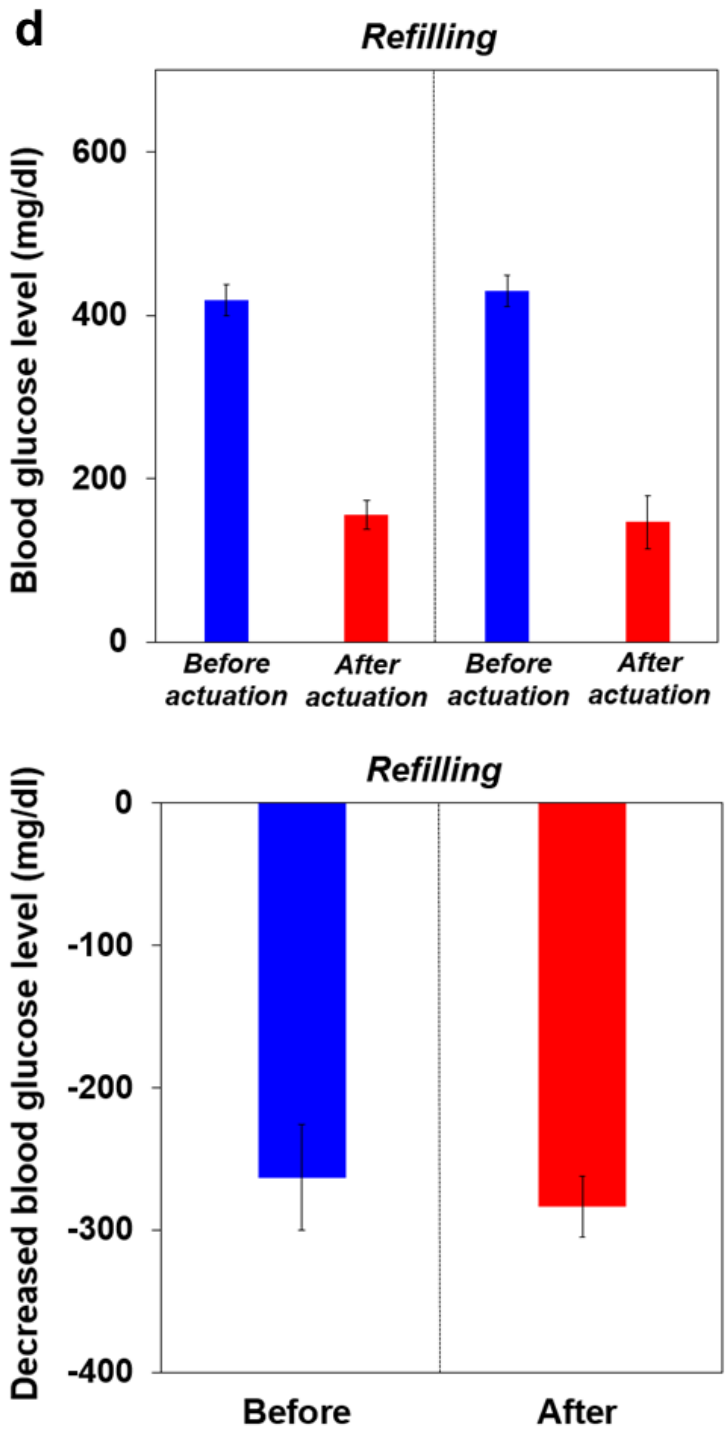
d
Refilling
Blood glucose level (mg/dl)
600
400
200
0
Before actuation
After actuation
Before actuation
After actuation
Refilling
Decreased blood glucose level (mg/dl)
0
-100
-200
-300
-400
Before
After

Figure 3.12 Reproducibility assessment of the MDP after a refilling procedure. For this evaluation, I first simulated consumption of insulin by intentionally withdrawing 0.4 ml of the insulin solution in the drug reservoir and then injected the same volume of fresh insulin solution through the septum port of the MDP using a 30G needle. **(a)** Schematic description of the refilling procedure. *(i)* The refill port is located with a localization magnet (M_L) with a donut shape and polarity opposite that of M_R; *(ii)* a syringe needle is inserted through the refill port, and 0.4 ml of insulin solution (109 U/ml) is injected; and *(iii)* the drug reservoir is filled with the insulin solution. **(b)** *In vitro* insulin release profiles before and after a refilling procedure. The MDP was fully immersed in phosphate-buffered saline (PBS; pH 7.4) at 37 ° C. Initially, three actuations were conducted at 10-min intervals. After each actuation, the amount of released insulin was measured. Then, a refilling procedure was performed, and the experiments were repeated. Three MDPs were tested for this experiment. **(c, d)** *In vivo* profiles of plasma insulin concentration and glucose level in blood before and after the refilling procedure (n = 3). The refilling procedure was performed while the MDP was implanted in STZ-induced diabetic rats. The septum port was found from outside of skin using a localization magnet (M_L) with a polarity opposite that of M_R. To measure the plasma insulin concentration, blood was collected at 60 min after actuation. The blood glucose levels were measured at −1 and 120 min after actuation.

After 11 days, with two consecutive actuations at each administration, the MDP_1A/2A group exhibited an insulin concentration and decreased glucose level of 741.8 ± 4.13 μU ml^{-1} and −300.3 ± 10.8 mg dl^{-1}, respectively, both higher than in MDP_1A and, importantly, similar to the values in the S.C. injection group. During the non−actuation periods in the MDP_1A and MDP_1A/2A groups, plasma insulin concentrations were low (Fig. 3.3) and similar to the control group, indicating that there was no leakage of insulin from the implanted MDP. To examine a long−term efficacy, I continued the experiment with the MDP_1A/2A group until 60 days, where the insulin in the MDP was fully replenished at 31 days. As shown in Fig. 3.10(c, d), the insulin concentration and decreased glucose levels from 31 days (743.9 ± 10.9 μU ml^{-1} and −323.8 ± 19.9 mg dl^{-1}, respectively) were similar to those observed during the earlier period at 16−30 days (Fig. 3.10(a,b)). This result implied a long−term applicability of the MDP herein that could infuse the insulin in a reproducible manner even after a replenishing procedure. After a replenishing procedure, I did not observe any sign of hypoglycemia with all tested animals. Due to the valve located at the outlet, a slight change in reservoir pressure did not appear to cause considerable insulin burst release. For a more detailed analysis, I also assessed the dynamic profiles of insulin concentration and decreased glucose level at shorter time scales (i.e., 720 minutes) after administration in the S.C. injection, MDP_1A and MDP_1A/2A groups. These extensive measurements were performed at 1, 16 and 30 days after MDP

implantation. As shown in Fig. 3.4 and 3.10, on 1 day, the profiles of insulin concentration and decreased glucose levels were similar among all three groups. However, on days 16 and 30, the overall decrease in the insulin concentration and decreased glucose level were greater in the MDP_1A group than in the S.C. injection group. The areas under the curve for insulin concentration and decreased glucose level ($AUC_{PK,\ insulin}$ and $AUC_{PD,\ glucose}$, respectively) in the S.C. injection group were 84,392 μU ml^{-1} min and 60,035 mg dl^{-1} min, respectively, which decreased to 50,236 μU ml^{-1} min and 41,325 mg dl^{-1} min on day 16 and 47,162 μU ml^{-1} min and 36,510 mg dl^{-1} min on day 30, respectively. In the MDP_1A/2A group, the maximum insulin concentration and decrease in glucose level were comparable to those in the S.C. injection group on days 16 and 30. However, both $AUC_{PK,\ insulin}$ and $AUC_{PD,\ glucose}$ were larger in the MDP_1A/2A group (129,204 μU ml^{-1} min and 93,364 mg dl^{-1} min at day 16 and 129,267 μU ml^{-1} min and 90,360 mg dl^{-1} min at day 30, respectively) than in the S.C. injection group. In the MDP_1A/2A group, a larger dose of insulin was administered into the subcutaneous space and appeared to slowly diffuse into the blood stream across the fibrotic capsule around the MDP, resulting in greater systemic insulin exposure. This process appeared to be completed within hours after MDP actuations (Table 3.2). Regardless of the period after implantation, the times of the maximum insulin concentration and decrease in glucose level were constant (i.e., $T_{max,\ insulin}$ = 60 min and $T_{max,\ glucose}$ = 120 min, respectively) in all groups.

Table 3.2 Insulin amount left in fibrotic capsules. To assess the insulin amount possibly left in the fibrotic capsule, I biopsied the whole capsule including the MDP at two different days after implantation, i.e., at 16 days and 60 days, respectively (n = 5; 16 days, n = 4; 60 days). At each day, the MDP was actuated twice consecutively (1.6 U insulin delivery) and after 360 min, the biopsy was performed. From each of the biopsied capsule, I extracted the MDP and the surrounding capsule tissue was fully immersed in 5 ml of pH 7.4 PBS at 37 °C for 6 h. Then, the supernatant was analyzed with HPLC, as described in the Methods, to measure the insulin amount. Our results revealed that more than 97.5% of the total amount of delivered insulin was diffused out from the fibrotic capsule during the first 360 min after actuations.

Day	Insulin amount in fibrotic capsule (U)
16	0.032 ± 0.011
60	0.030 ± 0.008

Values ± s.d.

3.3.4 Histopathology

To assess *in vivo* biocompatibility, biopsied tissue samples around the MDP were examined by hematoxylin and eosin (H&E) and CD68 staining. As shown in Fig. 3.13 (a, b), the overall inflammatory and foreign body reactions were minimal for all tested tissue locations around the MDP. Also, elevation of inflammatory markers in plasma, such as IL−1b, IL−6 and TNF−α, was not observed at 30 and 60 days after MDP implantation (Table 3.3).

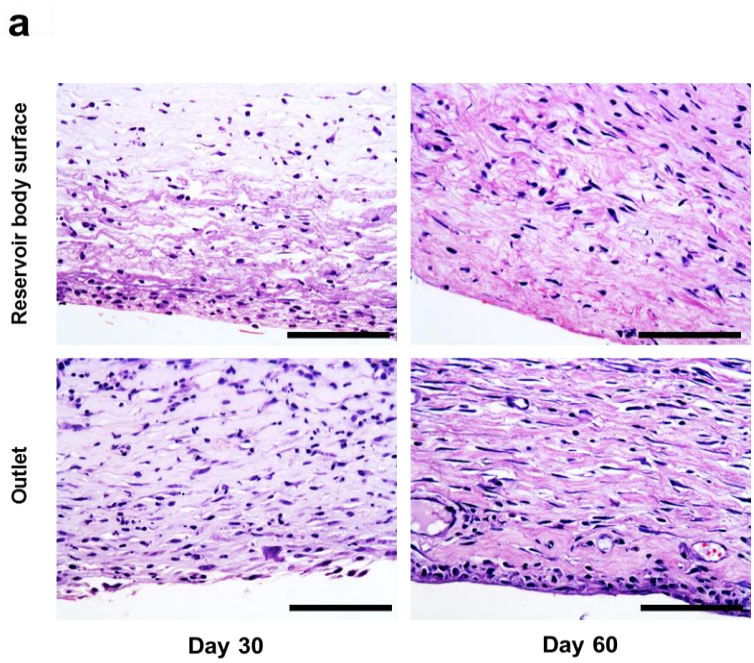
a
Reservoir body surface
Outlet
Day 30
Day 60

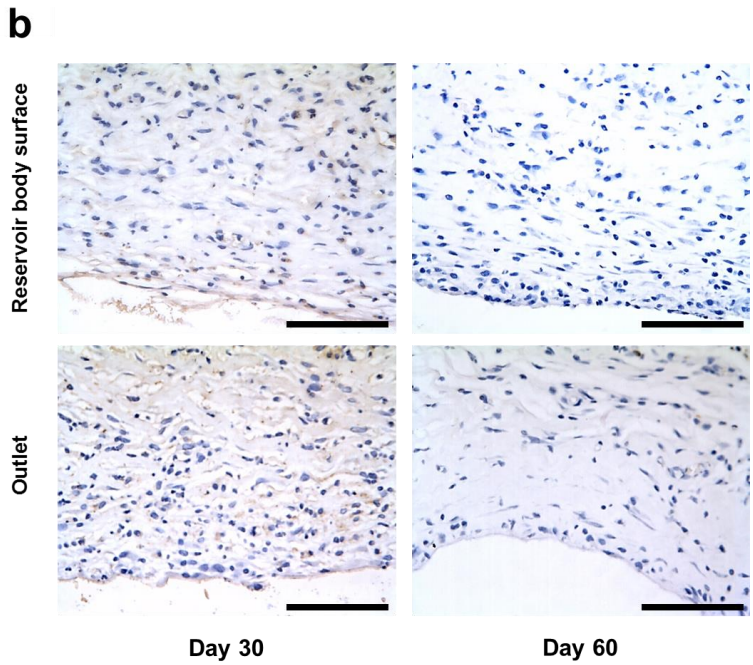
b
Reservoir body surface
Outlet
Day 30
Day 60

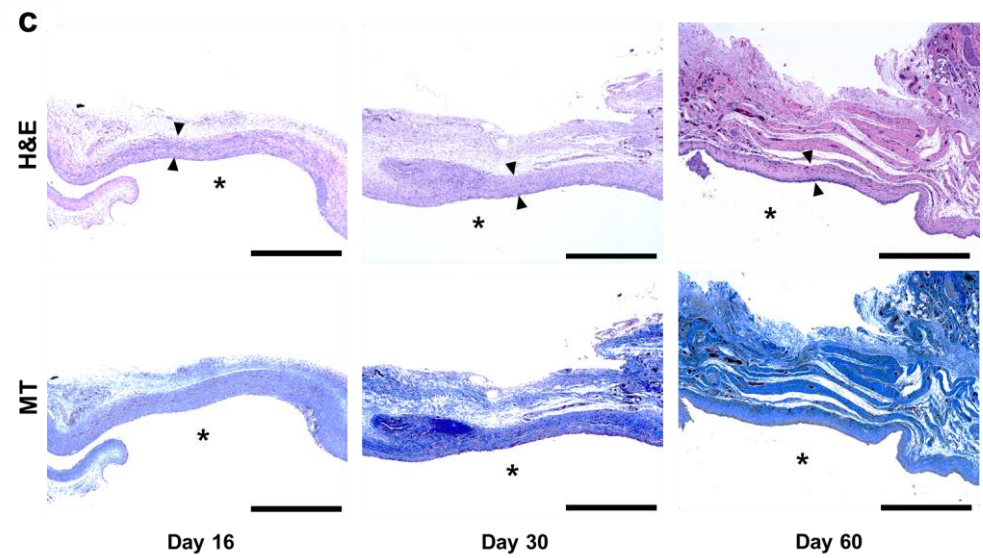

Figure 3.13 Representative histological images of the tissues around the MDP. Two distinct locations in the tissue were observed: the tissues near the reservoir body surface and near the outlet of the MDP. The asterisk (*) indicates the location of the implanted MDP. n = 4; 16 days, n = 5; 30 days and n = 4; 60 days. To evaluate biocompatibility, I assessed the degree of inflammatory response in **(a)** H&E-stained and **(b)** CD68-stained tissues near both the reservoir body surface and the outlet of the MDP at 30 and 60 days after implantation. The scale bars are 100 μm. **(c)** Formation of collagen was assessed in both H&E- and MT-stained tissues near the outlet of the MDP at 16, 30 and 60 days after implantation. To measure the capsule thickness, the thinnest region of the capsule was selected in each image of the H&E-stained samples, as indicated by the arrows. The scale bars are 1 mm.

Table 3.3 Inflammatory markers in plasma. Inflammatory markers in plasma, such as IL−1b, IL−6 and TNF−α, were measured at 30 and 60 days after MDP implantation (n = 3; 30 days, n = 3; 60 days). For all animals, elevation of inflammatory markers was not observed and their levels in plasma were not different from the ones with the control animal group (i.e., the animals without MDP implantation).

	IL-1b (pg ml^{-1})	IL-6 (pg ml^{-1})	TNF-α (pg ml^{-1})
Day 30	68 ± 10	53 ± 4.0	82 ± 11
Day 60	68 ± 4.0	56 ± 3.0	87 ± 8.2
Control	71 ± 8.6	60 ± 3.2	94 ± 3.0

Values ± s.d.

These results support the biocompatibility of the MDP, which is attributable to the biocompatible Parylene C coating used in this work(58). The fibrotic capsule close to the outlet of the MDP, which could influence the pharmacokinetics and pharmacodynamics profiles of infused insulin, was also examined. As shown in Fig. 3.13c, fibrotic capsule formation was evident, and in the capsule tissues, minimal proliferation of bland-looking fibroblasts with rich collagenous stroma and some lymphoplasmacytic, histiocytic and eosinophilic infiltration were observed. The capsule thickness was 242 ± 56.9 μm after 16 days, similar to the thicknesses at 30 and 60 days (243 ± 56.9 μm and 246 ± 41.7 μm, respectively). No sign of clogging was observed with the valve in the MDP at 60 days (Fig. 3.14). This constant thickness may explain the reproducible values of insulin concentration and decreased glucose level measured from 16 days in the MDP_1A and MDP_1A/2A groups. The capsule thickness did not appear to vary at the different locations of the MDP surface.

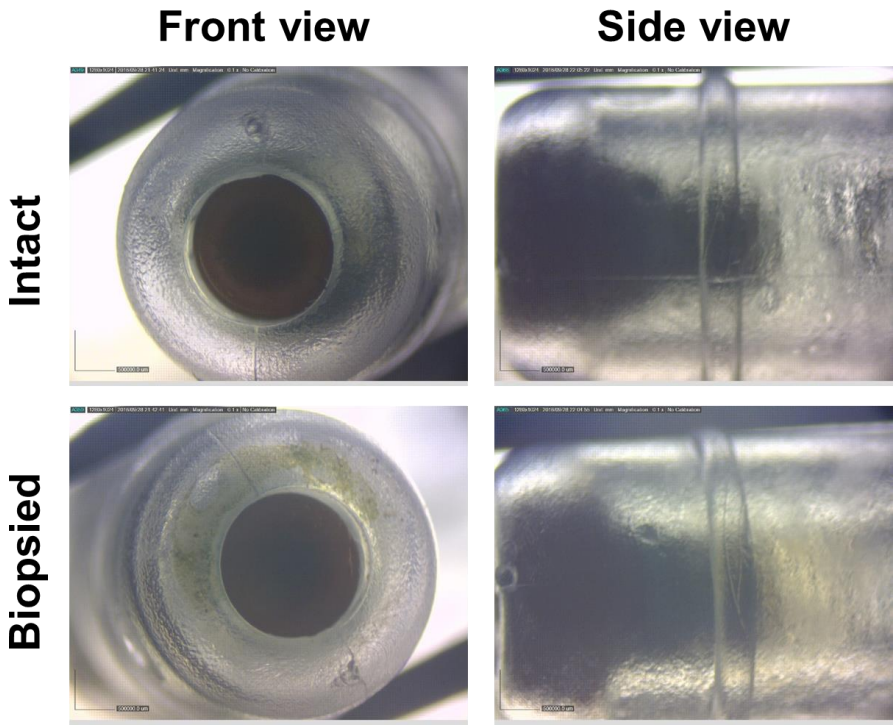

Figure 3.14 Representative images of the intact valve and the one extracted from the MDP biopsied at 60 days after implantation. No sign of clogging was seen with the valve in the implanted MDP.

3.4 Discussion

In this work, I designed a fully-implantable MDP for semi-permanent use. Compared to previous implantable systems for insulin delivery (13, 54, 65), the MDP is advantageous due to its batteryless operation by infusing insulin based on actuation via a magnetic field. The magnetic field strength used in this study (~ 0.1 T) can propagate through tissue without damage(66), and thus, the MDP can be actuated noninvasively. This approach also allows the MDP to be patient-driven to provide on-demand release of insulin. This is an important aspect of clinical modulation for maintaining blood glucose levels after each meal(67). Along with the batteryless design, I also prepared a refill port in the drug reservoir to enable periodic refilling of insulin. Currently, Medtronic's synchromed Ⅱ and Iprecio pump are refilled with external marking or hand recognition from outside body. However, drug administration errors are frequently reported. Unlike these devices, the locations of the refill port can be easily recognized due to the presence of a magnet, M_R, even with subcutaneous implantation of the MDP similar to tissue expanders in clinical use(60). As a result, the MDP exhibited similar infused insulin doses per actuation before and after the refilling procedure, and thus the *in vivo* pharmacokinetics and pharmacodynamics profiles did almost not change after a refilling procedure (Fig. 3.12). In this work, to examine the feasibility, I prepared the MDP as a prototype, small enough to be implantable in STZ-induced diabetic rats. Therefore,

envisioning implantation in human, the MDP could be prepared to possess a larger volume, hence allowing for a larger drug reservoir. This could be designed more efficiently as the MDP herein does not need a space for battery. Previous trials have employed magnetic fields to trigger drug release from implantable devices. For example, a drug reservoir in an implantable device was sealed with a porous membrane in which the pores could be opened and closed by an externally applied magnetic field(68). In other examples, a membrane with an aperture or porous capsule was deformed to squeeze the drug depot and initiate its release by a magnetic field(69-71). However, due to the presence of pores and apertures in the sealing membrane, drug leakage during non-actuation periods was not avoidable. This inherent drawback may hamper the application of these devices for insulin delivery because uncontrolled exposure of insulin can cause undesirable events, such as hypoglycemia(72). I therefore designed the MDP to be leak-free when the external device is not in use. Two magnets each having 1000 G magnetic field strength are embedded in the MDP and become attached to immobilize the plunger and barrel subunits, preventing unwanted infusion. The force between two magnets is 1.25 N. Therefore, since the magnet having a magnetic field strength of 3000 G or more needs to be driven at an accurate position from the outside body, the possibility of malfunction is remarkably low. However, a fundamental solution requires a design that can be composed of patterned magnets inside and that can be driven only by the outer

magnet of the same pattern. I also employed a check valve at the outlet to further prevent leakage possibly caused by diffusion (Fig. 3.3). Another advantage of our MDP is the relatively fast infusion of insulin, where the delivered doses of insulin per actuation were quite similar regardless of the period for the external device application (Fig. 3.15). Upon removal of the external device, the magnet in the plunger immediately attracts the magnet in the barrel, causing the plunger to push insulin toward the outlet nearly instantaneously. Although not the same as the biological system, such as islets(73), this rapid infusion more closely mimics insulin delivery via the established clinical modalities, such as with an insulin pen or needle-syringe injections(74). In addition, the longevity of the device can be improved by compensating the negative pressure inside the device through a flexible drug reservoir such as, PU (polyurethane) or SEBS (Styrene-Ethylene-Butylene-Styrene) and valve system. Furthermore, MRI compatible issue can be resolved like a programmable CSF (Cerebrospinal Fluid) shunt valve or a cochlear implant. Currently, the shut valve with a 1-mm diameter, 1.3-mm NdFeB magnet has been proven safe in 3 T MRI (generally 1.5 T MRI is the most widely used), and new developed cochlear implant equipped with a rotatable pattern magnet (remanent magnetization of 1.15-1.25 T inside the device) is known to be compatible with 3 T MRI. The pharmacokinetics and pharmacodynamics profiles of insulin release in the MDP group were similar to those in the S.C. injection group, even at shorter time scales (Fig. 3.11). Therefore, the MDP

herein could be applicable for a variety of insulin formulations and regimens to achieve a profile of blood glucose level needed for specific diabetic treatment (Figs. 3.16 and 3.17).

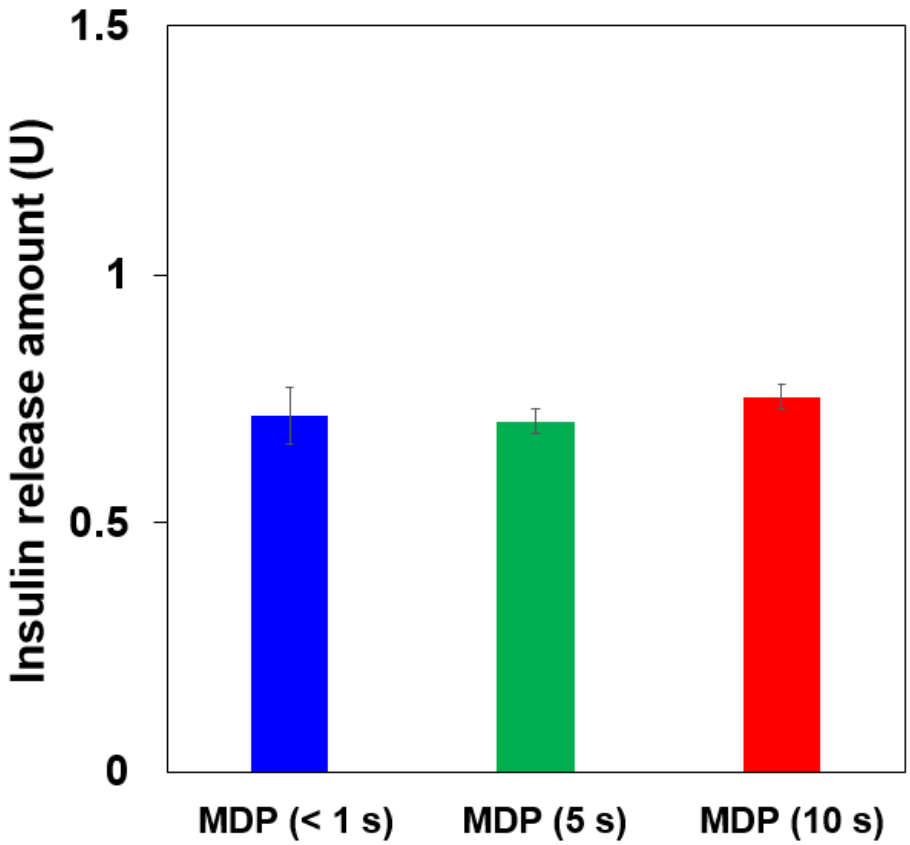

Figure 3.15 Reproducibility assessment of the MDP with varying the periods for the external device (M_E) application. Under the *in vitro* drug release experimental condition depicted in Fig. 3.2, the external device was applied and removed to the MDP during the periods of < 1 s, 5 s and 10 s, respectively (i.e., MDP (< 1 s), MDP (5 s) and MDP (10 s), respectively). The results revealed that the delivered doses of insulin per actuation were quite similar regardless of the period for the external device application. Three distinct MDPs were tested for each period for the external device application.

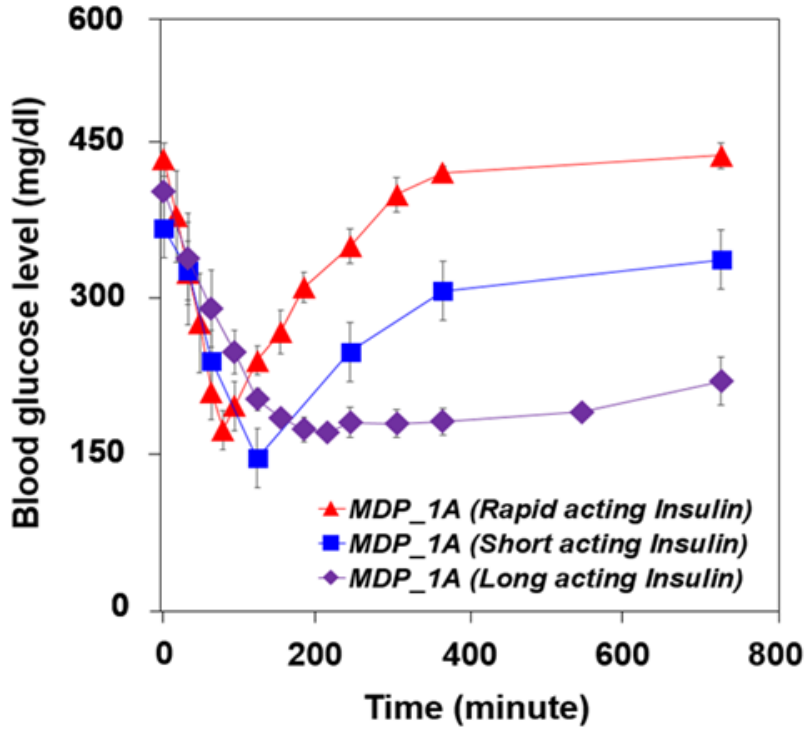
600
450
300
150
0
Blood glucose level (mg/dl)
0
200
400
600
800
Time (minute)
MDP_1A (Rapid acting Insulin)
MDP_1A (Short acting Insulin)
MDP_1A (Long acting Insulin)

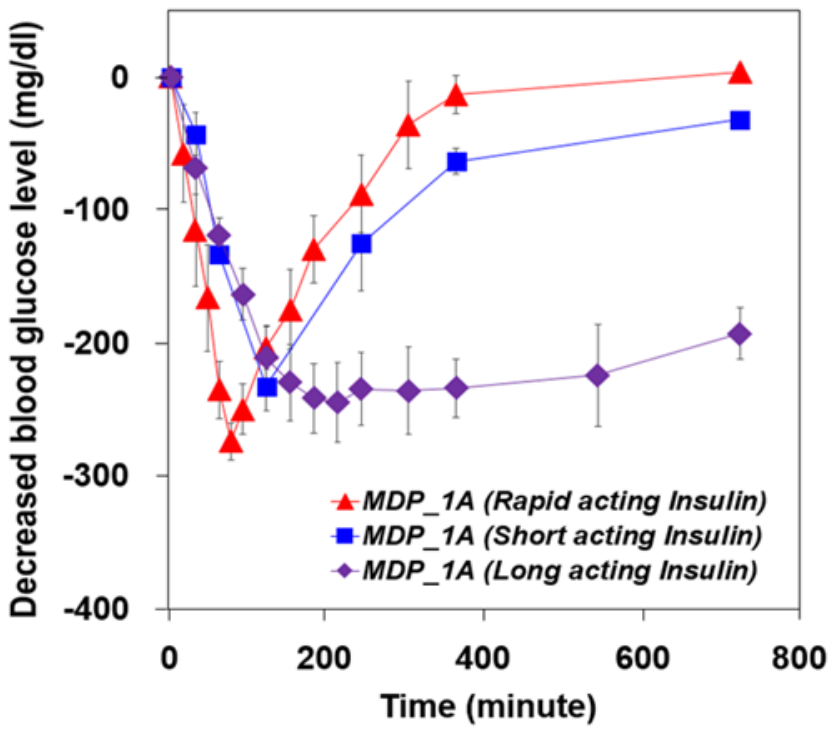
0
-100
-200
-300
-400
Decreased blood glucose level (mg/dl)
0
200
400
600
800
Time (minute)
MDP_1A (Rapid acting Insulin)
MDP_1A (Short acting Insulin)
MDP_1A (Long acting Insulin)

Figure 3.16 Profiles of blood glucose level obtained with the three different insulin formulations. In addition to a short acting insulin mainly used in this study (i.e., MDP_1A (short acting insulin)), I additionally prepared the MDP filled with a rapid acting or long acting insulin formulation (NovoRapid[1] or Lantus[2], respectively) to give the animal groups of MDP_1A (rapid acting insulin) or MDP_1A (long acting insulin), respectively. At 1 day after the MDP was implanted in STZ-induced diabetic rats, the blood glucose level was obtained at −1 to 720 min after insulin administration by a single actuation of the MDP. A similar dose of insulin was administered for all experimental groups (rapid acting: 0.74 U; short acting: 0.80 U; and long acting 0.74 U). For each animal group, 4 rats were employed for statistics. For all formulations, the decrease in blood glucose level was apparent after actuation and as expected, a specific profile of blood glucose level was observed for each type of the insulin formulations filled in the MDP. For rapid acting insulin, the blood glucose level decreased and increased back more rapidly. For long acting insulin, the blood glucose level dropped relatively slowly and this lowered level was maintained for a longer period.

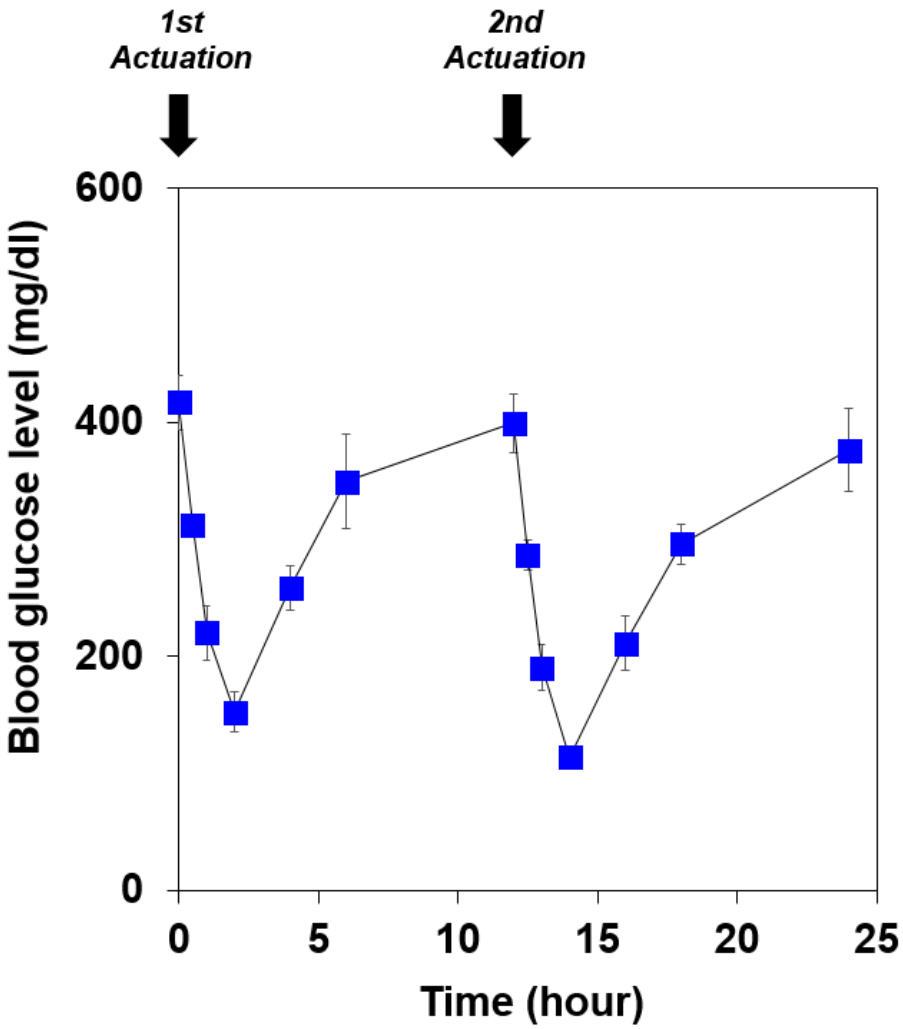

Figure 3.17 *In vivo* profiles of blood glucose level with multiple daily actuations of the MDP. To give an insight of insulin delivery after each of the meal times, the MDP was actuated twice with an interval of 12 h. After the first actuation, a glucose level dropped and increased back to a high level as expected with diabetic rats, which was observed to be repeated in a similar pattern after the second actuation (n=4).

Dose adjustment by varying the number of consecutive external device applications can also be easily performed because of the fast mechanical response between the plunger and barrel. At each actuation, the MDP infuses a specific volume of liquid, and therefore the dose of each actuation can also be varied by changing the concentration of insulin solution stored in the drug reservoir. Thus, I envision that a dose of prandial insulin can be customized within the typically prescribed range of 0.5–1.0 U, depending on the patient's needs for precise insulin dosing(75). This dose adjustment would be more effective and convenient when combined with a closed-loop glucose sensor(76, 77).

Even with the presence of fibrotic capsules, the MDP produced plasma insulin concentrations and decreased glucose levels similar to those in the early period after implantation, simply by increasing the number of actuations (Fig. 3.8). Although the overall inflammatory and foreign body reactions were acceptable (Fig. 3.12), fibrotic capsule formation around the nondegradable implant like the MDP was natural and inevitable(78). Fibrotic capsule formation occurs gradually over weeks(79), and thus to ensure reproducible systemic drug exposure, I envision delaying the operation of the MDP herein until formation of the fibrous capsule is complete(64). Another clinical issue is local lipohypertrophy at the site of subcutaneous insulin injection(80). In this scenario, a catheter-connected MDP can be advantageous. For example, insulin can be infused via a catheter into the intraperitoneal space while implanting the MDP

subcutaneously for improved access to the external magnetic device(81) (Table 3.4).

Table 3.4 Amount of released insulin with varied catheter lengths. The MDP without a catheter (i.e., a catheter, 0 cm in length) and the ones connected with a catheter, 10 and 15 cm in length, respectively, were each actuated under the *in vitro* experimental condition. Although the amount of released insulin decreased with the catheter length, insulin could still be released in a reproducible manner with a catheter length of up to 15 cm and this was reported to be similar to an anatomical distance between the subcutaneous and intraperitoneal space in humans[4]. The result indicated a reproducible volume of liquid infused per actuation and thus, the dose of insulin could be accommodated by employing a proper concentration of insulin formulation to be filled in the drug reservoir.

Catheter length (cm)	Insulin release amount (U)
0	0.81 ± 0.04
10	0.74 ± 0.04
15	0.68 ± 0.04

3.5 Conclusion

In conclusion, I have proposed a simple-assembly, implantable infusion pump enabled with on-demand, pulsatile release of insulin. The pump can be actuated to infuse insulin via an externally applied magnetic field, thus enabling non-invasive insulin delivery after one-time implantation. Most importantly, the pump can be operated without a battery and can be designed to be refilled, enabling potentially semi-permanent use. The desired dose of insulin can be accurately and reproducibly controlled by varying the number of actuations, resulting in pharmacokinetics and pharmacodynamics profiles similar to those of conventional subcutaneous insulin injections. This control can be achieved simply by varying the number of applications of a pen-type magnet on the outside skin above the implanted insulin-infusion pump. Therefore, I conclude that the system proposed in this work is promising for noninvasive, on-demand pulsatile insulin administration for diabetic treatment.

Chapter 4

Conclusion and Perspective

To treat chronic diseases that are the cause of death of 67 percent of the world's population is urgent. The most common way to treat them is long-term drug therapy such as frequent injection and oral administration. However, it causes a lot of pain and economic burden to the patient. To resolve this, implantable drug delivery device enabled with controlled drug release has been emerging because it

can replace frequent injections and oral administration with a single implant. It is mainly classified as a passive drug delivery device and an active implantable drug delivery device.

A passive drug delivery device can preprogram the drug release rate before implanting the device into the body. Additionally, it is capable of delivering drugs in a self-controlled manner and is suitable for the treatment of diseases requiring long-term continuous drug release.

On the other hand, an active drug delivery device can be on-demand controlled after implantation. Thus, it is suitable for diseases requiring precise and complex drug regimens.

In this study, a microchannel-based implantable microchip as a passive device and implantable battery-less device as an active device were presented as next innovative patient-customized implantable devices.

In Chapter 2, I presented a microchannel-based implantable microchip that can be operated in self-controlled manner by preprogramming the drug release rate. The core of the study was the ability to adjust the desired amount of drug release by controlling channel dimensions such as, length and cross-sectional area based on Fick's first law of diffusion and diffusion flux equation. Therefore, it is suitable for diseases requiring a long-term continuous release profile such as, pain disorder, type 2 diabetes, brain tumor, eye diseases, contraceptive, and androgen deficiency. For clinical applications, several improvements are required. First, the device can be constructed efficiently and easily for implantation such as a

tube shape because it is simply composed of a drug reservoir and a microchannel without the need for a battery or driving parts. Furthermore, if the device itself is composed of biodegradable polymers such as PLGA, PLLA, and PCL, there is no need to consider second surgery. With these advantages, it can be simply applied by adding to existing implantable devices as a combination product and multi-drug delivery is also possible because it can be composed of multiple reservoirs and channels. For example, if a drug for the treatment of diseases and an anti-fibrous capsule agent are enclosed, the disease treatment and the anti-capsule effect can be achieved at the same time.

In Chapter 3, I presented an implantable battery-less device that can be driven externally without a battery after implanting the device.

The essence of this study is that it can be operated by magnetic field as 'no power source'. So, just putting a magnetic field on the skin instead of an injection needle, the drug can be non-invasively delivered. Therefore, it is suitable for diseases requiring a precise and complex drug regimens such as, osteoporosis, diabetes, multiple sclerosis, cancer (chronotherapy), contraceptive, and human growth hormone deficiency. However, some points should be improved in clinical application. Currently, it is composed of prototypes of sufficient size to be implanted into rats, but envisioning implantation in human, drug reservoir and driving parts should be modified. Unlike other devices, it does not require a battery, which makes it possible to construct a device with a high proportion of drug reservoir in total

volume. In addition, as mentioned in Chapter 3, the negative pressure issue of the device can be compensated by the flexible drug reservoir and the valve system, and the problem of malfunction due to external factors can be solved by adjusting the strength of the inner magnet and using the pattern magnet. Additionally, if the case is made of titanium, the safety of the device will be enhanced. Furthermore, MRI compatibility is expected to be available if the inner magnet is configured to be rotatable, such as a cochlear implant(82). Also, if an external controller, such as an electromagnet or a motor equipped with magnet is employed, safety and practicality can be improved. In particular, it is possible to implement a closed-loop system if it is used in conjunction with CGMS (i.e., continuous glucose monitoring system). In addition, if a multi-channel based implantable microchip and a battery-less implantable device are combined, they can be expected to be promising new innovative implantable drug delivery device in near future.

Therefore, microchannel-based implantable microchip and implantable battery-less device that can replace frequent injections and oral administration with a single implant are of great significance in that they offer patient-specific new concept biomedical technology and expected to be promising new innovative implantable devices in near future.

References

1. Statistics NCfH, Research NCfHS. Health, United States: US Department of Health, Education, and Welfare, Public Health Service, Health Resources Administration, National Center for Health Statistics; 2002.
2. Serban MA. Translational biomaterials—the journey from the bench to the market—think 'product'. Current opinion in biotechnology. 2016;40:31-4.
3. Grayson ACR, Choi IS, Tyler BM, Wang PP, Brem H, Cima MJ, et al. Multi-pulse drug delivery from a resorbable polymeric microchip device. Nature materials. 2003;2(11):767-72.
4. Westphal M, Ram Z, Riddle V, Hilt D, Bortey E, Group ECotGS. Gliadel® wafer in initial surgery for malignant glioma: long-term follow-up of a multicenter controlled trial. Acta neurochirurgica. 2006;148(3):269-75.
5. Lee SH, Park M, Park CG, Kim B-H, Lee J, Choi S, et al. Implantable micro-chip for controlled delivery of diclofenac sodium. Journal of Controlled Release. 2014;196:52-9.
6. Funk S, Miller MM, Mishell DR, Archer DF, Poindexter A, Schmidt J, et al. Safety and efficacy of Implanon™, a single-rod implantable contraceptive containing etonogestrel. Contraception. 2005;71(5):319-26.
7. Fischer K, Degenkolb K, Fischer W, Mendelsohn A. Nanoscale Constrained Delivery: A Novel Technology for Subdermal Implants. Nanoprecision Medical Inc White Paper. 2014.
8. Verma RK, Arora S, Garg S. Osmotic pumps in drug delivery. Critical Reviews™ in Therapeutic Drug Carrier Systems. 2004;21(6).
9. Henry RR, Rosenstock J, Logan D, Alessi T, Luskey K, Baron MA. Continuous subcutaneous delivery of exenatide via ITCA 650 leads to sustained glycemic control and weight loss for 48 weeks in metformin-treated subjects with type 2 diabetes. Journal of Diabetes and its Complications. 2014;28(3):393-8.
10. Tan T, Watts SW, Davis RP. Drug delivery: enabling technology for drug discovery and development. iPRECIO® micro infusion pump: programmable, refillable and implantable. Frontiers in pharmacology. 2011;2:44.
11. Lang AE, Gill S, Patel NK, Lozano A, Nutt JG, Penn R, et al. Randomized controlled trial of intraputamenal glial cell line-derived neurotrophic factor infusion in Parkinson disease. Annals of neurology. 2006;59(3):459-66.
12. Santini JT, Jr., Cima MJ, Langer R. A controlled-release microchip. Nature. 1999;397(6717):335-8.
13. Prescott JH, Lipka S, Baldwin S, Sheppard NF, Maloney JM, Coppeta J, et al. Chronic, programmed polypeptide delivery from an implanted, multireservoir microchip device. Nature biotechnology. 2006;24(4):437-8.
14. Farra R, Sheppard NF, McCabe L, Neer RM, Anderson JM, Santini JT, et al. First-in-human testing of a wirelessly controlled drug delivery

microchip. Science translational medicine. 2012;4(122):122ra21-ra21.
15. Van Lintel H, Poscio P, Neftel F. Piezoelectric micropump having actuation electrodes and stopper members. Google Patents; 1998.
16. Gensler H, Sheybani R, Li PY, Mann RL, Meng E. An implantable MEMS micropump system for drug delivery in small animals. Biomedical microdevices. 2012;14(3):483-96.
17. Li PY, Shih J, Lo R, Saati S, Agrawal R, Humayun MS, et al. An electrochemical intraocular drug delivery device. Sensors and Actuators a-Physical. 2008;143(1):41-8.
18. Santini JT, Cima MJ, Langer R. A controlled-release microchip. Nature. 1999;397(6717):335-8.
19. Tuncay M, Calis S, Kas H, Ercan M, Peksoy I, Hincal A. In vitro and in vivo evaluation of diclofenac sodium loaded album in microspheres. Journal of microencapsulation. 2000;17(2):145-55.
20. Cormio M, Citerio G, Spear S, Fumagalli R, Pesenti A. Control of fever by continuous, low-dose diclofenac sodium infusion in acute cerebral damage patients. Intensive care medicine. 2000;26(5):552-7.
21. Gohel M, Amin A. Formulation optimization of controlled release diclofenac sodium microspheres using factorial design. Journal of Controlled Release. 1998;51(2):115-22.
22. Arias JL, López-Viota M, López-Viota J, Delgado ÁV. Development of iron/ethylcellulose (core/shell) nanoparticles loaded with diclofenac sodium for arthritis treatment. International journal of pharmaceutics. 2009;382(1):270-6.
23. Manconi M, Mura S, Sinico C, Fadda A, Vila A, Molina F. Development and characterization of liposomes containing glycols as carriers for diclofenac. Colloids and Surfaces A: Physicochemical and Engineering Aspects. 2009;342(1):53-8.
24. Hua S, Ma H, Li X, Yang H, Wang A. pH-sensitive sodium alginate/poly (vinyl alcohol) hydrogel beads prepared by combined Ca< sup> 2+ </sup> crosslinking and freeze-thawing cycles for controlled release of diclofenac sodium. International journal of biological macromolecules. 2010;46(5):517-23.
25. Vilar G, Tulla-Puche J, Albericio F. Polymers and drug delivery systems. Current drug delivery. 2012;9(4):367-94.
26. Bravo SA, Lamas MC, Salomon CJ. In-vitro studies of diclofenac sodium controlled-release from biopolymeric hydrophilic matrices. J Pharm Pharm Sci. 2002;5(3):213-9.
27. Tsai N-C, Sue C-Y. Review of MEMS-based drug delivery and dosing systems. Sensors and Actuators A: Physical. 2007;134(2):555-64.
28. Shawgo RS, Richards Grayson AC, Li Y, Cima MJ. BioMEMS for drug delivery. Current Opinion in Solid State and Materials Science. 2002;6(4):329-34.
29. Judy JW. Microelectromechanical systems (MEMS): fabrication, design and applications. Smart materials and Structures. 2001;10(6):1115.
30. Potts E, Fleming H, McFeeters R, Guinnup D. Equilibration of solutes in nonfermenting, brined pickling cucumbers. Journal of Food Science.

1986;51(2):434-9.
31. Kim GY, Tyler BM, Tupper MM, Karp JM, Langer RS, Brem H, et al. Resorbable polymer microchips releasing BCNU inhibit tumor growth in the rat 9L flank model. Journal of Controlled Release. 2007;123(2):172-8.
32. Nasir F, Iqbal Z, Khan A, Ahmad L, Shah Y, Khan AZ, et al. Simultaneous determination of timolol maleate, rosuvastatin calcium and diclofenac sodium in pharmaceuticals and physiological fluids using HPLC-UV. Journal of Chromatography B. 2011;879(30):3434-43.
33. Zeplin PH, Larena-Avellaneda A, Schmidt K. Surface modification of silicone breast implants by binding the antifibrotic drug halofuginone reduces capsular fibrosis. Plastic and reconstructive surgery. 2010;126(1):266-74.
34. Anderson J, Niven H, Pelagalli J, Olanoff L, Jones R. The role of the fibrous capsule in the function of implanted drug-polymer sustained release systems. Journal of biomedical materials research. 1981;15(6):889-902.
35. Jansen J, Van Der Waerden J, De Groot K. Development of a new percutaneous access device for implantation in soft tissues. Journal of biomedical materials research. 1991;25(12):1535-45.
36. Nasir F, Iqbal Z, Khan JA, Khan A, Khuda F, Ahmad L, et al. Development and evaluation of diclofenac sodium thermorevesible subcutaneous drug delivery system. International journal of pharmaceutics. 2012;439(1):120-6.
37. Huang X, Brazel CS. On the importance and mechanisms of burst release in matrix-controlled drug delivery systems. Journal of Controlled Release. 2001;73(2):121-36.
38. Lee KJ, Yang SY, Ryu W. Controlled release of bupivacaine HCl through microchannels of biodegradable drug delivery device. Biomedical microdevices. 2012;14(3):583-93.
39. Grattoni A, Shen H, Fine D, Ziemys A, Gill JS, Hudson L, et al. Nanochannel technology for constant delivery of chemotherapeutics: beyond metronomic administration. Pharmaceutical research. 2011;28(2):292-300.
40. Yang SY, Yang J-A, Kim E-S, Jeon G, Oh EJ, Choi KY, et al. Single-file diffusion of protein drugs through cylindrical nanochannels. ACS nano. 2010;4(7):3817-22.
41. Rastogi A, Luo Z, Wu Z, Ho PS, Bowman PD, Stavchansky S. Development and characterization of a scalable microperforated device capable of long-term zero order drug release. Biomedical microdevices. 2010;12(5):915-21.
42. Tao SL, Lubeley MW, Desai TA. Bioadhesive poly (methyl methacrylate) microdevices for controlled drug delivery. Journal of controlled release. 2003;88(2):215-28.
43. Kim SB, Kim YJ, Yoon TL, Park SA, Cho IH, Kim EJ, et al. The characteristics of a hydroxyapatite–chitosan–PMMA bone cement. Biomaterials. 2004;25(26):5715-23.
44. Bjugstad K, Redmond J, Lampe K, Kern D, Sladek J, Mahoney M. Biocompatibility of PEG-based hydrogels in primate brain. Cell transplantation. 2008;17(4):409-15.
45. Schwartz SS, Epstein S, Corkey BE, Grant SF, Gavin JR, Aguilar RB.

The Time Is Right for a New Classification System for Diabetes: Rationale and Implications of the β-Cell-Centric Classification Schema. Diabetes Care. 2016;39(2):179-86.
46. Inzucchi SE, Bergenstal RM, Buse JB, Diamant M, Ferrannini E, Nauck M, et al. Management of hyperglycemia in type 2 diabetes, 2015: a patient-centered approach: update to a position statement of the American Diabetes Association and the European Association for the Study of Diabetes. Diabetes care. 2015;38(1):140-9.
47. DeWitt DE, Hirsch IB. Outpatient insulin therapy in type 1 and type 2 diabetes mellitus: scientific review. Jama. 2003;289(17):2254-64.
48. Eugster EA, Francis G. Position statement: continuous subcutaneous insulin infusion in very young children with type 1 diabetes. Pediatrics. 2006;118(4):e1244-e9.
49. Dunstan DW, Kingwell BA, Larsen R, Healy GN, Cerin E, Hamilton MT, et al. Breaking up prolonged sitting reduces postprandial glucose and insulin responses. Diabetes care. 2012;35(5):976-83.
50. Mura S, Nicolas J, Couvreur P. Stimuli-responsive nanocarriers for drug delivery. Nature materials. 2013;12(11):991-1003.
51. Nair M, Guduru R, Liang P, Hong J, Sagar V, Khizroev S. Externally controlled on-demand release of anti-HIV drug using magneto-electric nanoparticles as carriers. Nature communications. 2013;4:1707.
52. Yavuz MS, Cheng Y, Chen J, Cobley CM, Zhang Q, Rycenga M, et al. Gold nanocages covered by smart polymers for controlled release with near-infrared light. Nature materials. 2009;8(12):935-9.
53. Haveman JW, Logtenberg SJ, Kleefstra N, Groenier KH, Bilo HJ, Blomme AM. Surgical aspects and complications of continuous intraperitoneal insulin infusion with an implantable pump. Langenbeck's Archives of Surgery. 2010;395(1):65-71.
54. Tan T, Watts SW, Davis RP. Drug delivery: enabling technology for drug discovery and development. iPRECIO (R) Micro Infusion Pump: programmable, refillable, and implantable. Frontiers in Pharmacology. 2011;2.
55. Li Y, Ho Duc HL, Tyler B, Williams T, Tupper M, Langer R, et al. In vivo delivery of BCNU from a MEMS device to a tumor model. Journal of controlled release : official journal of the Controlled Release Society. 2005;106(1-2):138-45.
56. Kan JW, Yang ZG, Peng TJ, Cheng GM, Wu B. Design and test of a high-performance piezoelectric micropump for drug delivery. Sensors and Actuators a-Physical. 2005;121(1):156-61.
57. Kang N, Alexander G, Park JK, Maasch C, Buchwalow I, Luft FC, et al. Differential expression of protein kinase C isoforms in streptozotocin-induced diabetic rats. Kidney international. 1999;56(5):1737-50.
58. Linder M, Huther S, Reinacher M. In vivo reactions in mice and in vitro reactions in feline cells to implantable microchip transponders with different surface materials. Vet Rec. 2009;165(2):45-50.
59. McCoy EK, Wright BM. A review of insulin pen devices. Postgraduate medicine. 2010;122(3):81-8.
60. Elliott MP, Dubrul W. Magna-Site tissue expander: an innovation for

injection site location. Plastic and reconstructive surgery. 1988;81(4):605-7.
61. Gibney MA, Arce CH, Byron KJ, Hirsch LJ. Skin and subcutaneous adipose layer thickness in adults with diabetes at sites used for insulin injections: implications for needle length recommendations. Current medical research and opinion. 2010;26(6):1519-30.
62. Takeuchi H, Ishida M, Furuya A, Todo H, Urano H, Sugibayashi K. Influence of skin thickness on the in vitro permeabilities of drugs through Sprague-Dawley rat or Yucatan micropig skin. Biological and Pharmaceutical Bulletin. 2012;35(2):192-202.
63. Hashim IIA, Higashi T, Anno T, Motoyama K, Abd-ElGawad A-EH, El-Shabouri MH, et al. Potential use of ɣ-cyclodextrin polypseudorotaxane hydrogels as an injectable sustained release system for insulin. International journal of pharmaceutics. 2010;392(1):83-91.
64. Farra R, Sheppard NF, Jr., McCabe L, Neer RM, Anderson JM, Santini JT, Jr., et al. First-in-human testing of a wirelessly controlled drug delivery microchip. Sci Transl Med. 2012;4(122):122ra21.
65. Gin H, Renard E, Melki V, Boivin S, Schaepelynck-Belicar P, Guerci B, et al. Combined improvements in implantable pump technology and insulin stability allow safe and effective long term intraperitoneal insulin delivery in type 1 diabetic patients: the EVADIAC experience. Diabetes & metabolism. 2003;29(6):602-7.
66. Schaefer DJ, Bourland JD, Nyenhuis JA. Review of Patient Safety in Time-Varying Gradient Fields. Journal of magnetic resonance imaging. 2000;12(1):20-9.
67. Burdick J, Chase HP, Slover RH, Knievel K, Scrimgeour L, Maniatis AK, et al. Missed insulin meal boluses and elevated hemoglobin A1c levels in children receiving insulin pump therapy. Pediatrics. 2004;113(3):e221-e4.
68. Cai KY, Luo Z, Hu Y, Chen XY, Liao YJ, Yang L, et al. Magnetically Triggered Reversible Controlled Drug Delivery from Microfabricated Polymeric Multireservoir Devices. Adv Mater. 2009;21(40):4045-+.
69. Pirmoradi FN, Jackson JK, Burt HM, Chiao M. On-demand controlled release of docetaxel from a battery-less MEMS drug delivery device. Lab on a chip. 2011;11(16):2744-52.
70. So H, Seo YH, Pisano AP. Refillable and magnetically actuated drug delivery system using pear-shaped viscoelastic membrane. Biomicrofluidics. 2014;8(4):044119.
71. Shi J, Zhang H, Jackson J, Shademani A, Chiao M. A robust and refillable magnetic sponge capsule for remotely triggered drug release. Journal of Materials Chemistry B. 2016;4(46):7415-22.
72. Pickup JC, Hammond P. NICE guidance on continuous subcutaneous insulin infusion 2008: review of the technology appraisal guidance. Diabet Med. 2009;26(1):1-4.
73. Veiseh O, Tang BC, Whitehead KA, Anderson DG, Langer R. Managing diabetes with nanomedicine: challenges and opportunities. Nature Reviews Drug Discovery. 2015;14(1):45-57.
74. Lee LJ, Li Q, Reynolds MW, Pawaskar MD, Corrigan SM. Comparison of utilization, cost, adherence, and hypoglycemia in patients with type 2

diabetes initiating rapid-acting insulin analog with prefilled pen versus vial/syringe. Journal of medical economics. 2011;14(1):75-86.
75. Clark PE, Okenfuss CR, Campbell M. Half-unit dose accuracy with HumaPen® Luxura™ HD: an insulin pen for patients who need precise dosing. Journal of diabetes science and technology. 2010;4(2):353-6.
76. Bergenstal RM, Tamborlane WV, Ahmann A, Buse JB, Dailey G, Davis SN, et al. Effectiveness of sensor-augmented insulin-pump therapy in type 1 diabetes. New England Journal of Medicine. 2010;363(4):311-20.
77. El-Khatib FH, Russell SJ, Nathan DM, Sutherlin RG, Damiano ER. A bihormonal closed-loop artificial pancreas for type 1 diabetes. Science translational medicine. 2010;2(27):27ra-ra.
78. Ward WK. A review of the foreign-body response to subcutaneously-implanted devices: the role of macrophages and cytokines in biofouling and fibrosis. Journal of diabetes science and technology. 2008;2(5):768-77.
79. Park S, Park M, Kim BH, Lee JE, Park HJ, Lee SH, et al. Acute suppression of TGF-ß with local, sustained release of tranilast against the formation of fibrous capsules around silicone implants. Journal of Controlled Release. 2015;200:125-37.
80. Rademecker R, Pierard G, Scheen A. Lipodystrophy reactions to insulin: effects of continuous insulin infusion and new analogs. Am J Clin Dermatol. 2007;8:21-8.
81. Spaan NA, Teplova AE, Renard E, Spaan JA. Implantable insulin pumps: an effective option with restricted dissemination. The Lancet Diabetes & Endocrinology. 2014;2(5):358-60.
82. Shew M, Lin J, Staecker H. MRI Imaging in an NF2 Patient with a Novel MRI Compatible Auditory Brain Stem Implant. Journal of Neurological Surgery Part B: Skull Base. 2017;78(S 01):P180.

Abstract in Korean

국문 초록

만성 질병 치료를 위해 일반적으로 사용하는 방법은 장기간 약물 치료 요법이다. 대표적으로 잦은 주사 및 경구투여 방법이 있으나, 이들은 환자에게 많은 고통과 경제적인 부담을 안겨주는 제약점이 있다. 이의 해결을 위하여, 본 논문에서는 단 한번의 이식으로 잦은 주사 및 경구 투여를 대체하고 만성질병의 치료 효과를 극대화 시킬 수 있는 혁신적 이식형 약물 전달 디바이스들을 제안하고자 한다.

지속적인 약물전달이 요구되는 질병치료를 위하여, 전달하고자 하는 약물 방출량을 미리 프로그램하고 조절 전달 가능한 마이크로채널기반 마이크로칩을 개발하였다. 이 연구의 핵심은 Fick's first law of diffusion과 diffusion flux equation 기반 채널의 단면적과 길이변화를 통하여 원하는 양의 약물 방출량을 조절 가능했다는 점이다. 생체적합한재료인 폴리메틸메타크릴레이트 기반의 디바이스는 마이크로제작기술로 널리 이용되는 CO_2 레이저의 출력 및 가공 속도, 레이저의 조사 높이 등의 조건 등을 변화하여 약물을 탑재할 수 있는 약물저장고와 약물 확산벽 역할을 하는 마이크로채널을 정밀 제작할 수 있었다. 약물 저장고에는 관절염에 널리 사용되는 diclofenac을 채워 넣었고, 마이크로채널의 경우 생분해성 고분자인 폴리에틸렌글리콜(PEG)을 밀하게 채워 넣어, 8가지의 서로 다른 약물 전달 프로파일을 50일 이상 재현성 있게 구현 할 수 있었다. 이와 같은 여러 마이크로채널과 약물 저장고를 함께 구성한 마이크로칩은 초반 급격한 약물 방출 및 지연 없이 70일 동안 지속적인 약물 전달 (31일 동안 선형 약물 패턴, $R^2 > 0.996$)이 가능함을 *in vitro* 실험을 통해 보였고, 혈중 내 30일 동안 148 ng/ml-225 ng/ml의 약물 농도가

지속적으로 유지됨을 *in vivo* 약동학 테스트를 통해 증명하였다.

정밀하고 복잡한 약물 요법이 요구되는 질병치료를 위하여, 디바이스 이식 후 외부에서 약물 조절전달이 가능한 이식형 인슐린 주입 펌프를 개발하였다. 이 연구의 핵심은 '무(無)전원' 으로 자석에 의해 구동 된다는 점으로 피부에 주사 바늘 대신 자석을 대는 것만으로 통증 없이 원할 때마다 펄스형 약물 전달을 할 수 있다. 현재 기 개발된 능동형 이식형 디바이스들은 내부에 장착된 배터리로 인해 디바이스 전체 크기가 다소 크고 배터리 수명이 다하면 재수술이 필요한 제약점이 있다. 하지만 자기력 기반 이식형 인슐린 주입 펌프의 경우 디바이스 내부에 배터리가 필요 없어 교체를 위한 재수술이 필요 없다. 당뇨병이 유도된 동물 모델에 60일 동안 이식한 후 구동한 결과, 펌프의 혈중 인슐린농도와 혈당 감소량은 741.8 ± 4.13 μUml^{-1} and 300.3 ± 10.8 mg dl^{-1}으로 기존 인슐린 주사 방법으로 실험한 결과(683.3±16.9 μUml^{-1} and 251.1 ± 6.41 mg dl^{-1})와 거의 비슷한 수준으로 유지된다는 것을 증명할 수 있었다.

이 연구를 통하여, 마이크로채널기반 마이크로칩은 초반 급격한 약물 방출 및 지연 없이, 장기간 지속형 약물 전달이 가능함을 증명하였고, 자기력 기반 이식형 약물 전달 펌프는 디바이스 내부 전원 구동 없이 정밀하게 제어된 펄스형 약물전달이 가능함을 증명하였다. 그러므로 이 디바이스들은 단 한번의 이식으로 잦은 주사 및 경구 투여를 대체 할 수 있는 환자 맞춤형 신개념 의공학 기술을 제시했다는 점에서 큰 의미가 있음을 확인 할 수 있었다.

핵심어: 이식형 약물전달 디바이스, 마이크로채널, 자기력 구동, 무전원 구동, 조절 약물 전달, 지속형 약물 전달, 펄스형 약물 전달

Student Number : 2011-21126